Improving Dynamic Cyclic Rating Predictions for Cable Temperatures using the Finite Element Method

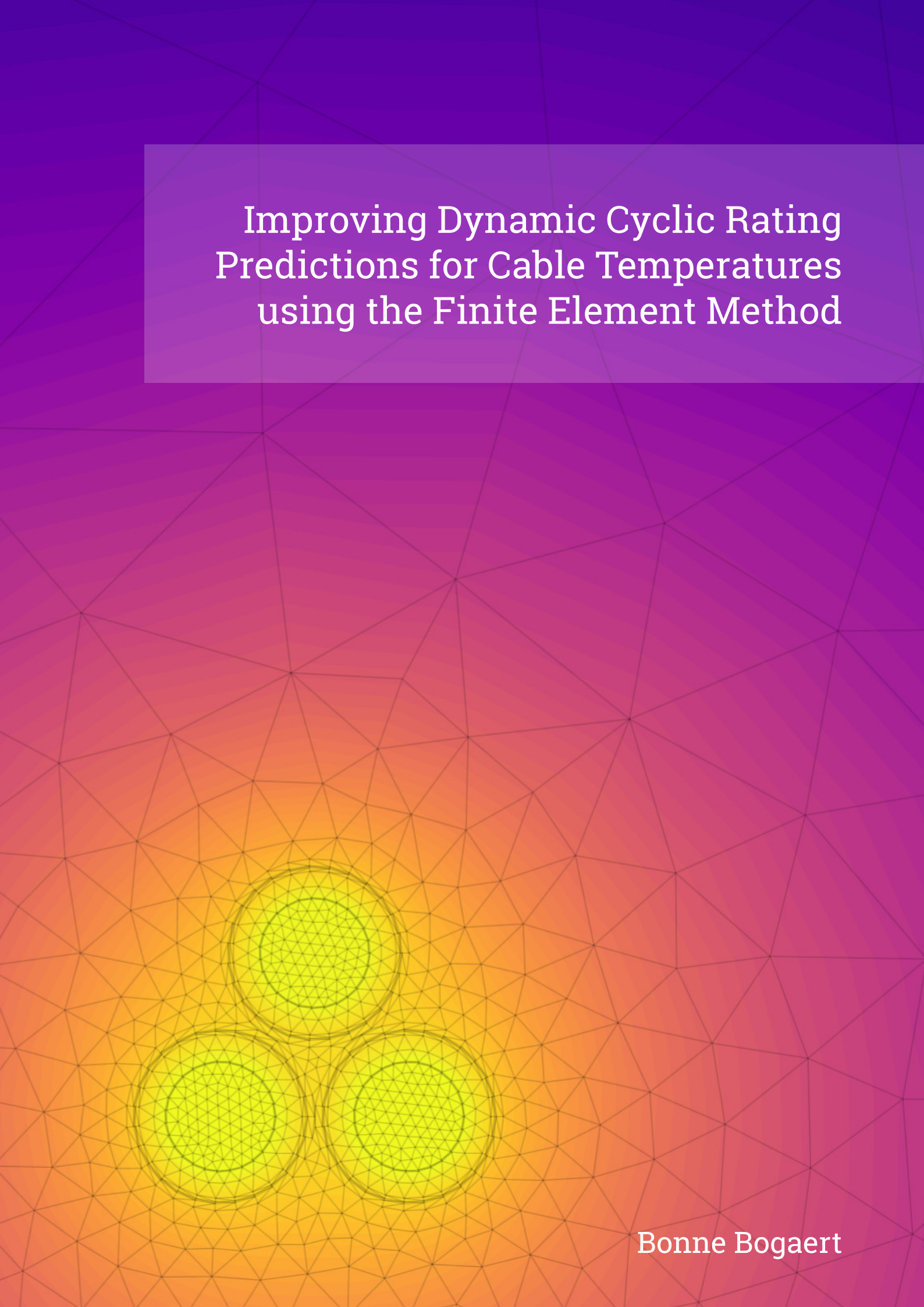

Bonne Bogaert

Improving Dynamic Cyclic Rating Predictions for Cable Temperatures using the Finite Element Method:

A Real-World Comparison

by

Bonne Bogaert

Thesis at the company Ventolines to obtain the degree of Master of Science
at the Delft University of Technology,

Student:	Bonne Bogaert	
Student number:	5107105	
Master program:	Electrical Engineering	
Track:	Electrical Power Engineering	
Project duration:	Nov 20, 2023 – June, 2024	
Thesis committee:	Prof.ir. P.T.M. Vaessen,	TU Delft, Thesis advisor
	Dr.ir. M. Ghaffarian Niasar,	TU Delft, Supervisor
	Dr.ir. H. Vahedi	TU Delft, Independent Member
	ir. B. Stobbe	Company, Supervisor
Company Info:	Ventolines	
	P.J. Oudweg 4, 1314 CH Almere	

An electronic version of this thesis is available at `http://repository.tudelft.nl/`

Cover graphics generated by *Ampwise*

Abstract

The thermal rating of power cables is a critical aspect of electrical cable design that determines their safe operational limits. Traditional rating methods rely on worst-case assumptions for weather conditions, such as constant ambient temperatures or steady-state loading with a 100% load factor. Given the significant thermal masses and variations in ambient conditions, these assumptions often do not reflect actual operational scenarios. As the integration of fluctuating renewable energy sources into power systems increases, the dynamic nature of these systems becomes more pronounced. Consequently, the thermal rating of the power cables must be considered dynamic to accommodate these changing conditions.

In this thesis, an improvement of dynamic cyclic rating predictions is explored for cable temperatures using the Finite Element Method (FEM). This improvement is performed by incorporating detailed weather and environmental data into the model.

The study begins with a comprehensive literature review that provides an overview of existing dynamic rating systems and their applications. Subsequently, an analytical and numerical thermal model was developed and compared with COMSOL and CIGRE standards. It is concluded that the developed numerical model demonstrates greater accuracy and usefulness. This numerical model is integrated into a web-based tool called *Ampwise*, which serves as the basis for all future improvements. Cable data from the Windpark Fryslân project is used to validate the predicted temperature against the measured cable temperature.

The research demonstrates that incorporating weather data significantly improves the precision of dynamic cyclic ratings, especially the inclusion of the real external air temperature and solar radiation of the location. Validation of the predicted conductor temperatures against measured DTS cable temperatures from the Windpark Fryslân project showed a mean absolute error (MAE) of 1.9 °C and a root mean square error (RMSE) of 2.3 °C. These results show the enhanced accuracy and reliability of the dynamic cyclic ratings when real weather data are incorporated. However, the rate of change in the real temperature is significantly higher than the predicted temperature, leading to short-term differences between the predicted and actual temperatures.

In addition, a sensitivity analysis is conducted to assess the impact of various factors. The analysis highlights the importance of correct initial conditions, particularly ground temperature gradients and seasonal environmental variations.

The thesis concludes that integrating weather and environmental data into dynamic rating models is crucial to achieving reliable and precise cable performance predictions over an extended period, thus supporting better operational decisions and infrastructure management.

Preface

This thesis concludes my M.Sc. degree in Electric Power Engineering at the Delft University of Technology (TU Delft), carried out during the last 3 quarters of the school year 2023/2024. Diving into high-voltage cables and their role in a future of renewable energy has opened my eyes to the many possibilities and challenges in this field. I hope that with the knowledge I gained through this thesis I can one day contribute to a more sustainable and greener future.

First, my sincere appreciation goes to my family for being supportive and encouraging throughout my study period. A special thanks goes to my girlfriend Evelien for giving feedback on the final presentation.

This work was carried out at the company Ventolines, where I spent 8 months working on the graduation and an additional 2 months in an internship before. During this period, I gained invaluable experience and insight into working in a corporate environment.
Many thanks to everyone at Ventolines, especially my company supervisor, Benjamin, for the excellent support and guidance that I received throughout the thesis period. He helped me integrate into the business world and took me to various on-site locations to see the work first-hand. The quality of his feedback significantly shaped the substance of this thesis report.

Finally, my deepest gratitude goes to my University supervisor, Mohamad, whose expertise and passion for high-voltage cables were a source of inspiration. His willingness to assist with my questions or doubts, even during late hours and weekends, was immensely valuable and deeply appreciated.

Bonne Bogaert
Delft, July 2024

Contents

List of Figures

List of Tables

Abbreviations

Abbreviation	Definition
IEC	International Electrotechnical Commission
NEN	Nederlands Normalisatie-instituut
FEM	Finite Element Method
BC	Boundary Conditions
TRS	Temperature Rise by Superposition
ODE	Ordinary Differential Equation
TB	Technical Brochure
API	Application Programming Interface
WPF	Windpark Fryslân
DTS	Distributed temperature sensing
XLPE	Cross-linked polyethylene
AC	Alternating current
DC	Direct current
MAE	Mean Absolute Error
RMSE	Root Mean Squared Error
atm	Standard atmosphere (unit)

Symbols

Symbol	Definition	Unit
I	Current/Ampacity	A
U	Voltage	V
P	Heat loss or power dissipated	W
θ	Temperature	°C
W_d	Dielectric loss	W/m
W_c	Conductor power loss	W/m
W_{sh}	Sheath power loss	W/m
W_a	Armor power loss	W/m
n	Conductor count	-
T_i	Thermal resistance of material in layer i	$\mathrm{K \cdot m/W}$
ρ_i	Thermal resistivity of material in layer i	$\mathrm{K \cdot m/W}$
R_C	Conductor resistance	Ω/m
λ_1	Sheath loss factor	-
λ_2	Armor loss factor	-
L_f	Load factor	-
d_i	Diameter beneath layer i	mm
t_i	Thickness of layer i	mm
D_i	is the external diameter of the insulation (excluding screen)	mm
d_c	is the diameter of the conductor, including the screen, if any	mm
d_x	Dielectric dividing diameter	mm
Q	Heat capacitance per unit length	$\mathrm{J/(K \cdot m)}$
A	Area of material	m^2
C_v	Volumetric heat capacity	$\mathrm{J/(K \cdot m^3)}$
D_{ex}	External diameter	mm
D_{in}	Internal diameter	mm
p_{soil}	Thermal resistivity of soil	$\mathrm{K \cdot m/W}$
p	Van Wormer coefficient for long duration transients	-
p^*	Van Wormer coefficient for short duration transients	-

Symbol	Definition	Unit
T_{env}	Ambient temperature	°C
L	Burial depth	mm
s	Laplace variable	-
$H(s)$	Transfer function	-
W_c	Conductor loss per meter cable	W/m
α	Thermal diffusivity	m^2/s
τ	Time constant	s
$\theta_m(t)$	is the temperature rise at node m at time t	°C
T_{mj}	is the coefficient from the thermal equivalent	-
P_j	is the time constant determined from the poles of the transfer function	s^{-1}
t	is the time from the beginning of the step	s
n	is the number of loops in the network	-
m	is the node index	-
$x_{(n-m)m}$	is the coefficient of the numerator equation of the transfer function	-
y_n	is the first coefficient from the denominator equation of the transfer function	-
Z_{km}	are the zeros of the transfer function	-
P_j, P_k	are the poles of the transfer function	-
ρ_{soil}	is the thermal resistivity of the soil	$K \cdot m/W$
$C_{v,soil}$	is the volumetric heat capacity of a unit volume of soil	$j/m^3 \cdot K$
d_{soil}	is the density of the soil	kg/m^3
$c_{p,soil}$	is the volumetric heat capacity of soil at constant pressure	$J/kg \cdot K$
d_w	is the density of water	kg/m^3
$c_{p,w}$	is the volumetric heat capacity of water	$J/kg \cdot K$
v_{soil}	is the moisture content of the soil	%
R_{20}	is the conductor resistance at 20 °C	Ω
$\rho_{c,20}$	is the conductor resistivity at 20 °C	Ωm
A_c	is the conductor area	m^2
α_{20}	is the temperature coefficient	1/K
θ_c	is the conductor temperature	°C
R_{AC}	is the AC resistance of the conductor at operating temperature per unit length	Ω/m
U_0	is the voltage to earth	V
C	is the capacitance per unit length of a cable	F/m
ω	= 2 π f, is the radial frequency	rad
$tan\delta$	is the loss factor of the insulation at power frequency and operating temperature	-
ϵ_0	is the permittivity of the vacuum	F/m
ϵ_r	is the relative permittivity of the insulation	-
C_{LL}	is the length correction factor for considering laying up cores	-
R_λ	Thermal resistivity of soil	K · m/W
λ_{sat}	thermal conductivity, saturated soil	$W/K \cdot m$
λ_{dry}	thermal conductivity, dry soil	$W/K \cdot m$
K_e	Kersten function	-
α	soil-specific factor	-
S_r	Degree of saturation	%
λ_s	thermal conductivity in solid soil components	$W/K \cdot m$
n	porosity	%
λ_w	thermal conductivity water	$W/K \cdot m$

Symbol	Definition	Unit
λ_q	thermal conductivity quartz fraction	$W/K \cdot m$
q	quartz fraction as mass percentage of dry soil	%
λ_0	thermal conductivity other minerals	$W/K \cdot m$
θ_0	is the initial temperature	°C
$W_{c,20}$	is the conductor loss at 20 °C	W/m
α_{20}	is the temperature coefficient	1/K
$SR(t)$	is the step response function	-
δ	is the thermal diffusivity of the medium	m^2/s
c	is the volumetric specific heat of the material	$J/K \cdot m^3$
W_{int}	is the heat generation rate in the cable	W/m
T_{max}	Maximum operating temperature	°C
λ_{soil}	Thermal conductivity of soil	W/(K · m)
k	Thermal conductivity	W/(K · m)
L_f	Length of buried cable	m
H	Conductivity matrix	-
Q	Capacity matrix	-
K	Heat generation vector	-
h_e	Element conductivity matrix	-
g_e	Element capacity matrix	-
k_e	Element heat generation vector	-
h	is the convective heat flux	$W/m^2 \cdot K$
k	is the thermal conductivity of air	$W/m \cdot K$
L	Characteristic length	m
T	Temperature of the surface	$^\circ C$
T_{ext}	External temperature	$^\circ C$
g	Acceleration due to gravity	m/s^2
β	Thermal expansion coefficient	$1/K$
ν	Kinematic viscosity of air	m^2/s
α	Thermal diffusivity of air	m^2/s
T_0	Average annual temperature	°C
ΔT	Maximum annual temperature variation from average	°C
D_h	Thermal diffusivity of soil	m^2/day
t	Number of days after coldest day	-
z	Depth of burial	m
ω	Angular frequency	$1/day$
z_0	Damping depth	m

1 Introduction

This thesis aims to develop and validate a model for dynamic cable rating that incorporates detailed weather and soil data to improve the accuracy and efficiency of temperature predictions for underground power cables. The validation is done by comparing the predicted temperature from the model with real measured cable temperature data.

This chapter first provides an introduction where the underlying background and motivation for the thesis are given. In addition, a scientific and overall contribution is given, and the problem definition and scope of the thesis are described.

The *Ampwise* tool, developed by the author, is an interface where a user can experiment with various scenarios to understand the thermal heating effects of the cables. The user can enter the various inputs (cable data, layout, soil info, load profile, etc.) and the Python-based server-side solves the numerical system with the Finite Element Method (FEM) and displays the results. The numerical model has been implemented with improvements in the weather and soil. The program is explained in Appendix A.

1.1. Background and Motivation

The integration of renewable energy sources into power grids has increased significantly in recent years, driven by the global desire to find sustainable and environmentally friendly energy solutions. This shift presents new challenges for the efficient and reliable operation of electrical power systems, especially in the thermal management of underground power cables. Renewable energy sources, such as wind and solar energy, are highly variable and introduce fluctuating load conditions that traditional static cable rating methods cannot adequately address.
These variable ratings are referred to in the literature as *dynamic*, *time-dependant*, or *real-time*. In this thesis, the term *dynamic rating* is used.

The existing electrical infrastructure was not designed for these variable energy sources. Consequently, power grids are becoming increasingly congested, with cables and overhead lines often approaching their design limits. This congestion forces wind and solar farms to curtail their output, meaning they must reduce or turn off power production to avoid overloading or unbalancing the grid. This not only leads to inefficiencies and financial losses, but also undermines the potential environmental benefits of renewable energy.
By improving the model, the real thermal limit can be increased. Accurate prediction and management of cable thermal limits are key to maximize the integration of renewable energy into the power grid, reducing congestion, and ensuring reliable delivery of clean energy.

To avoid excessive thermal aging due to operating temperatures exceeding their limits, the correct ampacity rating of power system components, such as power cables, is important. The ampacity is defined as the maximum current that can be carried without violating these limits.

The ampacity of power components is often set with static thermal limits based on conservative heat transfer assumptions, worst-case scenarios of ambient conditions, and maximum load factor. Until recently, these static ratings have been sufficient, as electricity production and consumption have been predictable and relatively stable. However, if this rating method is used for a dynamic source like wind or solar, it will be noticed that the cable does not get as hot as expected since the cable has time to cool down at periods of less power (for example, at night in a solar farm). This also means that the cable can be overloaded or that a smaller cable is used with a smaller cross-sectional area, which is less costly and uses fewer materials.

Furthermore, since a dynamic approach is used, different load profiles can be combined onto the same cable. For instance, a solar farm can be added to an existing wind farm, as the cable can transmit more power during sunny hours when the wind farm's output might be lower. This approach can optimize the use of existing infrastructure, reduce costs, and improve the overall efficiency of the power grid.

Dynamic cable rating systems, which adapt to environmental conditions and load variations, are essential to optimize cable capacity utilization. This allows for a reduction in safety margins, enabling more efficient use of existing infrastructure. However, this also increases the pressure on accurate thermal modeling to prevent overheating and ensure the reliability and longevity of the cables.

Accurate thermal modeling must consider several factors, including seasonal dependencies and ground temperature gradients, which significantly affect the thermal behavior of buried cables. In a real cable, various thermal and environmental effects include moisture migration, changing water levels, and soil drying out around the cable. Figure 1.1 shows an example of the cable temperature over a year (measured from a fiber optic cable in the power cable). There is a clear trend where the cable is hotter in the summer compared to winter because of seasonal effects. So, modeling this environmental behavior is crucial for an accurate dynamic thermal model.

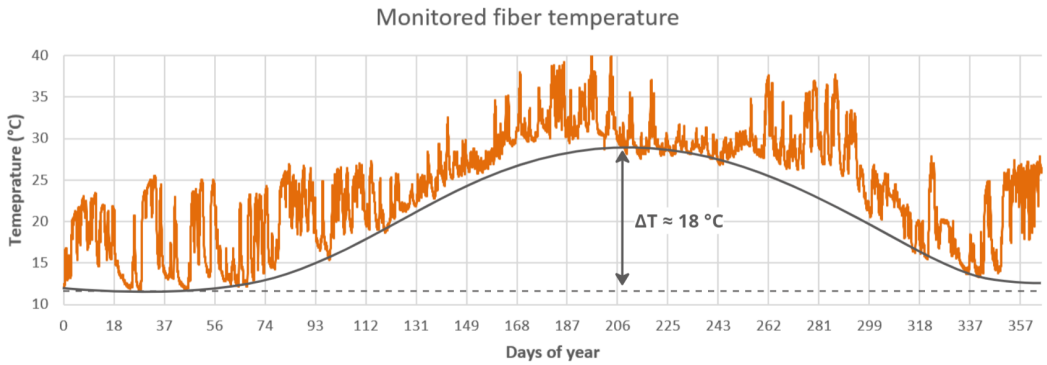

Figure 1.1: Fiber temperature trend over a year (data from Ventolines)

In this thesis, two improvements are proposed and tested for greater accuracy in the predicted temperature compared to the measured data.

- **Weather info**: This consists mainly of air temperature, air pressure, solar radiation, and precipitation. These all play a role in determining the temperature of the ground and cable. Furthermore, the air temperature changes the ground temperature with a certain convective heat flux, and depending on depth, the soil layers will all have a different temperature.
- **Soil info**: This consists of the division of the soil into different layers and assigning different parameters to these layers such as moisture content and thermal resistance. The water level and thermal resistance of the soil can play a big role in the cable temperature. The information can come from drillings of the ground that identifies these values.

By gaining a better understanding of the dynamics in the heating of the components of the power system, the utilization of the assets can be optimized. In this thesis, a model is developed to calculate the dynamic temperatures of underground power cables with incorporated weather data and detailed soil properties, which are compared with real-world measured cable data.

Contribution

The scientific contribution of this thesis lies in the development and validation of a model that integrates detailed environmental and weather data to improve the dynamic rating of underground cables. This model is compared with established benchmarks such as CIGRE and COMSOL to ensure its reliability and accuracy. Furthermore, the thesis introduces the *Ampwise* tool, a practical application designed to facilitate the implementation of these modeling techniques in real-world scenarios. By improving the accuracy of dynamic cable rating predictions, this research contributes to the overall efficiency and safety of the power distribution systems.

This thesis has been completed at the company **Ventolines**. They could greatly benefit from a cable calculation tool to check the thermal feasibility of new and existing cables to see if there is still space in the capacity of existing infrastructure. In addition, the monitored data of existing cables can be compared with the predicted temperature of the *Ampwise* tool, to verify and validate how accurate the prediction is and to perform an expansion analysis on the same cable with a new load profile to see if the cable will perform. This tool can be used in the development phase of a project, since all inputs can be known beforehand and the load profile can be extrapolated from the wind speed at the location. Furthermore, this tool can validate the dynamic prediction from other contractors and possibly even do the cable rating calculation in-house, which would be a great addition to the existing expertise of the company.

Furthermore, the *Ampwise* tool is also a cost-effective alternative to commercial cable rating tools, making advanced cable temperature predictions accessible without the need for in-depth knowledge of cable heating mechanisms or paid software. Users can simply input the required parameters, and the tool provides the results. *Ampwise* also offers educational insight by modeling and identifying hotspots and predicting future cable temperatures based on projected load profiles. It also provides valuable information on the temperatures of other critical components such as the cable sheath and the ground temperature rise. Contact the author to discuss accessing the *Ampwise* tool.

1.2. Scope and problem definition

From the developed thermal model, the main objective of the thesis is to illuminate these five research questions:

- **What is the most suitable technique for accurately modeling temperatures in underground power cables based on real measured data?**
- **How well does the chosen technique from this study compare with the established CIGRE and COMSOL models in predicting cable temperatures?**
- **How does the incorporation of dynamic weather data, as opposed to assuming a constant temperature, improve the accuracy of the predicted cable temperatures compared to monitored data?**
- **In what ways does the model improve when using detailed soil data, as opposed to assuming constant values compared to monitored data?**
- **How does the *Ampwise* tool, utilized in this study, improve the precision and usability of dynamic cable rating predictions for real-world applications?**

The Literature Review chapter 2 summarizes existing research and methodologies related to dynamic cable ratings, including IEC standards and various dynamic rating examples. The Thermal Modeling of Power Cables chapter 3 details the theoretical foundation and approaches to calculate the temperature variations within the conductors due to power transmission. Verification of the analytical and numerical thermal model chapter 5 verifies both models through comparisons with COMSOL, CIGRE TB 880, and measured data from the real world. Conclusions chapter 6 summarize the study findings, discussing improvements in cable temperature predictions and the effectiveness of the Ampwise tool. Finally, Further Work chapter 7 suggests potential areas for future research and development based on the results of the study. Appendix A covers the explanation of the user interface, cable crossings, and the Python, Matlab, and Javascript code of various parts.

2

Literature review of dynamic rating

An extensive literature review is conducted to provide an in-depth understanding of dynamic rating systems and their applications. This chapter introduces the concept of dynamic rating in power systems and examines various case studies that explore this approach. The review compiles and discusses collective knowledge, evolving interests, and ongoing research on the use of dynamic rating across power systems.

Dynamic rating systems have emerged as an important strategy for improving the efficiency and reliability of power systems. These systems, which are adaptive to real-time conditions, have been extensively studied and applied to various components of power systems, such as cables, overhead lines, and transformers. The literature reveals a broad spectrum of methodologies, ranging from the conventional International Electrotechnical Commission (IEC) standards to newer numerical methods, like the Finite Element Method (FEM), for evaluating and implementing dynamic ratings.

Dynamics ratings can be done to all parts of a power network: The transformers, switchgear, overhead lines, etc. [1] [2]. To limit the research in this thesis, the literature review has mainly focused on dynamic rating for underground cables. For the distribution grid, the Netherlands mostly uses underground cables to transport its electricity, which is an important part of the system to rate precisely.

In existing research, the emphasis on dynamic rating has mostly been directed toward overhead lines. The application of dynamic rating to underground cables presents additional complexities, largely attributed to the thermal properties of the soil, making it more challenging than its overhead counterparts. Consequently, most of the research dedicated to cable dynamic rating focuses on case studies and theoretical frameworks. Despite these challenges, a select number of grid operators have successfully implemented dynamic rating systems for underground cables, relying on direct temperature measurements [3].

2.1. IEC standards

Cable engineers have been using analytical solutions based on the original paper by Neher/McGrath(1957) [4] named *"The calculation of the temperature rise and load capability of cable systems"* or IEC Publication 60287 (1994) [5] for a long time. This method is based on standards such as IEC 60287 [5] [6] for steady-state calculations and IEC 60853 [7] [8] for dynamic, transient calculations.

- **Continuous calculations**, as outlined in the standard IEC 60287 offer a simplified approach, assuming steady-state conditions. The term "steady-state" means continuous constant current (100% load factor). This method is ideal for traditional power systems with minimal or predictable load variations. Covers aspects such as thermal resistance, cable laying configurations, and the influence of external conditions on cable performance. The standard is widely adopted for its efficiency in routine design and operational evaluations where conditions are relatively stable. It provides a reliable basis for cable sizing in more stable and predictable environments; it can be seen as a "worst case" scenario.

  The steady-state ampacity is calculated using Equation 2.1 from IEC 60287-1 [5]. Current **I** is proportional to a change in temperature $\mathbf{\Delta}\theta$ and various parameters of the cable ($T_1, T_2, T_3, W_d, n, R_C, \lambda_1, \lambda_2$, of Equation 2.1) and the environment (T_4, of Equation 2.1). This is inherently an approximation but can be found exceptionally useful for quite some practical cases where the current source remains relatively constant and the environment is relatively homogeneous. The steady-state method is a quick, easy, and widely used method of rating cables.

$$I = \sqrt{\frac{\Delta\theta - W_d[0.5T_1 + n(T_2 + T_3 + T_4)]}{R_C(T_1 + n(1 + \lambda_1)T_2 + n(1 + \lambda_1 + \lambda_2)(T_3 + L_f T_4))}} \tag{2.1}$$

- **Dynamic calculations**, like in the standard IEC 60853 are often used for systems with fluctuating load conditions (like renewables). This method considers the transient behavior of the cable under varying electrical loads and environmental conditions. It's particularly relevant where electrical demand varies significantly over time, such as in renewable energy systems affected by changing weather conditions. This approach is crucial for ensuring reliability in systems with non-constant load demands, providing a detailed and time-dependent analysis.
- **Numerical calculations**, as in the standard IEC 62095 from 2003. This standard makes a significant advancement in cable rating calculations by using the Finite Element Method (FEM) for more precise and dynamic calculations. This technical report acknowledges the limitations of traditional analytical models in capturing nuanced thermal interactions within complex cable environments. FEM offers a solution to these limitations by enabling detailed simulations of thermal and electrical phenomena, which are especially critical to accurately determine the dynamic ratings of underground cables.

The reason for including the steady-state current rating standard is that the thermal equivalent representation, boundary conditions, thermal resistivities, and losses calculated are the same for both rating methods and obtained from IEC 60287.

Rating of Power Cables by George J. Anders has been of great help in summarizing and describing common cable rating methods explained in standards and research in the field. It provides a comprehensive exploration of the electrical and thermal rating of power cables. The book delves into the physics of cable heating, methodologies for calculating cable capacity under both steady-state and transient conditions, and factors such as environmental conditions and cable configurations that influence cable performance. Advanced topics such as emergency ratings and the impact of load cycles on cable life are also discussed.

These standards are only theory, and in reality, the cables might give unexpected ampacities due to unforeseen parameters, often due to the non-homogeneous surrounding material (for an expanded view on this topic, read *"Rating of Electric Power Cables in Unfavorable Thermal Environment"* by J.Anders [9]).

2.2. Dynamic ratings

In the context of integrating renewable energy into power grids, dynamic cable ratings are essential. They adjust in real time to environmental conditions, optimizing cable capacity to handle the variable output. This section reviews key studies that have advanced our understanding and implementation of these ratings, crucial for maintaining grid reliability and efficiency amidst increasing renewable use.

The paper *Ampacity Calculation Method for Deeply Buried Wind Farm AC Submarine Export Cables* by Vree et al. [10] introduces a simplified dynamic ampacity calculation method for wind farm submarine export cables. This method calculates the cable capacity based on two load steps: a long-term average and a full-load scenario during peak wind farm output. A significant aspect of this method is the 10-year preloading phase, which represents the long-term average operational conditions and captures the thermal inertia of the soil surrounding the deep-buried cables. From this steady state temperature, it can be derived how much the wind farm can be overloaded until it reaches the maximal operational temperature. Furthermore, the researchers derived a current curve from the wind data as shown in Figure 2.1. This curve correlates the wind speed with the electrical current in the export cable, which accounts for the non-linear power output of the wind turbines. A load profile could be extracted from the wind speed at a location which can be used to predict the cable temperatures before there is a real cable on the ground.

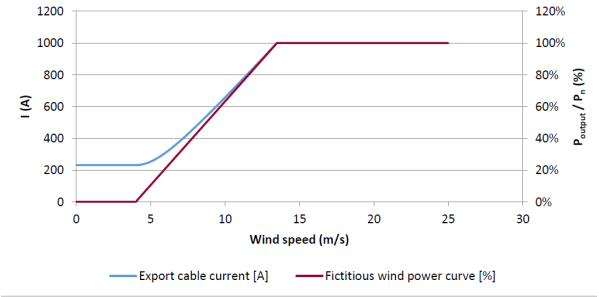

Figure 2.1: Power output and related export cable current plotted against the windspeed in [m/s] [10]

The paper *Cable Ampacity Calculations: A Comparison of Methods* by Bates [11] examines various analytical methods used to determine the ampacity of underground power cables. The paper covers traditional methods, including tabulated ampacities and the Neher–McGrath calculation procedure, and contrasts them with a recent method that considers the migration of moisture through the soil. The comparative study emphasizes the consequential risks associated with incorrect assumptions about the thermal resistivity and moisture content of the soil.

The paper *Dynamic Rating of Three-Core XLPE Submarine Cables Considering the Impact of Renewable Power Generation* by Nielsen et al. [12] delves into optimizing the selection of HVAC submarine cables during the design phase of projects, notably offshore wind farms. The paper leverages a thermal ladder network method (LNM) to assess thermal behavior within cables and presents a dynamic rating approach that iteratively combines static rating methods with thermal analysis of transient conditions. MATLAB simulations, validated against a Finite Element Method (FEM) benchmark, demonstrate the efficacy of the proposed method in modeling temperature transients in cable conductors, contributing to a more tailored and economically viable cable design process.

The study *Computer Method for the Calculation of the Response of Single-Core Cables to a Step Function Thermal Transient* presented by Gazzana-Priaroggia [13] introduces a computational model to analyze the thermal response of single-core power cables to transient thermal events. This model applies a superposition method that divides the cable and its surrounding environment into a series of elements, each with defined thermal resistance and capacitance. This division into finite elements allows for a detailed simulation of the flow of heat through the insulation of the cable and into the surrounding soil, capturing the dynamics of transient thermal behavior more accurately than traditional methods.

In the exploration of optimizing cable ampacity evaluation, the paper *New Approach to Ampacity Evaluation of Cables in Ducts Using Finite Element Technique* by Anders and Chaaban introduces a novel computational approach. This study enhances the understanding of thermal dynamics in cable systems, particularly those installed within ducts, by utilizing the finite element method to accurately model the nonuniform distribution of heat due to the cable's geometry and surrounding environment. Finite element analysis allows for a detailed investigation of thermal resistivity changes resulting from varying operational and environmental conditions, providing a more accurate assessment of cable performance in realistic scenarios. This method offers significant improvements over traditional ampacity calculation techniques, which often assume a uniform heat distribution and do not account for complex interactions between the cable and its environment showing the relevance of this paper.

The paper *Transient Thermal Response of Multiple Power Cables with Temperature-Dependent Losses* by Heinrich Brakelmann and George J. Anders [14] focuses on advancing the understanding of thermal behavior in multiple power cables under variable loading conditions. This study extends previously developed transient calculation methods for single cables to complex configurations involving multiple cables. By incorporating temperature-dependent power losses into their calculations, the authors provide a more accurate analytical solution for predicting the thermal response of cable systems during different loading scenarios. This approach helps in improving the design and safety protocols for power cable installations, ensuring that they operate within safe thermal limits under varying electrical loads and environmental conditions. The paper emphasizes the use of practical numerical examples to demonstrate the effectiveness of the proposed method and highlights its significance in real-world applications.

2.2.1. Finite Element Method

The paper *A 2-D Finite Element Mesh Generator for Thermal Analysis of Underground Power Cables*[15] presents an automatic program designed to create two-dimensional Finite Element (FE) grids. This tool is particularly adept at handling the unique geometrical challenges posed by underground cables and their associated thermal fields on nonuniform soil. The program simplifies the input data process and requires minimal user-defined parameters to control the generation of meshes. This includes specifications for circles, polygons, and the inclusion tree, ensuring well-shaped meshes and near-optimal FE solver performance.

The study titled *Development of a Web-Based User-Friendly Cable Ampacity Calculation Tool* presented by Eberg et al.[16] explores the advancement of cable ampacity calculation tools that integrate Finite Element Analysis (FEA) into a web-based platform. This tool aims to enhance the precision of ampacity assessments beyond traditional IEC 60287 standards, particularly for complex cable configurations found in critical power system applications such as mainland and wind farm connections. The research showcases comparisons between FEA simulations and empirical IEC calculations, emphasizing the tool's ability to handle diverse and intricate trench geometries with higher accuracy and flexibility. This paper shows the use of a web-based program to calculate numerical thermal ratings with FEM.

The study *Calculation of Cable Thermal Rating Using a Hybrid Method Based on IEC 60287 and Finite Element Method* by Aegerter [17] explores the integration of IEC standards with finite element analysis to optimize thermal rating calculations of power cables in complex configurations. The hybrid method combines the analytical approach of IEC 60287 with the detailed modeling capabilities of the finite element method (FEM), using the pyGIMLi software. This approach allows for a more accurate handling of nonhomogeneous soil conditions, multiple backfills, and intricate cable layouts that traditional methods may not adequately address. By calculating the external thermal resistances with FEM and integrating these with the analytical equations of the IEC, the method achieves a balance of computational efficiency and precision, offering a practical tool for modern cable design challenges.

The paper, *New Approach to Ampacity Evaluation of Cables in Ducts Using the Finite Element Technique*, by Anders and Chaaban [18], implemented a user-oriented suite of computer programs that utilize the finite element method. Addressing the challenge of accurately predicting cable ampacity in duct systems, the study introduces a novel model for non-uniform heat flux distribution within ducts, which contradicts the commonly used uniform heat distribution assumption. The research highlights the variation in heat flux along the duct's perimeter, with the maximum heat flux occurring at the top because of enhanced convection. This understanding is critical to designing more efficient cable systems in complex installations, as confirmed by laboratory experiments and field verifications.

The paper *Transient Heat Conduction Problems in Power Cables Solved by the Finite Element Method* by N. Flatabø [19] discusses the application of the finite element method (FEM) to solve transient heat conduction problems in power cables. This study specifically examines thermal transients in a 275 kV oil/paper-insulated buried power cable when subjected to time-varying load currents. Key highlights include the method's ability to handle complex geometries and discontinuities in material properties more effectively than traditional finite-difference methods. By modeling the dielectric loss, shield loss, and integrating changes in load current over time, the FEM provides a detailed thermal profile of the cable system. This approach not only improves the accuracy of thermal predictions under dynamic loading conditions but also supports the optimization of cable design for improved reliability and performance in power transmission systems.

2.2.2. Modeling the environment

The paper titled *An Improved Model for Predicting Soil Thermal Conductivity from Water Content at Room Temperature*[20], focuses on improving the precision of soil thermal conductivity (λ) models, which are essential for dynamic cable rating calculations. The authors introduce a new model that incorporates the volumetric water content (θ), the bulk density of the soil (ρ_b), and the sand fraction to predict λ in a wide range of moisture conditions. Among the many factors that influence the thermal conductivity λ, θ is the one that varies the most under field conditions. In situ monitoring of λ as a function of θ can represent a significant challenge. Consequently, much effort has been made to develop $\lambda(\theta)$ models based on easily measurable soil parameters. The study introduces an improved model that correlates thermal conductivity with volumetric water content, bulk density, and sand (or quartz) fraction. For sand, clay, and loam, the thermal resistivity can be calculated with the Horton model [20]:

$$R_\lambda = \frac{1}{(\lambda_{sat} - \lambda_{dry}) \cdot K_e + \lambda_{dry}} \tag{2.2}$$

$$K_e = \exp\left[\alpha \cdot \left(1 - S_r^{(\alpha - 1{,}33)}\right)\right] \tag{2.3}$$

$$\lambda_{sat} = \lambda_s^{(1-n)} \cdot \lambda_w^n \tag{2.4}$$

$$\lambda_s = \lambda_q^q \cdot \lambda_o^{(1-q)} \tag{2.5}$$

$$\lambda_{dry} = -0.56 \cdot n + 0.51 \tag{2.6}$$

where

R_λ	thermal resistivity ($K \cdot m/W$)
λ_{sat}	thermal conductivity, saturated soil ($W/K \cdot m$)
λ_{dry}	thermal conductivity, dry soil ($W/K \cdot m$)
K_e	Kersten function
α	soil-specific factor (0.27 or 0.96 for fine and coarse textured soils, respectively)
S_r	Degree of saturation (%)
λ_s	thermal conductivity in solid soil components ($W/K \cdot m$)
n	porosity
λ_w	thermal conductivity water (0.594 $W/K \cdot m$)
λ_q	thermal conductivity quartz fraction (7.7 $W/K \cdot m$)
q	quartz fraction as mass percentage of dry soil
λ_0	thermal conductivity other minerals (3 or 2 $W/K \cdot m$ for fine and coarse-textured soils, respectively)

This model is tested and validated against measured data from twelve different soil types, demonstrating substantial improvements over existing models such as Johansen (1975) and Côté & Konrad (2005), especially at lower water content. The findings are crucial because they provide a more reliable method for predicting the thermal behavior of the soils surrounding the buried cables, leading to better designed and safer power distribution systems. This paper is very relevant to this thesis since it explains a model to calculate the thermal resistivity from the drilling information, which can be used to model the environment more precisely.

2.3. Temperature monitoring of cables

In the real world, it is important to accurately determine the current-carrying capacity of cables for the safety and performance of the specific cable. This section therefore presents the most used temperature monitoring methods for power cables. Modern approaches to cable ampacity calculation often involve the use of temperature sensing technologies, which provide real-time data on cable conditions. This gives the option to compare with theoretical calculations.

Distributed Temperature Sensing (DTS) systems can continuously monitor the temperature along the entire length of a cable, offering a detailed picture of its thermal condition. This approach offers extensive and detailed insight into the cable's thermal profile, which is not possible with traditional point-based temperature measurements. By using optical fibers for temperature monitoring, hot spots and ampacity-limiting sections where dynamic thermal rating should be applied can easily be detected.

DTS operates using a fiber optic cable as a continuous temperature sensor. The process begins with a laser that emits light pulses into the optical fiber. As the light travels through the fiber, it interacts with the molecular structure of the glass, causing a small portion of the light to be scattered back towards the source. This backscattered light, known as the Raman signal, consists of two components: Stokes and anti-Stokes signals. The intensity of the anti-Stokes signal is temperature-dependent, allowing the system to measure temperature variations along the fiber. An optical splitter directs the backscattered light to a detector and signal-processing unit, which analyzes the signals and generates temperature data. The processed data are then displayed as a temperature profile over distance, providing a continuous temperature measurement along the entire length of the fiber. Figure 2.2 shows the workings of this process in a schematic diagram. DTS systems provide high temperature resolution, typically ranging from 0.1°C to 1°C. Furthermore, calibration is essential for DTS systems to maintain accuracy. It involves comparing the system's temperature readings with known standards to correct for any measurement deviations or drift over time. To calibrate, fixed coefficients are generally used to convert raw Stokes and anti-Stokes measurements into temperature values.

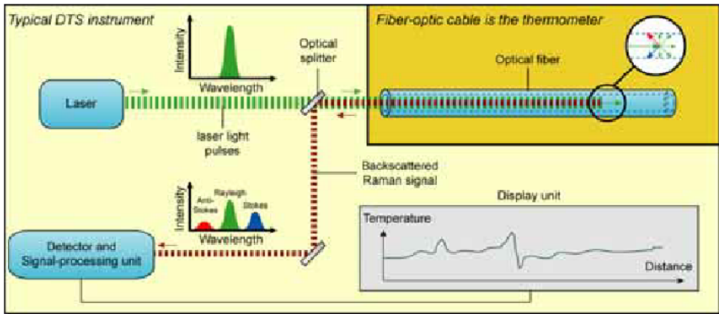

Figure 2.2: Diagram of a typical distributed-temperature-sensing system [21]

This data is crucial for implementing **Real-time thermal rating (RTTR)** systems, which dynamically adjust the ampacity of cables based on real-time temperature measurements. In addition, these systems can be configured with thresholds for maximum, minimum, and gradient temperatures, automated alarms, and protective actions when these thresholds are breached.
For insulated cables, the conductor temperature cannot be directly measured and must be calculated based on sheath temperature measurements, since the fiber optic cable is placed alongside the metal sheath. Some DTS systems can also measure current density, tilt angle, or sag [2].

The paper *Real-Time Monitoring and Dynamic Thermal Rating of Power Transmission Circuits* by Dale A. Douglass [1] discusses innovative approaches to optimizing the use of existing electrical infrastructure by implementing dynamic thermal ratings (DTR). The study highlights how real-time data from weather stations and electrical load measurements can replace traditional static thermal ratings with more flexible, condition-based ratings. Using sophisticated thermal models that adjust for real-time weather and load variations, utilities can improve the thermal capacity of power transmission equipment by 5% to 15%. This approach not only improves the reliability and efficiency of power systems, but also mitigates the need for extensive infrastructure upgrades, particularly beneficial in congested or

environmentally sensitive areas.

In practical applications, DTS systems are integrated into various infrastructure projects, including wind farms and underground power networks. For example, in the Windpark Fryslân (WPF) project [22], AP Sensing employed a DTS system to monitor the temperature of a single phase of the HV cables to the wind turbines, ensuring their safe and efficient operation [23]. EnergySolutions has a DTS system on the export cables to the mainland, which is 72 km long. For measuring export cables together with field cable strings [24], the same DTS equipment can be used at the same location.

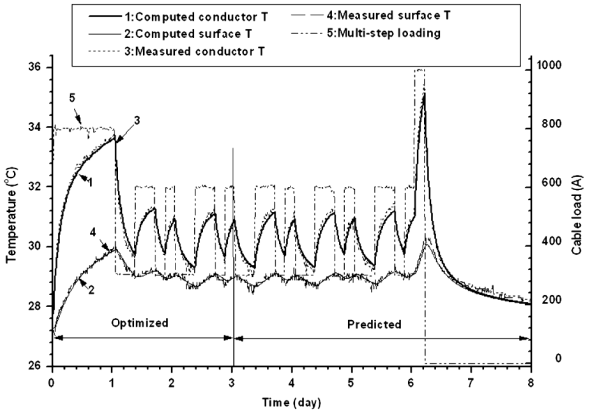

Figure 2.3: Measured and calculated cable surface and conductor temperature [25]

In the study conducted by Li [25], the potential of distributed temperature sensing (DTS) for the real-time evaluation of underground cable ratings. The paper delineates a methodical approach utilizing DTS data, which identify hot spots along the cable route and use them to evaluate the thermal parameters of the soil. An optimization procedure that combines finite element analysis with gradient-based optimization refines these parameters, which are then used to assess cable ratings under varying load conditions. This method provides a dynamic assessment tool that adapts to changing environmental factors, thereby improving operational reliability and cable load management. Figure 2.3 shows the measured and calculated cable surface temperature and conductor temperature when a multi-step load is applied for a period of eight days. This paper compares DTS data with the predicted temperature for a multi-step load and also uses the measured temperature to improve the predicted temperature.

2.4. Review of current dynamic cable rating programs

The market offers a variety of tools for calculating cable ampacity, each with distinct features fine-tuned to different project scales and requirements. Here is an overview of these tools:

- **Energy Solutions (ENSOL)** is an advisory agency dedicated to engineering and consulting. They conduct feasibility studies for renewable energy projects, mainly in The Netherlands. Their tool can also conduct dynamic cable ampacity calculations and loss calculations (see ENSOL report [26])
- **Twentsche Kabelfabriek (TKF)** is a cable manufacturer and they also are a popular option for conducting cable ampacity calculations and particularly relevant in the context of large-scale electrical engineering projects (see [27], [28], [29], [30], and [31]).
- **CYMCAP** is a dedicated software tool for performing cable ampacity and thermal analysis. Mostly for the capacity of underground and submarine cables (used by DNV).
- **COMSOL Multiphysics** is a powerful simulation software widely used in various scientific and engineering disciplines. Its core strength lies in its ability to perform advanced Finite Element Analysis (FEA) across multiple physics domains, thus it is not constrained to standards or fixed formats. In addition, COMSOL enables users to create custom applications based on their models.
- **Cable Pro Web** is a web-based cable sizing tool that allows quick calculations of cable sizes and ampacity based on user-defined parameters and also offers a free tool which is a basic version of the paid tool.
- **PowerFactory** is an advanced DIgSILENT tool that offers a variety of simulation capabilities, including the assessment of cable performance under various load conditions.

Chapter conclusion

Dynamic rating systems for power cables have become crucial tools in enhancing the efficiency and reliability of power transmission networks. This comprehensive literature review has explored various methodologies and case studies related to dynamic rating, focusing primarily on underground cables and their unique challenges.

The review highlighted the evolution from traditional steady-state methods prescribed by standards such as IEC 60287 to more advanced techniques such as dynamic and numerical calculations utilizing Finite Element Method (FEM). These advances are essential to accurately predict cable ampacity under varying load and environmental conditions, particularly critical for integrating renewable energy sources.

Key studies showcased the application of dynamic rating in real-world scenarios, such as wind farm export cables and offshore installations. Furthermore, temperature monitoring technologies, notably Distributed Temperature Sensing (DTS), were discussed for their role in enabling real-time thermal rating systems. These systems provide continuous temperature monitoring along cables, facilitating dynamic adjustments in ampacity based on actual environmental conditions, thereby improving operational safety and efficiency.

In general, this review underscores the importance of ongoing research and technological advancements in dynamic rating systems, providing insights into future directions to optimize power cable performance in modern electrical grids.

3

Thermal modeling of power cables

In this chapter, we present the theoretical foundation for calculating the variation of the temperature within a conductor due to the power transmitted through the cable. As the energy sector transitions towards more dynamic sources, such as wind and solar power, accurately modeling the variability in current becomes crucial. These variations significantly affect the conductor's temperature, marking a departure from the traditional steady-state ratings that assume constant power.

The goal of precise cable modeling is to improve the reliability and efficiency of power transmission systems. By understanding and predicting the thermal behavior of cables under various load conditions, we can optimize their design and operation, thus extending their useful life and reducing the risk of failure.

The approaches to modeling the thermal behavior of power cables can be broadly categorized into two methods: analytical and numerical.

1. **The Analytical Method**: This approach uses a ladder network for its simplicity and straightforward implementation, effectively substituting the cable with an electrical analogy for easy analysis. The temperature is calculated using equations that are evaluated at each time step.
2. **The Numerical Method**: This method applies finite element modeling (FEM), segmenting the domain into small elements. This granularity enables temperature modeling in more specific scenarios, accommodating complex situations with greater precision. The temperature is calculated using an Ordinary Differential Equation (ODE) involving matrices.

These methods are detailed and evaluated in various scenarios. Analytical methods facilitate the derivation of current rating equations in a closed form, offering a more direct solution. In contrast, numerical methods rely on iterative solutions to determine cable ampacity, offering enhanced flexibility and the ability to simulate complex cable configurations and more accurate boundary conditions.

To accurately model the thermal model of a power cable, it is crucial to understand the different mechanisms how heat is transferred. There are three main methods of heat transfer: conduction, convection, and radiation.
Conduction is the transfer of heat through a material via direct contact, without involving the movement of the substance itself. In the context of cables, conduction serves as the primary mode of heat transfer, with the surrounding environment influencing more than 70% of the total heat accumulated within the cable conductor.
Convection involves heat transfer through the physical movement of a fluid, which can be either a liquid or a gas. In a thermal model, a convective layer exists at the cable's surface where heat can be exchanged with the surrounding air.
Finally, **Radiation** is heat generated from electromagnetic waves such as the Sun and can be included in the model as a heat flux on a boundary like solar radiation.

3.1. Method 1: Analytical approach, superposition principle

The analytical approach, in which the cable is converted to an RC ladder network, provides a straightforward and computationally efficient means to approximate temperature profiles under steady-state and transient conditions. This method, leveraging the concept of thermal resistance and capacitance networks, offers a clear visualization of the heat flow paths and facilitates the identification of critical thermal bottlenecks within the cable system.

It is a quick and often accurate approximation for dynamic situations, which makes it especially useful for incorporating load profiles. Due to its speed and widespread use, this method is included in the thesis to provide a reliable and efficient method for initial assessments and temperature predictions in dynamic cable rating scenarios.

3.1.1. Ladder network representation of a power cable

The analysis of heat conduction in power cables leverages the fundamental similarity between thermal and electrical flow. Specifically, the movement of heat, driven by temperature differences between the current-carrying conductor and its environment, mirrors the flow of electrical current induced by potential differences. This analogy defines temperatures as analogous to voltages and heat flows to electrical currents, as highlighted by Anders [32]. Like an electrical RC circuit where the voltage at a certain node is required, with the thermal RC network, the temperature at a certain node is calculated. By segmenting the cable into discrete volumes characterized by their thermal resistance and heat capacitance, a lumped parameter method is used to solve the differential equations in the heat conduction problem.

For a steady-state scenario, it is presumed enough time has passed so there are only thermal resistances in series and no thermal capacitances.
To build a ladder network, the cable is considered to extend up to the inner surface of the soil for buried cables. Thermal capacitances that are placed in parallel can be summed up just like the electrical analogy.

Whether the thermal transient is long or short depends on the cable construction. For transient rating computations, long-duration transients are those that last longer than $\frac{1}{3}\sum T \cdot \sum Q$ where $\sum T$ and $\sum Q$ are the total thermal resistance and capacitance of the internal cable, respectively. The derivations of T and Q are discussed below. Short-duration transients usually last between 10 min and 1 hour [32].

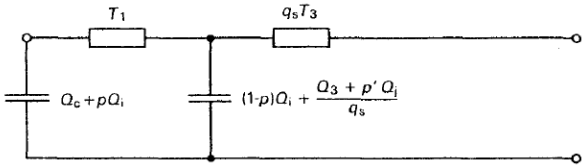

Figure 3.1: Equivalent cable network for long transient response calculations [8]

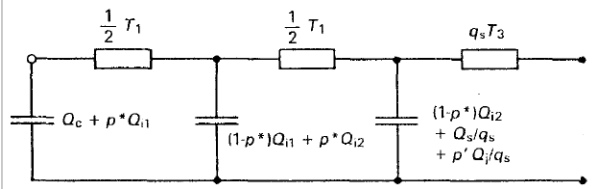

Figure 3.2: Equivalent cable network for short transient response calculations [8]

Figure 3.1 and Figure 3.2 show the equivalent circuit for a typical cable for long and short transients respectively. The thermal resistances of the insulation T_1 and the outer sheath T_3 are placed in series, and the thermal capacitances of all the layers are placed in parallel with each other at the correct location. The total thermal capacity of a dielectric is divided between the inner and outer diameters.

For short transients, the dielectric is divided into two parts with equal thermal resistance, divided at point $d_x = \sqrt{d_c \cdot D_i}$, utilizing the adjusted Van Wormer equation (Equation 3.6) [32].

To account for the presence of sheath/armor losses, the thermal resistance beyond the metallic layer must be multiplied, and the thermal capacitance must be divided by the ratio of the losses in the conductor and the metallic layer to the conductor losses. The sheath losses are represented as the loss factor multiplied times the conductor losses, as explained in IEC 60287-1 [5].

3.1.2. Thermal resistance of the cable parts and surrounding soil

All non-conductive materials in the cable will impede heat flow away from the cable as a result of their thermal resistance. By taking advantage of the circular geometry of the cable layers, the thermal resistance of these parts may be calculated. For all cylindrical parts of a single-core cable, the thermal resistance per unit length is calculated from Equation 3.1 [5]. The index i can be 1, 2, or 3 referring to the insulation, metallic screen, and sheath, respectively. However, the thermal resistance of metallic layers can be neglected in rating computations due to the low thermal resistivity [5].

$$T_i = \frac{\rho_i}{2\pi} \ln\left(1 + \frac{2t_i}{d_i}\right) \tag{3.1}$$

where

T_i	is the thermal resistance of the material ($W/K \cdot m$)
ρ_i	is the thermal resistivity of the material in layer i (K·m/W)
d_i	is the diameter below the layer i (mm)
t_i	is the thickness of layer i (mm)

The ampacity rating of cables is significantly influenced by the thermal resistance of the surrounding environment. For buried cables, this resistance accounts for more than 70% of the increase in conductor temperature. For air-insulated cables, this resistance predominantly affects the conductor temperature, primarily through natural or forced convection [9].
Soil has a higher thermal resistance and less efficient heat dissipation compared to other media such as air. The heat generated by the buried cables must travel through the dense, less conductive soil, causing a significant temperature rise. In contrast, air provides better convective cooling, allowing heat to dissipate more effectively.

When a cable cannot get rid of heat anymore, it can damage the insulation, increase the risk of electrical failures such as short circuits, and accelerate aging of components. Safety hazards, including fire risks, may arise in flammable environments.

For directly buried cables laying in a uniform soil where the depth of burial is much greater than the diameter of the cable, a short form of the Kennelly formula (Equation 3.2) can be used to calculate the thermal resistance of the soil [32]. To improve the heat dissipation underground, the cables are often laid in a backfill, a material of known and often lower thermal resistivity.

$$T_4 = \frac{\rho_{soil}}{2\pi} \ln\left(\frac{4L}{D_{ex}}\right) \tag{3.2}$$

where

ρ_{soil}	is the thermal resistivity of the material around the cable (K·m/W)
L	Cable burial depth (mm)
D_{ex}	is the external diameter of the cable (mm)
T_4	is the thermal resistance of the soil

3.1.3. Thermal capacitance of the cable parts

For addressing dynamic cable rating challenges, it's important to factor in the material's thermal storage capacity. The lumped capacitance method is utilized for the analytical resolution of heat equations

relevant to cable rating calculations. The heat capacitance per unit length for a material is expressed as shown in Equation 3.3, following Anders [32].

$$Q = A \cdot C_v \tag{3.3}$$

where

Q	is the heat capacitance of a material (J/K ·m)
A	Area of a material (m^2)
C_v	is the volumetric heat capacity of a material (J/K ·m^3)

The heat capacitance for a concentric configuration, such as the cable insulation and outer sheath, is established from Equation 3.4.

$$Q = \frac{\pi}{4}(D_{ex}^{*2} - D_{in}^{*2}) \cdot C_v \tag{3.4}$$

Where D_{in} and D_{ex} are the internal diameter and external diameter, respectively.

However, for insulation materials and other dielectrics, the heat capacity does not linearly correlate with thickness, and the thermal capacitance is not uniformly distributed between the inner and outer diameters. To enhance the precision of the lumped parameter model, Van Wormer devised a strategy for apportioning the heat capacity between the conductor and the screen. The heat capacity of the dielectric is divided into a portion pQ_{in} placed at the inner diameter D_{in} and a portion $(1 - pQ_{ex})$ at the external diameter D_{ex}, where p is the Van Wormer Coefficient for long duration transients and p^* for short duration transients given by [32]:

$$p = \frac{1}{2\ln\left(\frac{D_{ex}}{D_{in}}\right)} - \frac{1}{\left(\frac{D_{ex}}{D_{in}}\right)^2 - 1} \tag{3.5}$$

$$p^* = \frac{1}{\ln\left(\frac{D_{ex}}{D_{in}}\right)} - \frac{1}{\left(\frac{D_{ex}}{D_{in}}\right) - 1} \tag{3.6}$$

An assumption made in the derivation of the van Wormer coefficient is that the temperature distribution in the dielectric follows a steady-state logarithmic distribution for the period of the transient and that it can be equally divided between the conductor and sheath. However, a steady-state temperature distribution was assumed even for transient conditions in IEC 60853 [7]. This can bring errors and inaccuracies to the cable dynamic thermal rating, especially for the short transient.

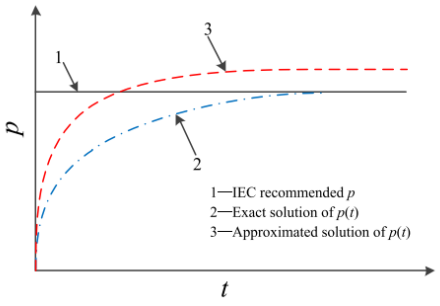

Figure 3.3: Comparison of constant and dynamic Van Wormer coefficient [33]

It can be observed from Figure 3.3 that before the cable reaches a steady state, the recommended IEC p and the approximate solution of p(t) are larger than the exact solution of p(t). A larger p means that more thermal capacitance of insulation is assigned to the conductor [33]. The blue line is the exact solution, and the black line is what is used in the equations.

Therefore, adopting either the recommended IEC solution p or the approximate solution of p(t) will bring a negative error to the dynamic temperature evaluation of the cable. Especially for the IEC

recommended p, at the early stage of cable temperature rise, an error will be expected due to the large difference in p in terms of the exact solution.

3.1.4. Transient cable conditions

To calculate the total temperature rise of a cable, the IEC standard [8] divides the temperature rise into one portion caused by the internal parts of the cable and one portion caused by the surrounding (soil). The rise in temperature due to internal parts is modeled based on the thermal equivalent such as Figure 3.1 or Figure 3.2, while the rise in temperature due to the environment of the cable can be evaluated by representing the cable as a line source in an infinite homogeneous medium [34]. The sum of these individually calculated responses is the total temperature rise of the cable above ambient.

Temperature rise in the internal parts of the cable

To analyze the linear network within a ladder framework, it is essential to derive the expression for the response function, which represents the temperature rise above the cable surface in response to a forcing function (the heat loss from the conductor). The determination of the response function is accomplished using the transfer function (Equation 3.7) of the thermal equivalent. The transfer function can be solved for all loops of the ladder network, thus calculating the temperature at any part (node) of the cable. The polynomials Y(s) and X(s) depend on the number of loops in the network [32]. The transfer function for the conductor node (θ_c) of the network is given by Equation 3.8.

$$H(s) = \frac{Y(s)}{X(s)} \tag{3.7}$$

$$H_c(s) = \frac{\theta_c}{W_c} = Z_{tot} \tag{3.8}$$

In which Z_{tot} is the impedance "downstream" of the conductor node, which equals the total impedance of the network:

$$Z_{tot} = \cfrac{1}{s\Omega_\alpha + \cfrac{1}{T_\alpha + \cfrac{1}{s\Omega_\beta + \cfrac{1}{T_\beta + \cfrac{}{\cdots + \cfrac{1}{s\Omega_v + \frac{1}{T_v}}}}}}} \tag{3.9}$$

The Laplace transform of the ladder network of the thermal impedance of the circuit $T_\alpha Q_\alpha$ to $T_v Q_v$ is given by Equation 3.8 and Equation 3.9. Furthermore, by solving the complex fraction of Equation 3.9, to only one simplified numerator and denominator, the root coefficients can be seen when all orders of s are grouped, and the poles and zeros can be calculated relatively easily by setting the denominator/nominator to zero and solving for s.

The time response may calculate the temperature of each node in the network obtained by the transfer function as in Equation 3.10 [32].

$$\theta_m(t) = W_c \sum_{j=1}^{n} T_{mj}(1 - e^{P_j t}) \tag{3.10}$$

where
Further, the coefficients T_{mj} are obtained from the poles and zeros of the transfer function. The coefficients are given by Equation 3.11 [32].

$$T_{mj} = -\frac{x_{(n-m)m}}{y_n} \frac{\prod_{k=1}^{n-m}(Z_{km} - P_j)}{P_j \prod_{k=1,k\neq j}^{n}(P_k - P_j)} \tag{3.11}$$

where

$\theta_m(t)$	is the temperature rise at node m at time t (°C)
W_c	is the conductor loss per meter cable (W/m)
T_{mj}	is the coefficient from the thermal equivalent (see Equation 3.11)
P_j	$= -\frac{1}{\tau}$, is the time constant determined from the poles of the transfer function (s^{-1})
t	is the time from the beginning of the step (s)
n	is the number of loops in the network
m	is the node index

$x_{(n-m)m}$	is the coefficient of the numerator equation of the transfer function
y_n	is the first coefficient from the denominator equation of the transfer function
Z_{km}	are the zeros of the transfer function
P_j, P_k	are the poles of the transfer function

Cable environment impact on the temperature rise

The Kennelly hypothesis, which suggests that the earth's surface is an isotherm, serves as a foundation for calculating the temperature rise attributable to the surroundings. Using this assumption in conjunction with representing the cable as a line source in an infinite homogeneous medium, the resulting temperature increase due to environmental factors can be determined using Equation 3.12 [34]. This approach also operates under the assumption that the earth's surface maintains a constant temperature. Practically, cables are typically buried at depths approximately ten times their external diameter, and given the range of temperatures these cables typically encounter, treating the earth as an isothermal entity is a valid approximation.

$$\theta_e(t) = W_c \frac{\rho_{soil}}{4\pi}\left[-Ei\left(-\frac{D_{ex}^2}{16\delta t}\right) + Ei\left(-\frac{L^2}{\delta t}\right)\right] \tag{3.12}$$

Where ρ_{soil} and δ are the thermal resistivity and the diffusivity of the soil, respectively, while the parameters L and D_{ex} are described earlier in subsection 3.1.2. Popular mathematical computer programs often have a built-in function to calculate the exponential integral.

The diffusivity (δ) of soil, which influences the efficiency of heat transfer, varies with factors such as density, moisture content, and thermal resistivity. It is an indicator of the rate at which a temperature change will be transmitted through the soil by conduction. When the thermal diffusivity is high, temperature changes are transmitted rapidly. Often, the exact diffusivity of the soil is not known precisely, and a general approximation of $5 \cdot 10^{-7} m^2/s$ is often used. This value is based on the moisture content of 7% and a soil thermal permittivity of 1 $K \cdot m/W$ [32]. However, if the density, heat capacity, and thermal permittivity of a material are known, the diffusivity may be calculated from Equation 3.13 [35].

$$\delta = \frac{1}{\rho_{soil} d_{soil} c_{p,soil}} = \frac{1}{\rho_{soil} C_{v,soil}} \tag{3.13}$$

$$C_{v,soil} = d_{soil} c_{p,soil} + d_w c_{p,w} v_{soil} \tag{3.14}$$

where

ρ_{soil}	is the thermal resistivity of the soil ($K \cdot m/W$)
$C_{v,soil}$	is the volumetric heat capacity of a unit volume of soil ($j/m^3 \cdot K$)
d_{soil}	is the density of the soil (kg/m^3)
$c_{p,soil}$	is the volumetric heat capacity of soil at constant pressure ($J/kg \cdot K$)
d_w	is the density of water (kg/m^3)
$c_{p,w}$	is the volumetric heat capacity of water ($J/kg \cdot K$)
v_{soil}	is the moisture content of the soil (%)

The volumetric heat capacity of a unit volume of soil $C_{v,soil} = d_{soil} \cdot C_{p,soil}$ is the amount of energy required to raise the temperature of a unit volume of soil by one degree. Unlike thermal conductivity, the volumetric heat capacity increases strictly linearly as soil water content increases.

Densities, specific heat capacities, and thermal resistivities for common materials can be found on the website engineeringtoolbox.com [36]

Total temperature rise

The total temperature rise of the cable above ambient is a combination of the temperature rise in the internal parts of the cable and the temperature rise caused by the surroundings, given by:

$$\theta(t) = \theta_m(t) + \alpha(t) \cdot \theta_e(t) + \theta_d(t) \tag{3.15}$$

In which $\theta_m(t)$ and $\theta_e(t)$ are described in subsection 3.1.4 and Table 3.1.4, respectively and $\alpha(t)$ is the attainment factor for the transient temperature rise between the cable and its surroundings.

The attainment factor is used to take into account the heat developed in the cable during the early parts of a transient, as the effect of the increase in environmental temperature is not felt immediately [32]. The attainment factor can be described as the temperature rise across the cable at time t divided by the steady-state temperature rise across the cable.

$$\alpha(t) = \frac{\theta_c(t)}{W_c T_{tot}} \tag{3.16}$$

$\theta_d(t)$ is the heat generated due to dielectric losses if the cable is energized before t = 0, given by:

$$\theta_d(t) = W_d[\frac{1}{2}T_1 + n(T2 + T3 + T4)] \tag{3.17}$$

In Equation 3.17, it is assumed that half of the dielectric loss is produced by the conductor and the other half by the sheath. W_d is the dielectric loss and n is the number of internal conductors.

For the total temperature rise, the presence of other heat sources can also be modeled and also has a significant impact on the development of heat in the conductor [32].

The losses inside a cable

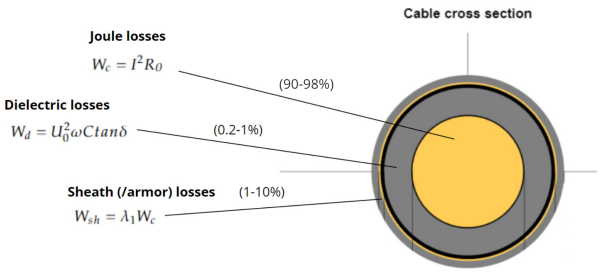

Figure 3.4: Cable losses and their share of total losses

Figure 3.4 shows an example cable with the major losses in a cable, with their respective share of total losses. The losses are dependant on several factors such as cable formation, grounding, material, etc. The biggest losses can be avoided by reducing the current or the resistance in the Joule losses (1).

1. **Temperature dependant resistance of the conductor**: The electrical resistance of the metallic parts of the cable changes with temperature, which in turn will affect total heat loss. Therefore, these changes should be taken into account when computing conductor losses. The following equation is used to calculate the temperature-dependent conductor loss [32]:

$$W_c = I^2 R_{AC} \tag{3.18}$$

In which I is the cable load carrying current and R_{AC} is the temperature-dependent conductor AC resistance per meter cable.

To calculate the AC resistance, the skin effect y_s, and proximity factor y_p needs to be determined, see IEC 60287 [5]. The AC resistance per unit length of the cable at its operating temperature is given in Equation 3.20. In the case of pipe-type cables, the AC resistance can be calculated with Equation 3.21.

$$R_\theta = R_{20}[1 + \alpha_{20}(\theta_c - 20)] \quad [\Omega/\mathrm{m}] \tag{3.19}$$

$$R_{AC} = R_\theta(1 + y_s + y_p) \tag{3.20}$$

$$R_{AC} = R_\theta[1 + 1.5(y_s + y_p)] \tag{3.21}$$

where

R_{20} $= \rho_{c,20}/A_c$ is the conductor resistance at 20 °C (Ω)
$\rho_{c,20}$ is the conductor resistivity at 20 °C (Ωm)
A_c is the conductor area (m^2)
α_{20} is the temperature coefficient (1/K)
θ_c is the conductor temperature (°C)
R_{AC} is the AC resistance of the conductor at operating temperature per unit length (Ω/m)

2. **Dielectric losses (only for AC)**: W_d is the heat dissipation factor/dielectric loss of the cable, which depends on the type of insulation and the construction of the cable. The dielectric loss is voltage-dependent and becomes significant only at voltage levels corresponding to the insulation material being used (for example: 63,5 kV for XLPE insulated cables). It is not necessary to calculate the dielectric loss for unscreened, multicore, or DC cables.

   The dielectric loss per unit length of the cable in each phase is given by Equation 3.22. The capacitance of cylindrical screens around circular conductors is given by Equation 3.23.

$$W_d = U_0^2 \omega C tan\delta \tag{3.22}$$

$$C = \frac{2\pi\epsilon_0\epsilon_r}{\ln(D_i/d_c)} C_{LL} \tag{3.23}$$

U_0 is the voltage to earth (V), $U_0 = U_n/\sqrt{3}$ for trefoil formation.
C is the capacitance per unit length of a cable (F/m)
ω $= 2\ \pi$ f, is the radial frequency (rad)
$tan\delta$ is the loss factor of the insulation at power frequency and operating temperature (given in IEC60287-1:2023 Table 3 [5])
ϵ_0 is the permittivity of the vacuum $\simeq 8,85410^{-12}$ (F/m)
ϵ_r is the relative permittivity of the insulation
D_i is the external diameter of the insulation (excluding screen) (mm)
d_c is the diameter of the conductor, including the screen, if any (mm)
C_{LL} is the length correction factor for considering laying up cores (the calculation is given in IEC60287-1:2023 Annex A [5])

3. **Loss factor for the metal sheath**: There is a certain loss in the sheath due to the circulating current that is lost from the conductor or the skin effect inside. Power loss in the sheath or screen (λ_1) consists of losses caused by circulating currents (λ_1') and eddy currents (λ_1'') as seen in Equation 3.25 from IEC 60287-1 [5]. This λ_1 is multiplied times the Joule losses to get the sheath losses.

$$W_{sh} = \lambda_1 W_c \quad (3.24) \qquad \lambda_1 = \lambda_1' + \lambda_1'' \quad (3.25)$$

The loss of circulating current (λ_1') is zero for installations where the sheaths are single-point bonded or cross-bonded and each major section is divided into three electrically identical minor sections.

Eddy currents generate resistive losses that transform some forms of energy, such as kinetic energy, into heat.

The change in conductor resistance with temperature during the transient result in the conductor losses being variable over time. Since the temperature depends on the conductor resistance and the resistance depends on the temperature in a cyclic manner, several iterations of the equations need to be performed to get satisfactory results or the temperature of the previous calculation needs to be taken, if any. Another approach is to use the Goldenberg equation. Allowance for the variation of the conductor loss with temperature gives the corrected temperature increase [37].

$$\theta_a(t) = \frac{\theta(t)}{1 + a[\theta(\infty) - \theta(t)]} \quad (3.26)$$

where $\theta(t)$ is the increase in the transient conductor temperature above ambient without correction for the variation in conductor loss, based on the conductor loss at the end of the transient. $\theta(\infty)$ is the increase in the steady state conductor temperature above ambient. a is the temperature coefficient of electrical resistivity of the conductor material at the beginning of the transient. $a = 1/[\beta + \theta(0)]$ with β being the reciprocal of the temperature coefficient at 0 °C and $\theta(0)$ is the starting transient temperature.

Transient temperature rise under variable loading (superposition principle)
The previously described equations are valid for a single step-current as input (constant current). To perform calculations for variable loading, a load curve must be divided into N current/power steps of constant magnitude (Δt). Using the superposition principle, the final temperature rise, as a function of time, can be calculated [32]. Figure 3.5 illustrates the principle of superposition and the temperature rise due to a two-step current (one step up and one step down).

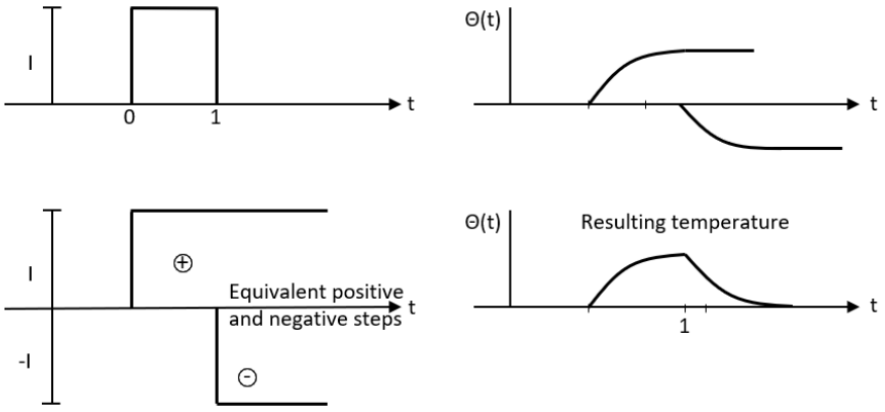

Figure 3.5: Illustration of the principle of superposition to calculate the resulting temperature rise due to a two-step current (one step up and one step down)

It can be seen from Figure 3.5 that the total temperature rise due to a multi-step current load is obtained by adding the movements of temperature towards a hypothetical steady-state temperature for all current steps. Mathematically, the total temperature increase can be modeled in terms of a summation of exponential expressions that describe the transient temperature rise caused by a step current change [32].

The Goldenberg formula works well for a single-step function. However, when we deal with the usual daily load variations with multiple load steps, the application of Equation 3.26 encounters difficulties because it requires a steady state temperature when a particular step load is applied. Another approach would be to iterate at each time step adjusting the electrical resistances to the temperature at the end of the step and going back to the beginning of the step with the new values. This process works well for simple systems, but can become cumbersome for multiple cable circuits considered together with complex load shapes [14].

The exact solution means that the response to each step must be adapted non-linearly to the magnitude of the loss step, and the superposition of different loss steps cannot be performed [14]. As an answer to this problem, G. J. Anders proposed the following equation:

$$\theta(t) = \theta_0 + W_{c,20}[c_{20} + \alpha_{20}\theta(t)]SR(t) = \theta_0 + \frac{W_{c,20}}{1 - \alpha_{20}W_{c,20}\theta(t)}SR(t) \tag{3.27}$$

where

θ_0	is the initial temperature (°C)
$W_{c,20}$	is the conductor loss at 20 °C (W/m)
c_{20}	$= 1 - \alpha_{20} \cdot 20$
α_{20}	is the temperature coefficient (1/K)
$SR(t)$	is the step response function $SR(t) = T(1 - e^{-t/\tau})$

This approximation has the advantage that the unmodified step response SR(t) of the system can be used. In the initial phase as well as in the final phase of the step response, which means that the initial (θ_0) and steady state (θ_∞) values are computed exactly. Additionally, the transient temperature is approximated on the safe side with sufficient accuracy and the peak deviation is present in the steep rise of the step response, so in the short transient.

The temperature dependence of the losses at time t leads to the following:

$$\theta(t) = \theta_0 + \frac{c_{20} + \alpha_{20}\theta_0}{1 - \alpha_{20}TRS(t)}TRS(t) \tag{3.28}$$

with the abbreviation TRS meaning *Temperature Rise by Superposition* with $t_i < t$. Any instant of time can be described as $t = i\Delta t$, $(i = 0, ..., N)$.

Starting with i = 0 and $\theta_c = \theta_0 = \theta_{amb} + \Delta\theta_d$, we consider the loss step $W_{c,20,i}$ by superimposing the thermal response on the existing TRS; that is, for all the following instants of time j the new values of the sum TRS in Equation 3.28 are computed as:

$$TRS^{new}(j) = TRS^{old}(j) + W_{c20,i}SR(j - i); \quad j = i + 1, ..., N \tag{3.29}$$

At all the following points in time i we have to execute two measures:
Verify any change in current and its associated losses $W_{c20,i}$. For computational efficiency, it's important to utilize only the previously computed and stored values of step responses, ensuring minimal computational effort.

1. Verify any change in current and its associated losses $W_{c20,i}$. For computational efficiency, it's important to utilize only the previously computed and stored values of step responses, ensuring minimal computational effort.
2. Compute the conductor temperature at time j using Equation 3.28.

This approach provides an algorithm for calculating the time-dependent temperature rise in cables due to current steps. It relies on the superposition of the step responses, which are derived from the system's predefined linear, temperature-independent step response SR(t) of the system [14].

Resulting calculation algorithm

To give an overview of the order in which the temperature increase calculations are performed in the algorithm developed, the resulting workflow chart can be seen in Figure 3.6.

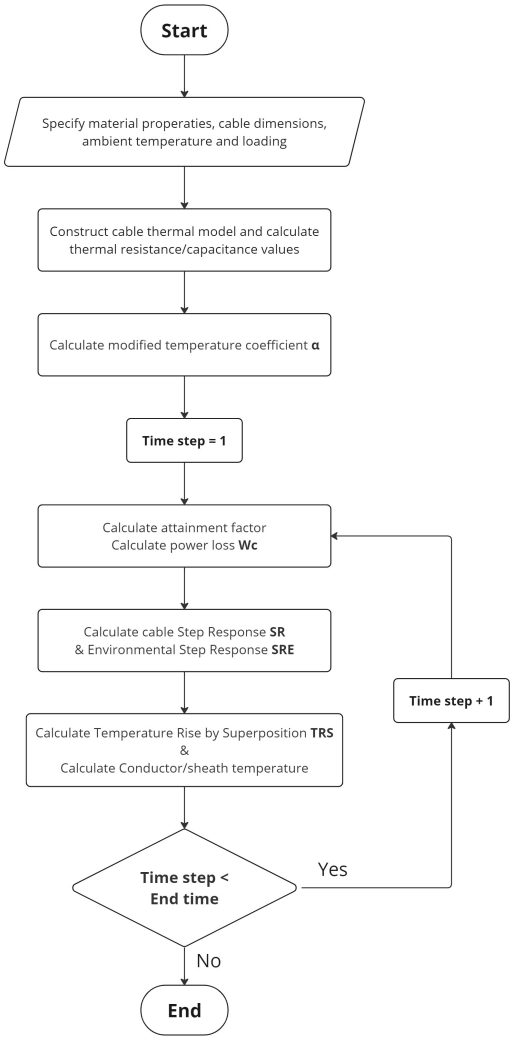

Figure 3.6: Flow chart of the developed algorithm for conductor and sheath temperature rise calculations based on IEC standards for cable ratings

Initially, material properties, cable dimensions, ambient temperature, and load conditions are defined. Following this, the transient thermal model is developed through analytical methods. Subsequent steps involve calculating the temperature response of the conductor and sheath until the designated simulation time frame is reached.

For the application of this principle, it is assumed that the thermal influence of adjacent cables, regardless of their operational status, does not interfere with the heat dissipation or generation in the primary cable. This assumption enables individual calculations for each cable, where the overall temperature increase results from the sum of the temperature increase attributable to the cable itself and those induced by neighboring cables. This approximation remains valid, provided that the cables are sufficiently spaced apart in the circuit. In situations where cables are near each other, such as in a touching formation, it becomes necessary to account for the temperature rise resulting from the concurrent operation of all cables. Solving the heat conduction equation using a numerical method facilitates such an analysis, offering a direct approach to considering the collective thermal effects.

3.2. Method 2: Numerical approach, FEM principle

The previous section provided an overview of analytical methods for determining cable ratings. Now, the Finite Element Modeling (FEM) is introduced, a robust numerical technique that avoids simplifying assumptions, such as lumped parameters and inaccuracies in complex scenarios including proximity to other heat sources, short transients, or soil layers with varying thermal properties. This method is particularly useful for custom or specialized cable configurations where standard approaches may fail to capture all relevant factors or the scenario falls outside the standardized guidelines.

This method is included in the thesis because it provides detailed and accurate temperature predictions for custom or specialized cable configurations where standard approaches may fail. Especially when trying to model a convective ground layer or detailed soil conditions with backfill around the circuits for example.

There are also advantages in using the finite element method in transient analysis. Like facilitating the coupling between internal and external circuits by assuming that the heat flow into the soil is proportional to the transient attenuation factor from the conductor to the cable's outer surface. The validity of these methods is substantiated not through analytical proof, but through empirical alignment with the responses produced by recommended circuit models. Here, the finite element method offers a solution with minimal simplifying assumptions.

It should be noted that the selected value for the thermal resistivity of the soil and its temperature will have a significant influence on any calculated current rating or cable temperature. In many cases, little can be gained by using a 'more accurate' calculation method if the soil conditions are not known with a degree of certainty [38]. Therefore, it is wise to use soil drilling information or to have a good idea of the type of soil used in the scenario, as well as the water level.

The numerical figures come from the web-based tool *Ampwise* which has been developed by the author, more explanation can be found in section A.1.

3.2.1. Finite element modeling (FEM)

The finite element method is a numerical technique for solving partial differential equations. Among many physical phenomena described by such equations, the problem of heat conduction and heat and mass transfer in the vicinity of power cables has been addressed in the literature [18] [19] [15].

FEM simulations do not require the simplifying assumptions (e.g. the lumped representation) inherent in the analytical algorithms. Instead, the FEM procedure is typically based on the discretization of partial differential equations that describe physical problems.

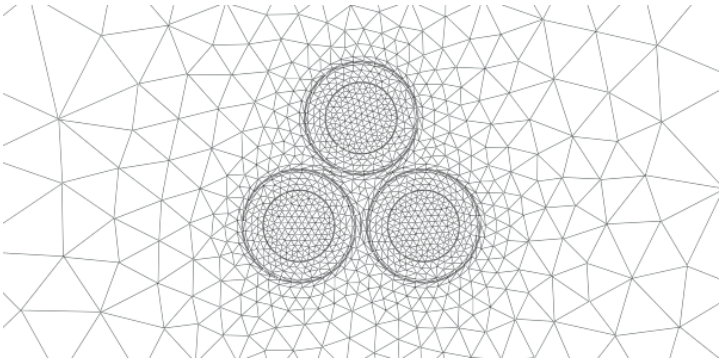

Figure 3.7: Example mesh (FEM) of Trefoil configuration from *Ampwise*

By discretizing the cable and its surrounding environment into a finite set of (triangular) elements (see Figure 3.7), FEM accommodates variable material properties, complex boundary conditions, and transient thermal responses, providing a comprehensive picture of temperature dynamics under a

wide range of scenarios. The downside is the need for relatively more computational power and time compared with analytical methods.

The core principle of the Finite Element Method (FEM) is that temperature distributions can be closely approximated through a discrete model. This model comprises a series of continuous functions that span a limited number of subdomains. The temperature at various points within the area of interest is represented by piecewise-continuous functions, establishing a foundation for the discrete model.

The discrete solution is constructed as follows:

- Identification of a finite set of points within the solution domain, known as nodal points or nodes.
- The domain of interest is segmented into a finite number of smaller areas, called elements. These elements are connected at common nodal points and collectively approximate the shape of the region. Elements are generally triangular or quadrilateral in shape. Triangular elements are the most common, connecting every closest node. The quadrilateral shape creates a quadratic equation along the edge and less total nodes than the triangular elements. For cable rating applications, two-dimensional triangular elements are the most commonly used [38].
- Within each element, the temperature is estimated using a polynomial expression of the nodal temperatures. Although a distinct polynomial represents each element, these polynomials are chosen to ensure a continuous temperature transition across element boundaries. The nodal temperatures are derived to provide the most accurate approximation of the actual temperature distribution. This approach results in a matrix equation whose solution vector contains coefficients of the approximating polynomials [38].

The user retains control over several parameters that influence the accuracy of the calculations.

1. **Size of the region to be discredited**: The objective is to select a large enough region so that the calculated values along the boundaries agree with those that exist in the physical problem. For the cable rating problem, this means that the side and bottom boundaries must be selected in such a way that the nodal temperatures at those boundaries all have the same value and the temperature gradient across the boundary is equal to zero.

   For transient analysis, the radius of the soil, out to which heat disperses, will increase with time. For practical purposes, it is sufficient to consider only the radius within which a sensible temperature rise occurs. This radius can be estimated from the following equation assuming that each cable is a line source of heat at

   $$\theta_{r,t} = \frac{W_r \rho_s}{4\pi} \left(-Ei \left(\frac{-r^2}{4\delta t} \right) \right) \tag{3.30}$$

   where $\theta_{r,t}$ is the threshold temperature value at the distance r from the cable axis and the remaining notation is that used in IEC 60853 [7]. The value of $\theta_{r,t}$can be taken as 0,1 K [38]. The above equation is applied for each cable. The region to be discretized will be an envelope around all circles.

2. **Size of the elements**: The element size within a network, encompassing various components such as cables, the earth, and backfill, is determined by the distance between boundary nodes. This spacing can be varied to obtain the desired element sizes (the elements should be smaller near the cable). The smaller the element size, the more accurate the results. However, it is important to note that computational time escalates exponentially with an increase in the number of elements, necessitating a balanced approach in the selection of optimal element sizes. The element size is often decided by the user (fine, normal, coarse, etc.) which corresponds with template values for mesh size.

3. **Type and Location of Boundary Definitions**: In contrast to traditional cable rating calculations that presume an isothermal earth surface boundary, the finite element method allows the representation of different boundary conditions and arbitrary boundary locations. Both straight-line and curved boundaries can be represented. In particular, circular boundaries that represent cable, water, or steam pipe surfaces can be easily handled.

   Three distinct boundary conditions are relevant for computing cable current ratings using the finite element method. The isothermal condition applies when a boundary segment maintains a constant temperature, which might vary along its length. Conversely, a convective boundary condition is recognized when heat transfer through convection occurs at the boundary, an essential consideration for installations of large-diameter cables near the earth's surface. Here, specifying the heat convection coefficient and the ambient air temperature becomes necessary. The heat transfer due to convection at the Earth's surface encompasses both natural and forced variants, with the latter significantly outweighing the former in strength. The precise determination of the convection coefficient, which fluctuates between 2 $W/m^2 \cdot K$ and 25 $W/m^2 \cdot K$ for free convection and reaches between 25 $W/m^2 \cdot K$ and 250 $W/m^2 \cdot K$ for forced convection, is crucial. The lower the value of this coefficient, the more severe heating occurs in the ground.

   Lastly, the constant heat flux boundary condition emerges in scenarios where external heat sources are close to the evaluated cables, with a definitive knowledge of their heat output.

4. **Representation of cable losses**: Conductor, sheath, and dielectric losses are represented in finite element studies as heat sources. Values of these losses are recalculated at each time step, using methods as explained in Equation 3.1.4.

5. **Time step selection for transient analysis**: Transient analysis necessitates the calculation of temperatures over successive time increments, care must be taken in the selection of a time step. Ideally, to minimize computational effort, the largest feasible time interval should be selected. However, the accuracy of these calculations may be compromised for large time steps. Luckily, modern solvers can dynamically adjust their time step, to satisfy aperiodic or irregular load profiles with enhanced precision.

3.2.2. Heat transfer equations

The general 2D heat conduction equation in a solid can be described as

$$\frac{\partial^2\theta}{\partial x^2} + \frac{\partial^2\theta}{\partial y^2} + W_{int}\rho = \frac{1}{\delta}\frac{\partial\theta}{\partial t} \tag{3.31}$$

where

θ	is the unknown temperature (°C)
δ	is the thermal diffusivity of the medium (m^2/s)
c	is the volumetric specific heat of the material ($J/K \cdot m^3$)
ρ	is the thermal resistivity of the material ($K \cdot m/W$)
W_{int}	is the heat generation rate in the cable (W/m)

The boundary conditions (BC) associated with Equation 3.31 can be expressed in two different forms. If the temperature is known along a portion of the boundary, then

$$\theta = \theta_B(s) \tag{3.32}$$

where θ_B is the boundary temperature that may be a function of the surface length s, this is also known as a Dirichlet boundary (see Figure 3.8).
If heat is lost or gained at the boundary due to a heat flux q or convection $h(\theta - \theta_{amb})$, (θ_{amb} can also change in time), then

$$-\frac{1}{\rho}\frac{\partial\theta}{\partial n} = q + h(\theta - \theta_{amb}) \tag{3.33}$$

where n is the direction of the normal to the boundary surface, h is the convection coefficient, and θ is an unknown boundary temperature, this boundary is also known as a Neumann boundary (see Figure 3.9). The negative sign indicates the direction of heat flow out of the domain.

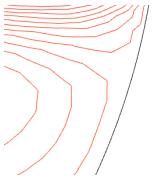

Figure 3.8: Dirichlet boundary

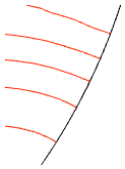

Figure 3.9: Neumann boundary

A thermal insulation boundary means that there is no thermal gradient orthogonal to the boundary and the heat flux is zero at that boundary ($-n \cdot q = 0$ or $n \cdot \nabla T = 0$).

It is important to note that for time-dependant studies, boundary conditions are not strictly necessary, since there is no converging needed. However, if a steady-state value is calculated, then it is important to set strict boundary conditions along the edges of the domain.

Temperature inside an element

To determine the temperature at precise points, such as the middle of the conductor or inside the metal sheath, it is necessary to be able to interpolate the temperature at this point using the temperature of the three nodes and the distances from these nodes. Consider a simple triangular element shown in Figure 3.10.

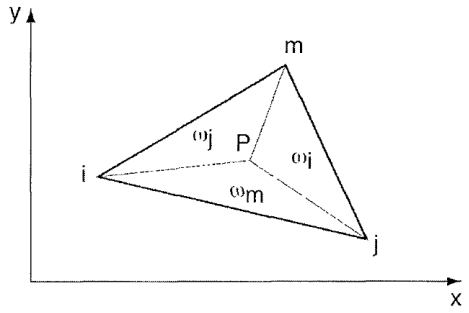

Figure 3.10: Area co-ordinates [38]

For this element, the temperature θ at any point inside can be uniquely specified as [32]:

$$\theta = \omega_i\theta_i + \omega_j\theta_j + \omega_m\theta_m = \begin{bmatrix}\omega_i & \omega_j & \omega_m\end{bmatrix}\begin{bmatrix}\theta_i \\ \theta_j \\ \theta_m\end{bmatrix} = \mathbf{N}^e \cdot \boldsymbol{\theta}^e \tag{3.34}$$

where $\omega_{i,j,m}$ are the area coordinates defined as in Figure 3.10. These coordinates define uniquely the position P inside the triangle. The inverse relationship between the area coordinates and the Cartesian coordinates yields the inverse relationship of the vector $\mathbf{N}^e$:

$$\begin{bmatrix}\omega_i \\ \omega_j \\ \omega_m\end{bmatrix} = \frac{1}{2A}\begin{bmatrix}(y_j - y_m) & (x_m - x_j) & (x_j y_m - x_m y_j) \\ (y_m - y_i) & (x_i - x_m) & (x_m y_i - x_i y_m) \\ (y_i - y_j) & (x_j - x_i) & (x_i y_j - x_j y_i)\end{bmatrix}\begin{bmatrix}x \\ y \\ 1\end{bmatrix} \tag{3.35}$$

where A is the area of the triangle. The temperature is a linear function in x and y, and thus the gradients are constant. A constant gradient within any element means that small elements must be used to approximate a rapid change in the value of θ.

Isothermal lines inside an element

Contour lines or isothermal lines are straight lines within an element that note a constant temperature. This is useful to see how heat flows within a domain. If the temperature is present inside an element, the isothermal line should cross two sides of that element. To obtain the coordinates of the intersection of the boundary lines of the element for a specific temperature θ, the following simple ratios can be used:

$$\frac{\theta_1 - \theta}{\theta_1 - \theta_2} = \frac{(x, y)_1 - (x, y)}{(x, y)_1 - (x, y)_2} \tag{3.36}$$

where $\theta_{1,2}$ are the temperature of nodes 1 and 2 and $(x, y)_{1,2}$ are the x and y locations of nodes 1 and 2, respectively. If the result is negative, this means the temperature is not present in the element. if the temperature at nodes 1 and 2 is the same, then that line is the isothermal line.

3.2.3. Finite element equations

To obtain all node temperatures, a property is used, where the functional χ is minimized over an area S bounded by a closed curve C [38].

Performing computations for each element e, the final set of linear algebraic equations is obtained for the whole region:

$$\frac{\partial \chi}{\partial \Theta} = \sum_{e=1}^{E} \left(\frac{\partial \chi}{\partial \theta_n} \right)^e = H\Theta + Q\frac{\partial \Theta}{\partial t} - K = 0 \tag{3.37}$$

where H is the heat conductivity matrix, Q is the heat capacity matrix, Θ and $\frac{\partial \Theta}{\partial t}$ are vectors that contain the nodal temperatures and their derivatives, K is a vector that expresses the distribution of heat sources and heat sinks over the region under consideration. In steady-state analysis, equation Equation 3.37 simplifies to $H\Theta - K = 0$.

The element conductivity matrix h_e is represented as:

$$h^e = \frac{1}{4A\rho}\left\{ \begin{pmatrix} a_i^2 & a_i a_j & a_i a_m \\ a_i a_j & a_j^2 & a_j a_m \\ a_i a_m & a_j a_m & a_m^2 \end{pmatrix} + \begin{pmatrix} b_i^2 & b_i b_j & b_i b_m \\ b_i b_j & b_j^2 & b_j b_m \\ b_i b_m & b_j b_m & b_m^2 \end{pmatrix} \right\} \tag{3.38}$$

$$+\frac{hd_{ij}}{6}\begin{pmatrix} 2 & 1 & 0 \\ 1 & 2 & 0 \\ 0 & 0 & 0 \end{pmatrix} + \frac{hd_{jm}}{6}\begin{pmatrix} 0 & 0 & 0 \\ 0 & 2 & 1 \\ 0 & 1 & 2 \end{pmatrix} + \frac{hd_{mi}}{6}\begin{pmatrix} 2 & 0 & 1 \\ 0 & 0 & 0 \\ 1 & 0 & 2 \end{pmatrix}$$

Where:

$$\begin{aligned} a_i &= x_m - x_j, & a_j &= x_i - x_m, & a_m &= x_j - x_i, \\ b_i &= y_j - y_m, & b_j &= y_m - y_i, & b_m &= y_i - y_j, \end{aligned}$$

Where, d is the distance between the respective nodes. The element capacity matrix is given by:

$$q^e = \frac{cA}{12}\begin{pmatrix} 2 & 1 & 1 \\ 1 & 2 & 1 \\ 1 & 1 & 2 \end{pmatrix} \tag{3.39}$$

and the element heat generation vector is equal to

$$k^e = \frac{W_{int}A}{3}\begin{pmatrix} 1 \\ 1 \\ 1 \end{pmatrix} + \frac{(h\theta_{amb} + q)d_{ij}}{2}\begin{pmatrix} 1 \\ 1 \\ 0 \end{pmatrix} + \frac{(h\theta_{amb} + q)d_{jm}}{2}\begin{pmatrix} 0 \\ 1 \\ 1 \end{pmatrix} + \frac{(h\theta_{amb} + q)d_{mi}}{2}\begin{pmatrix} 1 \\ 0 \\ 1 \end{pmatrix} \tag{3.40}$$

If there is no convective boundary along the segment of the element, the relevant term is committed in Equation 3.38 and Equation 3.40. Factor $W_{int}A$ represents the total heat in W/m generated in the element.

The set of ordinary differential equations (ODE) outlined in (Equation 3.37), which define the discretized problem, may be addressed via various recursive methods. Notably, two popular strategies for solving these equations to obtain the values of Θ at specific time points. The initial approach involves approximating the time derivative through a finite difference scheme. The alternative procedure is to use finite elements defined in the time domain. The IEC 62095 standard suggests for the application of Lee's three-level, time-stepping scheme [39] [38].

Popular computer programs offer a built-in option to solve the differential and a solver needs to be selected. Since this problem can be considered stiff (numerically unstable since some terms can lead to rapid variation in the solution), an implicit solution is necessary. A solver like the implicit Runge-Kutta method or an implicit multistep variable-order method is appropriate.

3.2.4. Underground thermal gradient

Seasonally and daily, the temperature of the air above the ground changes periodically due to environmental factors, such as the penetration of radiated solar heat into the ground. Depending on the time when this temperature change is present, a temperature change is also observed in the uppermost soil meters. The sun-induced heat flux is larger in summer and smaller in winter than the earth-induced heat flux, but the heat spreads through the ground more slowly than the annual cycle of the outside temperature.

To calculate the temperature for various depths and times, Equation 3.41, can be used. The equation is a cosine function with a damping depth $z_0 = \sqrt{2D_h/\omega}$

$$T(t,z) = T_0 - \Delta T e^{-z/z_0} cos(\omega t - z/z_0) \tag{3.41}$$

where

T_0	Average annual temperature (°C)
ΔT	Maximum annual temperature variation from average (°C)
D_h	Thermal diffusivity of soil (m^2/day)
t	Number of days after coldest day
z	Depth of burial (m)
ω	Angular frequency [$2\pi/365$] ($1/day$)
z_0	Damping depth (m)

Figure 3.11 shows the shallow geothermal temperature for the seasons.

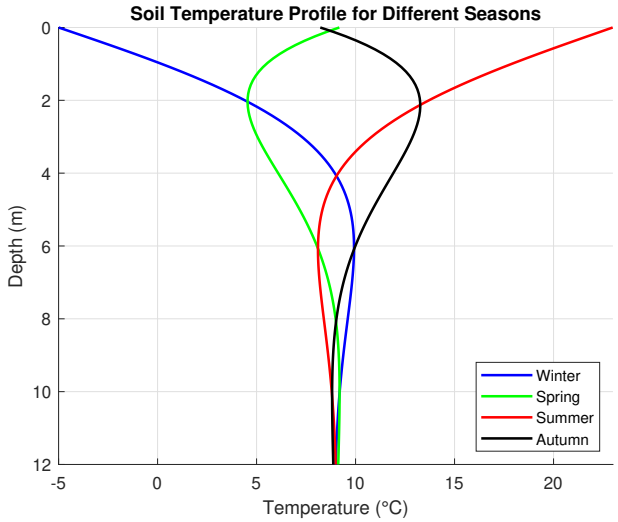

Figure 3.11: Annual soil temperature fluctuations for The Netherlands

The upper layers of the soil are heated in summer, while the deeper layers are still cold. While the heat spreads downward through the ground, it becomes colder again outside. The upper soil zones are cooled in winter when the summer heat has just reached the cooled layers of the last winter. This means that the annual cycle of the outside temperature continuously overtakes the annual cycle of the ground temperature.

Figure 3.11 is based for a seasonal ground temperature of $9 - 14 * cos((2 * pi/365) * t)$, which means the annual temperature is a cosine function with an average of 9 degrees and a deviation of 14 degrees. The thermal resistivity is 0.82 $K \cdot m/W$ and the diffusivity of the ground is 6.46 m^2/s.
This feature cannot be modeled by common analytical methods like IEC 60853 or IEC 60287 as these standards only model the environment by a single T_4 thermal resistance with constant ambient temperature.

Numerical modeling of geothermal temperature

To implement this geothermal gradient in a numerical system with FEM, the external air temperature can be included in the convective ground layer. In Equation 3.42, T_{ext} is the external ambient temperature. The external temperature can also be the real piecewise temperature at certain time intervals and location fetched from an API, instead of a cosine function. A cosine function can be a good annual approximation of temperature fluctuations. The changing temperature changes the heat flux generated at this ground layer.

Figure 3.12 shows the change of temperature in the ground when a temperature $(9-14*cos((2*pi/365)*t))$ is applied for the external temperature in the convective heat ground boundary (the x-axis is logarithmic to expand on the temperature effects at shallow depth). The cut-line also crosses the center of a power cable at 1m depth. Here, it is clearly visible that changing air temperature has a relatively big impact on both ground and cable temperature. The ground temperature fluctuates between 4 °C and 25 °C and the cable fluctuates between 42 °C and 54 °C for a steady state scenario.

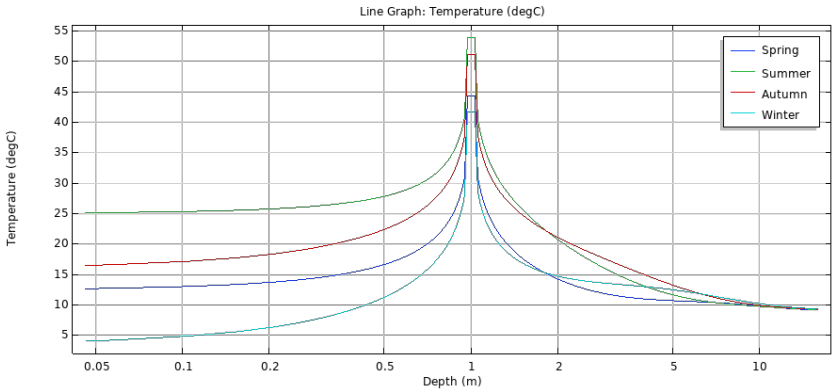

Figure 3.12: COMSOL logarithmic ground gradient with cable heating

To obtain a precise result, the real air temperature at a certain location can be fetched for the duration of the desired load profile output, instead of a cosine function. API's like *OpenWeather* or *Visual crossing weather* are perfect for this (A.8 shows Javascript code of how the fetching can be done). Only the geographical location and a time interval are included, and the hourly/daily air temperature at that location for that time period is outputted.

Initial conditions

Since the temperature changes with depth over time, it is important to get the initial conditions correct. For the numerical model, the initial conditions can be calculated with the analytical Equation 3.41. The temperature at various depths z can be found at time t = 0. This is just an approximation, but better than assuming all to be a constant temperature.

The problem with this approach is that it is not known how many days after the coldest day it is now or where on the cosine the first day is (The air temperature of 1 January is different in Australia from Iceland). So, the cosine could go upward or downward. What can be done to solve this problem is the following:

- **Fetch the temperature of the previous year**: The starting date is known from the first timestamp of the load profile. The air temperature is fetched of one year before. To reduce the load on the API, only monthly temperatures can be fetched.

- **Fit a single-period cosine on the temperature data**: Determine the amplitude and the phase shift of a fitted cosine function (the frequency is known since it is only one period).

  Figure 3.13, shows the temperature for the year 2023 (the first time stamp of the load profile is 01/01/2024 so one year is subtracted). The blue graph are 14 fetched records from *Visual Crossing Weather* of 2023 where the average temperature of that day is plotted for the city of Amsterdam. The red line is the fitted cosine function with an average temperature of 11.64°C, a temperature deviation of 15.31°C, and a phase-shift of 220.5 days. The green line shows the average measured temperature (from *weatherspark.com*) for the same location and time period. The average temperature is 10.04°C, and the temperature deviation is 16°C. The peak of the data occurs around the same time for the fitted cosine and the measured data. On the basis off these results, it can be concluded that a fitted cosine is a good approximation for the temperature fluctuations of a year for the determination of the initial conditions.

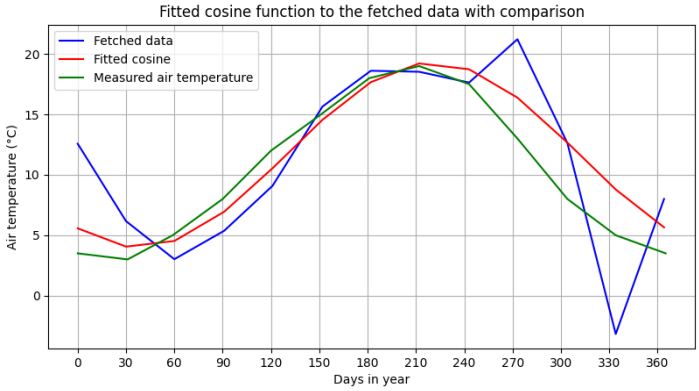

Figure 3.13: Fitted cosine function to the fetched data with comparison

From the fitted cosine function, the day after the coldest day can be known as the last point of the cosine function. Now T_0, ΔT and t can be entered in Equation 3.41 and the temperature can be known at all depths and the initial conditions can be established for that day and location.

Furthermore, to get an even better result, a steady-state preparation phase can be included to pre-run the model for some time (e.g. a year) to get accurate results at all layers, and then cable heating can be modeled from that time on (like the cable has been in the ground for a year before it is turned on). This approach is not used in the thesis since it takes a couple of minutes to model the whole year, and the analytical gives accurate results for the initial conditions.

3.2.5. Convective ground layer

The boundary layer that divides the ground and the air can be seen as a convective layer, since the air is a gas and uses convection to transfer heat produced by the cable. A convective heat flux q_0 is present at this layer. To model this correctly, in Equation 3.38 and Equation 3.40, an h-value is needed, also known as the convective heat transfer coefficient used in the Nusselt number [40]. It is assumed that the ground is a horizontal flat plate with external natural convection on top. The h-value for this situation can be found as follows:

$$q_0 = h \cdot (T_{ext} - T) \tag{3.42}$$

$$h = \begin{cases} \frac{k}{L} 0.54 Ra_L^{1/4}, & \text{if } 10^4 \leq Ra_L \leq 10^7, \text{and } T > T_{ext} \\ \frac{k}{L} 0.15 Ra_L^{1/3}, & \text{if } 10^7 < Ra_L \leq 10^{11}, \text{and } T > T_{ext} \\ \frac{k}{L} 0.27 Ra_L^{1/4}, & \text{if } 10^5 < Ra_L \leq 10^{10}, \text{and } T \leq T_{ext} \end{cases} \tag{3.43}$$

where Ra_L is the Rayleigh number [40]. This is a dimensionless number associated with buoyancy-driven flow, also known as free (or natural) convection. It characterises the fluid's flow regime: a value in a certain lower range denotes laminar flow; a value in a higher range, turbulent flow. Below a certain critical value, there is no fluid motion and heat transfer is by conduction rather than convection [40].

$$Ra_L = \frac{g\beta}{\nu\alpha}(T - T_{ext}) \cdot L^3 \tag{3.44}$$

where

h	is the convective heat flux $(W/m^2 \cdot K)$
k	is the thermal conductivity of air $(W/m \cdot K)$
L	Characteristic length (m)
T	Temperature of the surface $(^\circ C)$
T_{ext}	External temperature $(^\circ C)$
g	Acceleration due to gravity (m/s^2)
β	Thermal expansion coefficient $(1/K)$
ν	Kinematic viscosity of air (m^2/s)
α	Thermal diffusivity of air (m^2/s)

The characteristic length of the earth surface is the ratio of the surface area to the perimeter, as this represents the distance that heat must traverse to pass through the convective layer. For an infinite earth surface, L = 0.5. Calculating the density of dry air requires knowing the absolute pressure at the surface level. Therefore, the temperature of the ground, the absolute air pressure and external temperature collectively determine the heat flux on the ground, with all remaining factors remaining consistent for external natural convection involving air.

Figure 3.14 shows 10 meters of ground temperature above a cable (5m is directly above the cable). It is clear that the cable laid 0.3m under ground surface has a big influence on the ground temperature. The reason for the big temperature deviation is due to the cable being very close to the surface level.

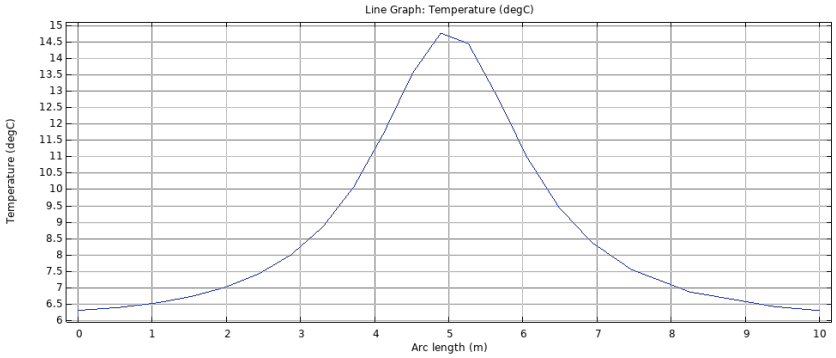

Figure 3.14: Convective ground layer with a ground gradient due to cable heating from COMSOL

The external air temperature and pressure can be time-varying as in a yearly temperature/air profile. The air pressure also changes over time and is needed to calculate the heat transfer coefficient h. There is no increase in temperature accuracy when using real air pressure data compared to the yearly average of 1013.25 hPa (section 4.7).

This feature cannot be modeled by common analytical methods like IEC 60853 or IEC 60287 as these standards only model the environment by a single T_4 thermal resistance with constant ambient temperature.

3.2.6. Boundary heat source - Solar radiation

Solar radiation is a general term for electromagnetic radiation emitted by the Sun. Solar radiation can be defined by the solar power in W/m^2 and the solar energy J/m^2. Both values can be obtained for various time steps from an API like *Visual Crossing Weather* or *OpenWeather*. The output is either a daily average or precise hourly values. The solar radiation heats the ground with a certain heat flux q, so this can have an impact on cable temperatures throughout the season.

For long simulations (like a year), it is undesirable to fetch hourly values, since then 8760 records of all datasets will be required. Furthermore, hourly detail is often unnecessary and does not increase accuracy compared to daily averages. However, in the case of solar radiation, the Sun is not averaged equally across the 24 hours. The solar radiation can be approximated as a Bell curve (see Equation 3.45), where the peak occurs around 13h and goes down on both sides, defined by the standard deviation.

$$S(t) = A \cdot e^{-\frac{t-13}{2 \cdot \sigma^2}} \tag{3.45}$$

$$\int S(t)\,dt = \frac{A}{\sqrt{2\pi\sigma^2}} = SolarEnergy \tag{3.46}$$

The standard deviation can be defined empirically to be 2.1 in winter and 3 in summer and interpolated sinusoidally in between (this is not universal yet, but a simplification for The Netherlands).
To calculate peak A, The area under the curve can be calculated by integrating Equation 3.45 and set equal to the solar energy as shown in Equation 3.46.

Figure 3.15 and Figure 3.16 both show the solar radiation for four days in Winter and Summer respectively (1 Jan, 7 July). Both graphs show the comparison between the real hourly solar radiation fluctuations during a day (Green, Red) and the approximated daily solar radiation from the daily average (Blue).

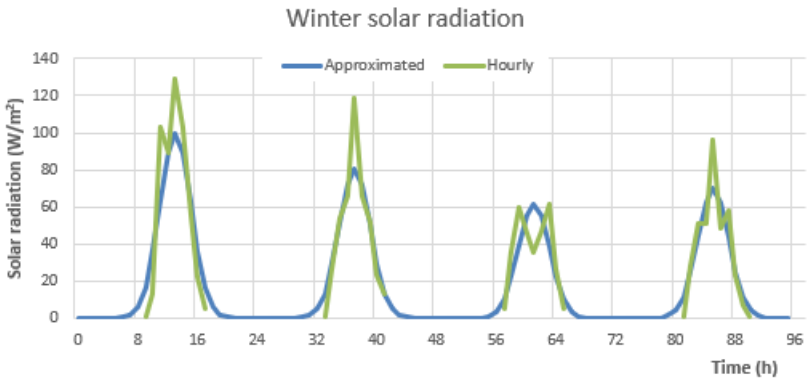

Figure 3.15: 4 days of Solar radiation in winter, hourly vs approximated data from Ampwise

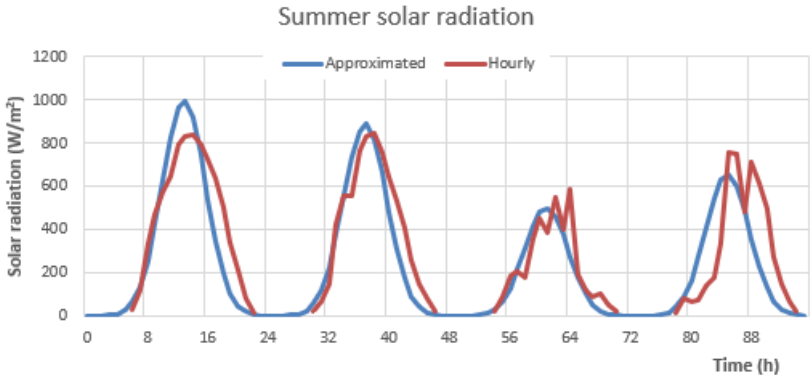

Figure 3.16: 4 days of Solar radiation in summer, hourly vs approximated data from Ampwise

Finally, not all solar energy is absorbed by the ground. The absorb factor depends on the angle of incidence of the light and the color of the ground material. Table 3.1 shows the absorb factor for various surface colors.

Surface color	Absorb factor (approximated)
White smooth surfaces	0.25 - 0.4
Grey to dark grey	0.4 - 0.5
Green, red and brown	0.5 - 0.7
Dark brown to blue	0.7 - 0.8
Dark blue to black	0.8 - 0.9

Table 3.1: Absorbed Solar Radiation vs. Surface Color (from www.engineeringtoolbox.com)

The approximated Bell curve follows the trend of the real hourly values, and for a year, the same amount of solar energy is used. Therefore, this method can be used to model the solar radiation daily variations for longer datasets.

3.2.7. Workflow

To give an overview of the order in which the calculations are done in the numerical algorithm developed in *Ampwise*, the resulting flow chart can be seen in Figure 3.17.

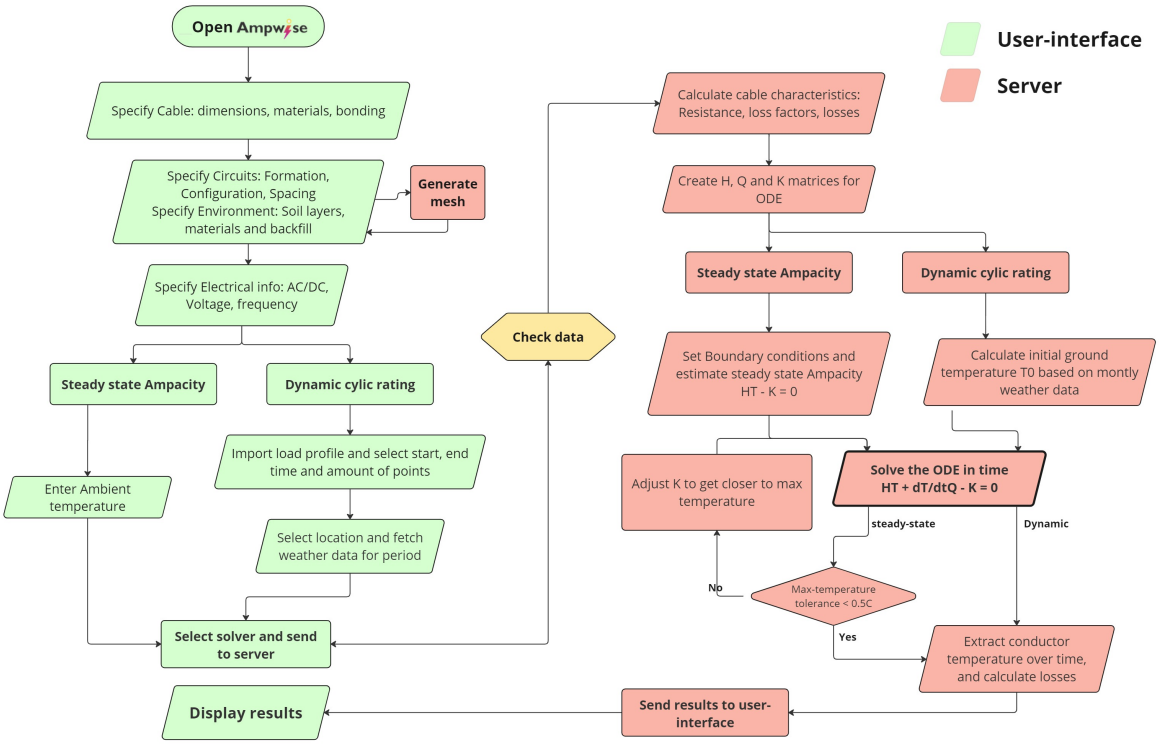

Figure 3.17: Flowchart Numerical model as implemented in *Ampwise* section A.1

The check data between the front end and the back end checks all incoming data if they are valid numbers and that they can be worked with in the server. If correct or missing values are found, the server gives an error code and tells the user what is missing or wrong in the console.

3.2.8. Description of numerical model in COMSOL

This subsection covers the description of the numerical modeling of the cable using the popular numerical program COMSOL Multiphysics, which utilizes the finite element method (FEM) procedure. COMSOL is a simulation platform that encompasses all of the steps in the modeling workflow like modeling, simulating, and adding physics. It can model real-world scenarios using multiple physics. It costs around 4600$ for one commercial license per year.

The results of the numerical COMSOL simulations were obtained to evaluate the numerical model explained in section 3.2. It is important to note that a model is inherently unrealistic, since it assumes perfect homogeneous materials and boundaries. However, it is the best method available to verify the mathematical accuracy of the methods explained in this thesis.

The process of modeling an underground power cable in COMSOL is as follows:

1. **New project creation**: First the space dimension need to be selected. As an underground power cable can be assumed straight and extremely long compared to its diameter, a two-dimensional (2D) domain is the most appropriate (A 3D model will introduce a lot more elements). A 2D modeling approach provides less complexity and computational effort than a full 3D simulation. Afterwards, it is required to select either a steady state or time-dependent study and for the physics, heat transfer in solids is the most appropriate.

2. **Component definitions**: Various expressions need to be defined. The first variable is the temperature-dependent resistance R which changes with temperature T [°C] with a certain temperature coefficient α. The second variable is the interpolated current profile in the case of a time-dependent study. Here, a daily load profile can be made or imported where current values are set per time interval. Next, the solar radiation can also be included as an interpolated function. Lastly, the ground gradient temperature can be defined as a function of depth.

3. **Model geometry**: Next, the domain (world) needs to be modeled. The outer domain, representing the soil was modeled as a semi-circle, illustrated in Figure 3.18. The bottom half represents the soil. The air is not modeled since every boundary has a boundary condition in COMSOL.

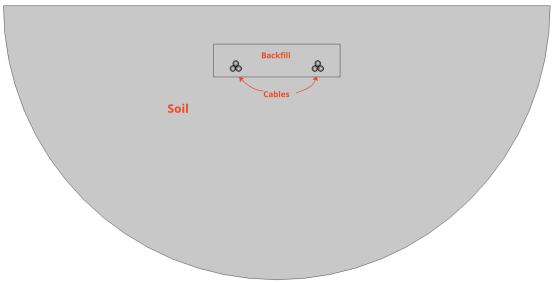

Figure 3.18: Total domain and burial depth of the cable in the COMSOL model

The required domain size can be established on the basis of the radius calculated in Equation 3.30. The domain radius is determined by factors such as the conductor size, the burial depth, the number of cables, and the spacing between circuits. In this case, a domain radius of 5m is sufficient, since a large radius does not change the conductor temperature (see section 4.3). Although a larger domain size can improve the accuracy of simulation outcomes (if there is a significant temperature gradient at the boundary), it might also result in an unnecessarily time-consuming simulation.

The different parts of the cable were modeled as several concentric circles. Figure 3.19 illustrates the cross section of the cable model.

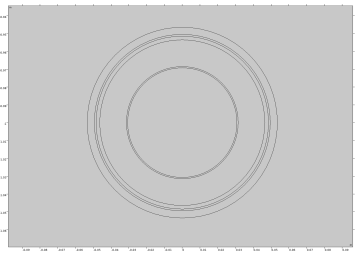

Figure 3.19: Cross section of a single core cable in COMSOL

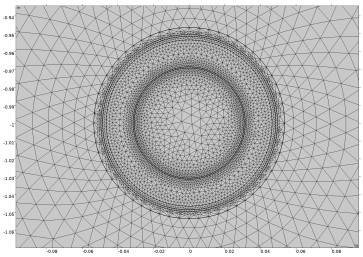

Figure 3.20: Mesh generation in cable COMSOL

4. **Material properties**: For the physic heat transfer in solids, the thermal conductivity $[W/K \cdot m]$, heat capacity at constant pressure $[J/kg \cdot K]$ and density $[kg/m^3]$ are necessary to define a material's thermal properties. This is done for all cable layers, the soil (and backfill). If a property is unknown, the material can also be selected from the material library in COMSOL.

5. **Physics interface**: For a directly buried cable, mainly conductive heat transfer is causing heat dissipation. To simulate the conductive heat transfer in the cable itself and its surrounding soil, the Heat Transfer in Solid physics was applied to the domain beneath the ground surface. This interface solves the differential equation described by Equation 3.31.

The initial temperature of the domain can be set at a constant temperature or a ground gradient. A convective heat flux is applied to the ground layer (horizontal plate, upside) with external natural

convection to simulate heat transfer from the ground to the air. The external temperature is set at 15 °C and a constant atomic pressure of 1.
To model the changing ground gradient, the model can be run for a full year with a cosine applied to the convective ground layer to set the temperature at various depths, or the initial temperature can be set in the beginning if the ground temperature is known.

To model solar radiation, a boundary heat source can be set to the ground layer with a solar radiation list in W/m^2 and multiplied by the world length and the absorb factor.

At the soil boundary (lower semicircle), thermal insulation is applied. Thermal insulation means that there is no heat flux across that boundary, or the temperature gradient across this boundary is zero (Neumann boundary).

3 heat sources with constant heat rates are present in the cable: (1) Joule losses in the conductor due to the current through the wire are defined in COMSOL as $R(T) * I(t)^2$ where R is the resistance variable, dependent on temperature and I is the current variable dependent on time, (2) the dielectric losses in the insulation defined as a constant value, and (3) the metallic sheath losses due to circulating and eddy current. This is a loss factor λ multiplied by the conductor losses.

6. **Mesh generation**: As a final preparation step, the mesh needs to be defined. COMSOL automatically creates the mesh based on a user-selected element size. Figure 3.20 shows the mesh of the cable with a *Finer* element size with refinement near the edges. Correct meshing affects the accuracy of the simulations as well as the computation time. Mesh elements should be small where temperature gradients are high and where the accuracy of the calculations is important. This is typically near the cable since interesting values are sheath and conductor temperatures.
7. **Solver configuration**: To investigate the transient temperatures, the *Time Dependent Study* step can be chosen. This study step solves the heat transfer physics in the time domain. The default solver is PARDISO and a range needs to be defined to tell the solver the end time and step size.
When clicking study, the solver will solve for temperature, and the result can be plotted at cut points/lines or visualized in a contour plot.

Chapter conclusion
Chapter 3 provided an exploration of thermal modeling for power cables using both analytical and numerical approaches. The analytical model theory, grounded in standards such as IEC 60287 and IEC 60853, offered a foundational understanding of thermal behavior under steady-state and transient conditions, respectively. Complementing this, the numerical model, particularly through the Finite Element Method (FEM), allowed for more precise simulations, accommodating complex boundary conditions and material properties.

Significant attention was paid to the convective boundary layer and solar radiation, crucial factors influencing cable temperature. Furthermore, the implementation of a real ground gradient as the initial temperature is also explained. Finally, the chapter explains the practical implementation of these models in COMSOL, which serves as a robust verification tool.

In summary, the methodologies discussed in Chapter 3 establish a solid framework for dynamic cable rating predictions. Using both analytical and numerical techniques, incorporating environmental considerations, and validating through COMSOL, this chapter sets a robust precedent for advanced thermal modeling in power cable systems.

4

Sensitivity Analysis

This chapter delves into the analysis of the sensitivity of various parts of the thermal modeling process and how this affects the conductor temperature. The parameters studied include mesh quality, world radius, the effect of stranding conductors, soil thermal resistivity, the use of weather data instead of constant temperature, and the effect of real vs constant air pressure. Each of these factors could significantly influence the accuracy and reliability of thermal predictions, making their study essential to optimize cable performance.

4.1. Effect of stranding vs solid conductors

Various cables have strands inside the conductor to make the cable more bendable. The space between the strands can be filled with a material or left empty (air). This could create a thermal difference compared to a solid conductor. There are various stranding configurations, such as the Milliken configuration; however, it is hard to model all the different stranding shapes individually so circles are chosen with equal radii to approximate the configuration. *Ampwise* is used to make the cable and the positions and radii of all strands. This model is imported into COMSOL as a DXF file. The daily profile from Table A.1 is used for the load profile. The 3 cases compared are 5-strand layers, 10-strand layers, and a solid conductor. The filling material used is the same as the semiconductive screen with a thermal resistivity of 2.5 $K \cdot m/W$.

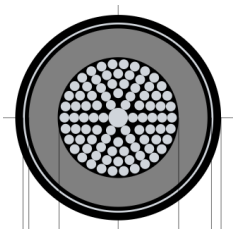

Figure 4.1: Stranding conductor with 5 layer strands from *Ampwise*

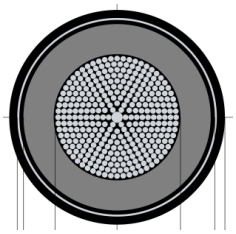

Figure 4.2: Stranding conductor with 10 layer strands from *Ampwise*

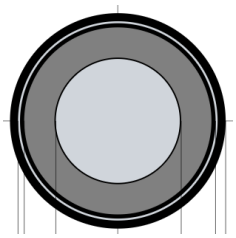

Figure 4.3: Solid conductor from *Ampwise*

Figure 4.5 shows the comparison. The stranding conductors give a higher conductor temperature than the solid conductor for the same power loss. This can be due to the same power being distributed over a smaller area, thus the strands get hotter. Also, the conductor might get hotter depending on the material between the strands. A higher thermal resistivity will make the conductor hotter.

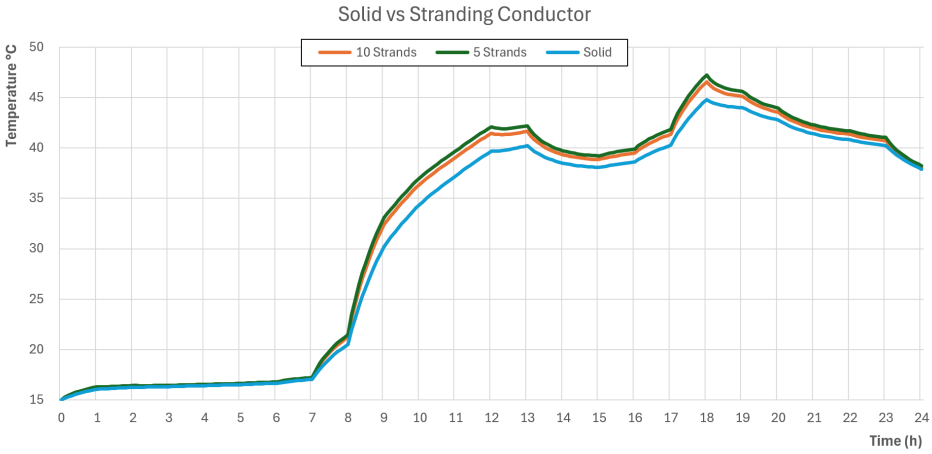

Figure 4.4: Conductor temperature for stranding and solid Conductors

The higher the strand layer count, the lower the conductor temperature since the filling factor is higher and there is less space in between the strands.

In reality, the strands are often squished together in the making process and there is not as much space between the strands. The strands are also never a perfect circle, evenly spaced. It is impossible to model a cable perfectly and to model it will create a huge amount of triangles extra compared to the solid conductor. Also, the effective conductor area is smaller for the 5- or 10-strand scenarios for the same power loss, so higher temperatures are expected. For simplification reasons, the stranding conductors are modeled as solid conductors in this thesis.

This comparison might not be fair, since the same power loss is applied to a different conductor area. Suppose that the effective area (the combined stranding area) would be the same in all three scenarios. In that case, the key factors that influence which cable is hottest are the total area and the thermal resistivity of the material that fills the remaining space between the strands. The hottest cable will be the cable with the lowest filling factor.

4.2. Effect of different mesh sizes

Next, the effect of different mesh sizes will be explored. COMSOL and *Ampwise* give the user the option between various mesh qualities (Extra Fine - Normal - Extra Coarse). This setting provides the mesh generator with a guideline on how many triangles are generated. This is also the largest determinant of the solve time of the computation. There is no clear difference between the different settings; choosing normal is appropriate in this case.

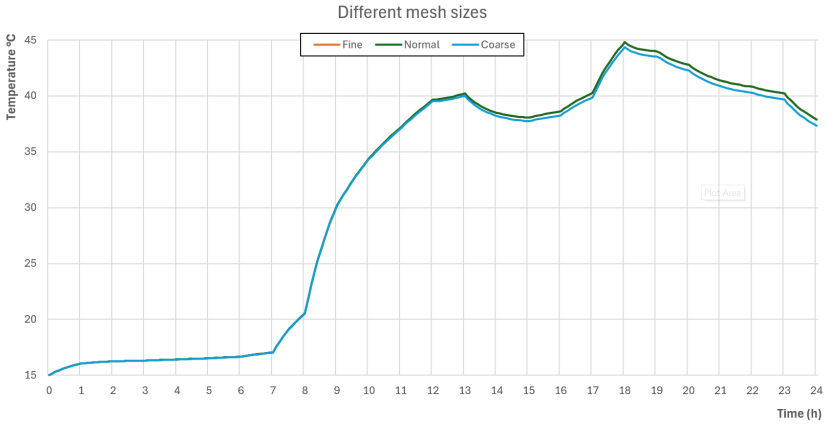

Figure 4.5: Conductor temperature of different mesh sizes

4.3. Effect of different world radii

Next, the effect of different world radii is studied. The domain can not be infinite since a mesh needs to be generated of the full domain. An outer boundary is set and chosen to be a circle since this is the most uniform and does not add any corners. The radius of the world could affect the conductor's temperature if it is too close. Figure 4.6 shows that there is hardly any change when the boundary is closer or further away (2m vs 12m). The reason there is no change is that there is no boundary condition on this edge and that there is also no heat sink/source present, so the conductor temperature does not notice this boundary. COMSOL applies a thermal insulation boundary on the world boundary. This will influence and form the thermal gradients near this boundary.

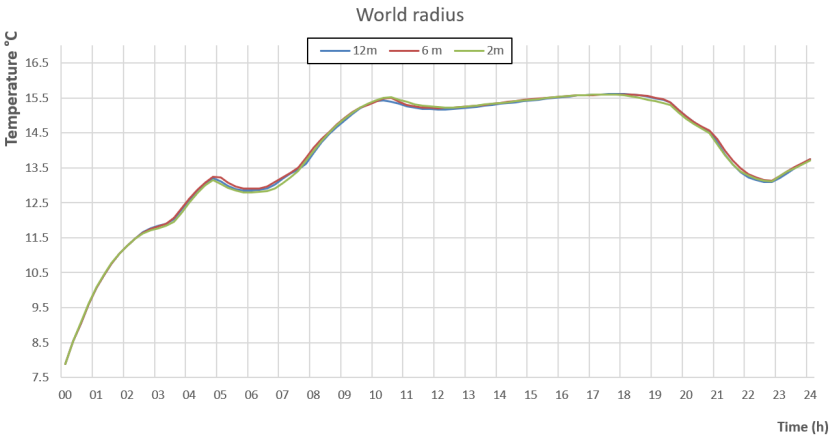

Figure 4.6: Conductor temperature of different world radii

4.4. Ground gradient vs constant temperature

Next, the effect of the initial conditions on the conductor temperature will be explored. The real temperature of the ground gradient based on depth is calculated using subsection 3.2.4. A gradient is found based on the temperature of the previous year. The gradient has a ground temperature of 5.11 °C, a cable temperature of 9.73 °C, and a bottom temperature of 12.28 °C. The constant case has a temperature of 15 °C for the whole domain. The initial temperature for the conductor is 16 °C.

Figure 4.7 shows that the difference is and remains quite substantial for the duration of the simulation.

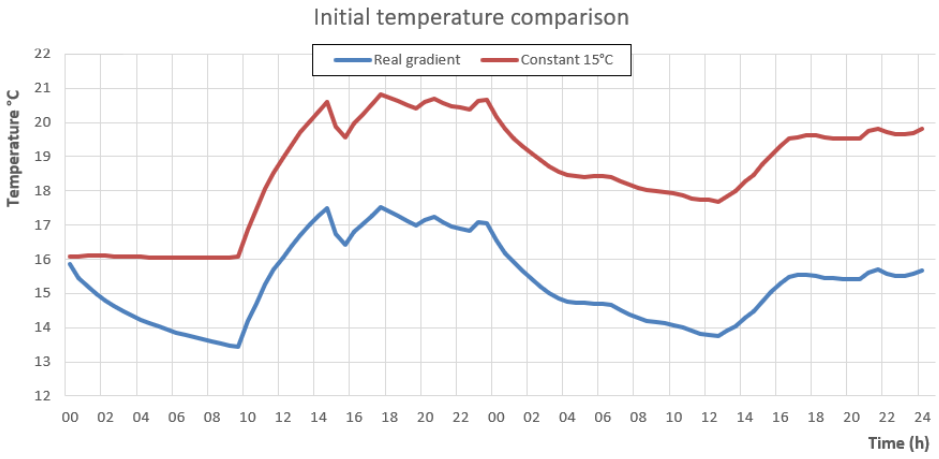

Figure 4.7: Real ground gradient temperature based on a date vs constant temperature

This difference shows the importance of correct initial conditions since the effect will continue since the thermal mass of the surroundings is greater than the cable. Assuming a constant temperature for the whole domain is incorrect, as these conditions change based on environmental/seasonal effects, and the temperature is also different depending on the depth.

4.5. Effect of soil thermal resistivity

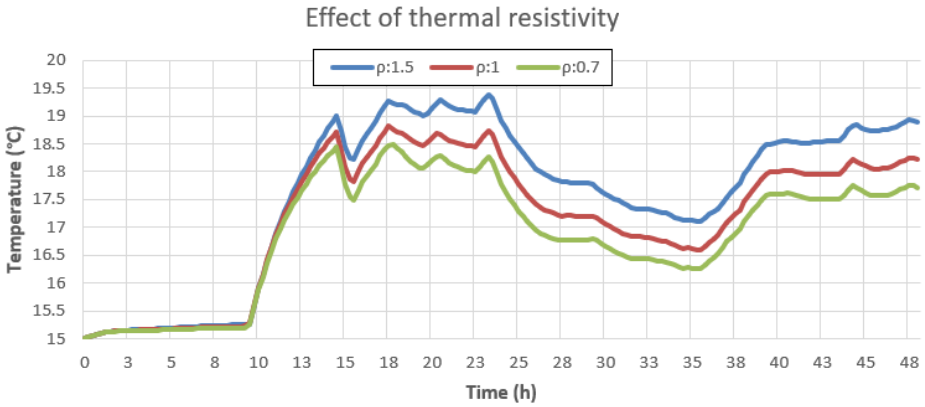

Figure 4.8: Effect of soil thermal resistivity on conductor temperature, from *Ampwise*

The thermal resistivity of the soil significantly impacts the temperature of an underground cable. Simulations were conducted over 48 hours for resistivity values of 0.7, 1, and 1.5 $K \cdot m/W$ with a trefoil cable configuration buried 1 meter deep.

For the initial 10 hours, the Conductor temperatures for all resistivity values remain close due to thermal inertia. Until 24 hours, the differences become evident. Higher resistivity (1.5 $K \cdot m/W$) leads to higher

temperatures (≈19.5°C), while lower resistivity (0.7 $K \cdot m/W$) results in lower temperatures (≈17.5°C). Until 48 hours, temperatures stabilize with cyclical variations. Higher resistivity consistently shows higher temperatures. Higher soil thermal resistivity results in higher conductor temperatures, affecting cable performance and lifespan.

In this example, it can be said that doubling the soil thermal resistivity increases the conductor temperature by around 2 °C.

4.6. Effect of weather data vs no weather data for a year

The effect of weather data on the conductor temperature is a crucial aspect of this thesis since this will prove if the including of weather data improves the fit of the predicted temperature to the real temperature. Figure 4.9 illustrates how air temperature and solar radiation influence the conductor temperature over a year.

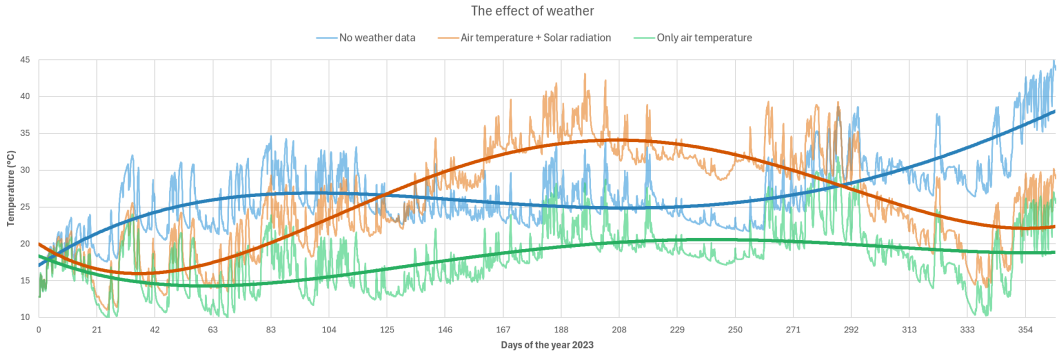

Figure 4.9: Effect of air temperature and solar radiation on the conductor temperature

The most important observation from Figure 4.9 is that incorporating both air temperature and solar radiation into the model provides a realistic representation of the seasonal variability in conductor temperature. The blue curve, which represents the model without any weather data, shows a steady linear increase in temperature. This linear trend is due to the absence of cooling, causing the heat to accumulate continuously without any cooling effect.

The green curve, which includes only air temperature data, shows some minor seasonal changes. However, it still fails to fully capture the correct seasonal variability. In particular, the temperature decreases in the winter, but not to the extent seen in the real data. This indicates that air temperature alone is insufficient to model the thermal behavior of the conductor accurately.

In contrast, the orange curve, which accounts for both air temperature and solar radiation, aligns closely with the observed data. This combination captures the full extent of the seasonal fluctuations, including the cooling effect during the winter months and the warming effect during the summer. The inclusion of solar radiation is critical because it significantly influences the conductor temperature during periods of high solar insolation. Solar radiation cannot be modeled without a convective layer since then the ground temperatures will skyrocket uncontrollably.

In summary, this analysis underscores the importance of incorporating comprehensive weather data, including air temperature and solar radiation, to accurately model the thermal behavior of power cables. Ignoring these factors or considering them in isolation leads to inaccurate predictions, as demonstrated by the linear increase in temperature without weather data and the minor seasonal changes with only air temperature.

4.7. Effect of variable vs constant air pressure

To calculate the kinematic viscosity and thermal diffusivity of air for the convective heat transfer coefficient h (Equation 3.44), the density of the air is needed. The density of air is calculated by dividing the absolute pressure of the air by the specific gas constant times the external temperature.

The hourly/daily external air pressures can also be obtained using a weather API like *Visual Crossing Weather*. To see how much variations in air pressure change the heat flux and the conductor temperature, it is compared to a constant air pressure of 1013.25 hPa (the global average air pressure, 1 atm). Figure 4.10 shows that both graphs perfectly overlap and there is no benefit in using real air pressure values in the solver. Approximating the air pressure to 1 reduces the computation time and complexity.

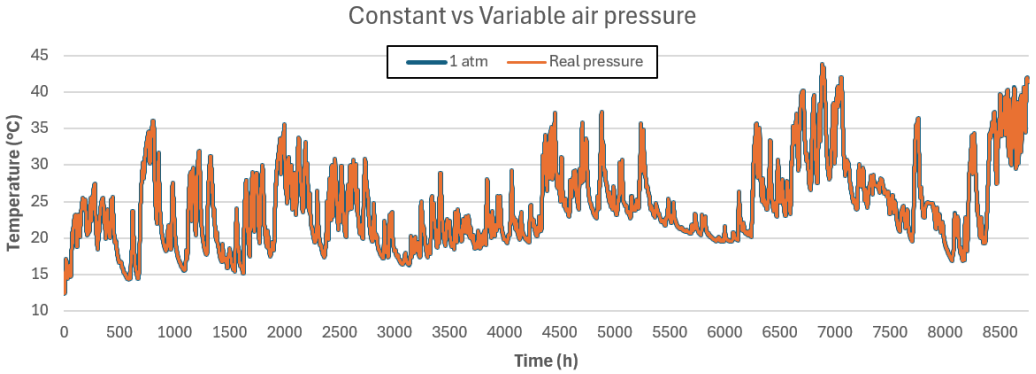

Figure 4.10: Constant vs variable pressure (Data from *Ampwise*)

Chapter conclusion

The sensitivity analysis highlights several critical factors that affect conductor temperature in underground cables. Higher soil thermal resistivity results in significantly higher conductor temperatures. For example, soil with a thermal resistivity of 1.5 $K \cdot m/W$ leads to temperatures around 19.5°C, while 0.7 $K \cdot m/W$ results in temperatures around 17.5 °C. This variation underscores the importance of accurately modeling the environment around the circuits.

In addition, the inclusion of comprehensive weather data, including air temperature and solar radiation, is crucial. The analysis shows that incorporating these factors provides a realistic representation of seasonal variability in conductor temperature. Ignoring these factors or considering them in isolation leads to inaccurate predictions. Therefore, both soil thermal resistivity and weather data must be carefully considered to ensure precise thermal modeling and optimize cable performance.

Furthermore, the initial ground gradient is very important as it significantly influences the conductor temperature throughout the simulation. Using accurate initial conditions helps in maintaining realistic temperature profiles, highlighting the need for precise ground temperature data based on depth and environmental conditions. Other factors such as the stranding detail, mesh size, and world radius are less critical but still contribute to the overall accuracy of the model.

5

Analytical and numerical thermal model verification

This chapter presents the results and the evaluation of the analytical and numerical model for dynamic cable rating calculations through three key comparisons.

First, both the analytical and numerical methods are compared with COMSOL simulations to determine which method is superior. This step verifies the accuracy and reliability of both approaches against a high-fidelity benchmark.

Second, the numerical model is compared with a case from CIGRE Technical Brochure 880, specifically against the analytical steady-state results provided by CIGRE. This comparison assesses the performance of the numerical model against established industry standards.

Finally, the numerical model is validated by comparing its predictions with real measured data from a distributed temperature sensing (DTS) system installed in the cables of Windpark Fryslân. This step ensures the model's practical applicability and accuracy in real-world conditions.

These comparisons collectively demonstrate the effectiveness and practicality of the numerical model of *Ampwise* for precise dynamic cable rating calculations.

5.1. Validation with COMSOL

The transient temperature analysis focused on a single core 110 kV cross-linked polyethylene (XLPE) insulated cable with a stranded aluminum conductor. Figure 5.1 shows the cross-sectional cable of the cable, including its dimensions. For all simulation scenarios, the cable was modeled with a burial depth of 1 meter, and the ambient soil temperature at this depth was maintained at 15 °C.

According to the IEC 60287 standard [5], the maximum rated current for the cable depicted in Figure 5.1, which features a conductor cross-section $2500mm^2$, is 2800 A under steady-state conditions (this high ampacity is due to the cable being the only heat source in the vicinity). This is the current level that, upon sustained application, results in a conductor temperature of 90 °C under equilibrium conditions. However, the conductor cross section area is often oversized to consider laying formation and environmental conditions.

In this context, the term *rated current* throughout this thesis is used to denote the current rating of an entire power system, rather than the maximal current capacity of the cable itself as determined by the IEC standard for continuous operation. Consequently, a more conservative value for the rated current was selected, set at 30% below the cable's maximum rated capacity. Therefore, the rated current for our purposes has been determined to be 2000 A for the single core cable. The high-rated current is due to the large cross-section of the conductor.

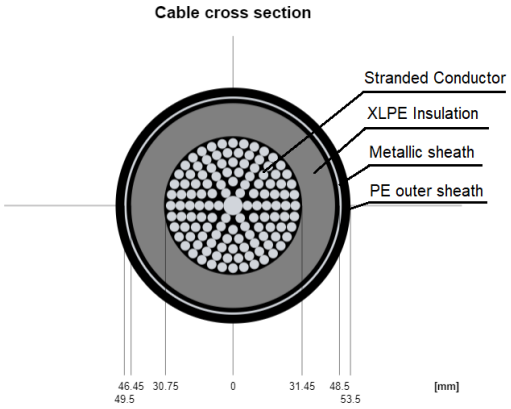

Figure 5.1: Example cable cross-section with dimensions from *Ampwise*

The cable comprises an aluminum conductor, XLPE insulation, an aluminum metallic sheath, and a protective polyethylene (PE) outer sheath. To distribute electrical stress uniformly across the cable insulation, thin semiconductive layers of XLPE/PE are situated between the conductor and the insulation, as well as between the insulation and the metallic sheath. Given their analogous material properties, this layer is treated as an insulation layer and is therefore included in the XLPE thickness in the calculations. The conductor strands are not modeled and the conductor is assumed to be a solid with the same outer diameter.

5.1.1. Analytical lumped parameter model

Based on IEC 60853 for cyclic loading and IEC 60827 for continuous loading, a method was implemented to calculate transient conductor temperatures. A MATLAB program was used to carry out the calculations as per the IEC standards. The MATLAB source code is available in Appendix A.

First, the material properties of the cable parts and the surrounding soil were specified. Thermal resistivity and specific heat for XLPE and PE were found in [32], while for copper, material properties were obtained from the Materials library in COMSOL. All material properties used in the calculations are recalled in Table 5.1.
The thermal equivalent for the single-core cable can be seen in Figure 5.2. A Python script is written to solve the temperature components, poles, and zeros of the ladder network, and the Python code is

	Thermal resistivity $[K \cdot m/W]$	**Density** $[kg/m^3]$	**Heat capacity** $[J/kg \cdot K]$
Aluminium	0.0042	2760	897
XLPE	3.2	930	1900
Semi-conductive screen	2.5	940	2300
PE	3.5	950	1900
Soil	0.82	1600	1180

Table 5.1: Material properties

available in A.8. The circuit (and the end capacitance) is a short circuit at the end. The capacitors in parallel can be added together to have a resulting 2 resistors and 2 capacitors, so a 2 loop system.

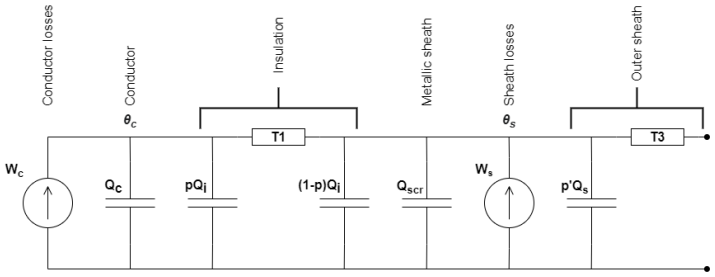

Figure 5.2: Long transient thermal equivalent ladder network of cable in Figure 5.1 directly buried

Based on the material properties in Table 5.1 and the cable dimensions recalled in Figure 5.1, the lumped parameters in the thermal equivalent circuit in Figure 5.2 were calculated from the equations described in subsection 3.1.2 and subsection 3.1.3. The calculated values can be seen in Table 5.2.

Q_c	7354.3	$[J/K \cdot m]$	T_1	0.2321	$[K \cdot m/W]$
Q_i	7808.8	$[J/K \cdot m]$	T_3	0.0433	$[K \cdot m/W]$
Q_{scr}	762.22	$[J/K \cdot m]$	p	0.4251	
Q_s	2336.3	$[J/K \cdot m]$	p'.	0.4871	

Table 5.2: Lumped calculated parameters

The transfer function can then be solved and simplified. The resulting poles, zeros, and T coefficients can be seen in Table 5.3.

P_1	-0.0044	$[s^{-1}]$	T_{11}	0.00037	$[K \cdot m/W]$
P_2	-0.0003	$[s^{-1}]$	T_{12}	0.275	$[K \cdot m/W]$
Z_1	-0.0043	$[s^{-1}]$			

Table 5.3: Lumped calculated parameters

Finally, the conductor temperature rise can be written as:

$$\theta_1(t) = W_c \sum_{j=1}^{n} T_{1j}(1 - e^{P_j t} = W_c[0.00037(1 - e^{-0.0044t}) + 0.275(1 - e^{-0.0003t})] \tag{5.1}$$

where W_c is the power loss per unit length in the conductor, which is calculated for each interval using Equation 3.18 and Equation 3.19. The conductor resistivity for aluminium is $2.826 \cdot 10^{-8}[\Omega m]$, the temperature coefficient α_{20} for aluminium is $0.00403[1/K]$, and the DC resistance at 20 °C is taken as $0.0000119\ [\Omega/m]$.

After solving the environmental transient for the laying condition and multiplying that by the attainment factor, finally, the Temperature Rise by Superposition (TRS) can be solved for every step with a certain resolution. The result will be the temperature profile for a certain current profile over time.

5.1.2. Numerical FEM model

Based on IEC 62095 for cyclic loading, the numerical model can be solved by completing the H, Q, and K matrices and solving for time using Equation 3.37. To fill in this matrix, first, a mesh is needed. So after the cable components are defined and the laying formation is visualized, the mesh can be generated with a certain precision. This defines all the nodes for which a value is found in the matrices.
The H matrix can be filled in using the thermal resistivity at each node. For world and ground nodes, the row will be set to all zeros except the diagonal index to one, then set as a Dirichlet boundary.
The Q matrix can be filled in using the heat capacity of the material present at the node. Like the H matrix, the row of the ground and world nodes is set to 0 except for the diagonal index, which is set to 1. For the K matrix, this sets the heat loss at each node. This is mostly 0, except for the nodes in the conductor, insulator, and sheath. For the world and ground nodes, the value is set at ambient temperature.

Afterwards, the end time and step size are chosen and the differential equation can be solved. During solving, the K matrix is also multiplied times the change in resistance due to temperature.

5.1.3. Validation with COMSOL

Both analytical and numerical methods will be compared with COMSOL to validate the practical usability of the method. The initial temperature is 15 °C. Three important scenarios are shown: (1) A long transient steady state load of 2000A, (2) A daily load profile, and (3) a short (10min) transient rise of 2000A.

The numerical model is chosen and implemented in the Web-based tool *Ampwise* section A.1. The cable generated in Ampwise can also be converted to a *.DXF* file that can be imported into COMSOL for quick modeling of the same cables.

The computation time for the numerical model is 2 min for COMSOL and 1 min for *Ampwise*.

1. **Long transient**: First, here a constant current of 2000A is applied to the cable for 1000 hours (≈ 42 days). Figure 5.3 shows the difference between the numerical model and the COMSOL model. The largest deviation of 1.3 °C under the COMSOL temperature occurs at the end after 1000h. Figure 5.4 shows the difference between the analytical model and the COMSOL model. Here there is always a deviation of more than 0.8 °C on the high side. The maximal deviation is in the short transient in the beginning where it rises asymptotically to 3 °C.

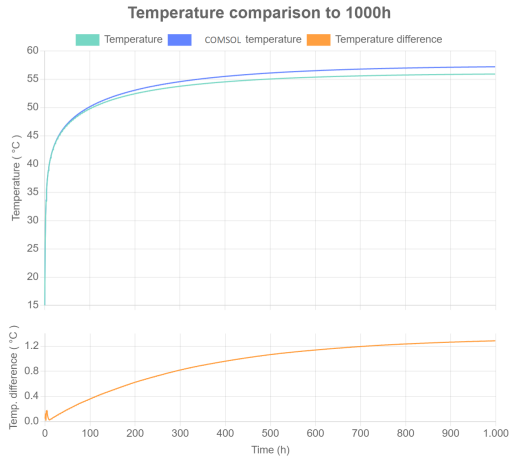

Figure 5.3: Long transient comparison between COMSOL and numerical model in *Ampwise*

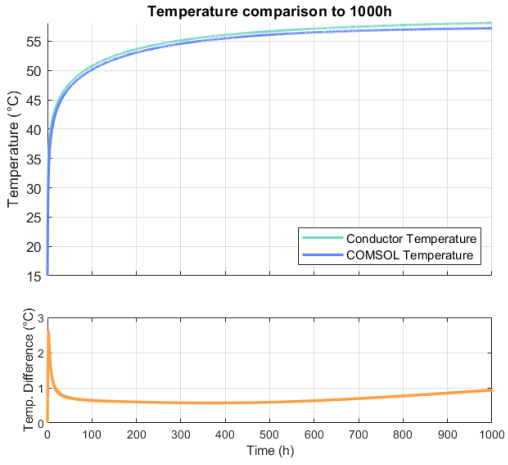

Figure 5.4: Long transient comparison between COMSOL and analytical model

2. **Daily load profile**: Second, here a daily load profile is applied to the cable, the current data can be seen in Table A.1. Figure 5.5 shows the difference between the numerical model and the COMSOL model. The largest deviation of 0.83 °C occurs during the steep rise from 290 to 1000A, on the safe side. Figure 5.6 shows the difference between the analytical model and the COMSOL model. The deviation here is also highest during the steep rise at around 3.2 °C.

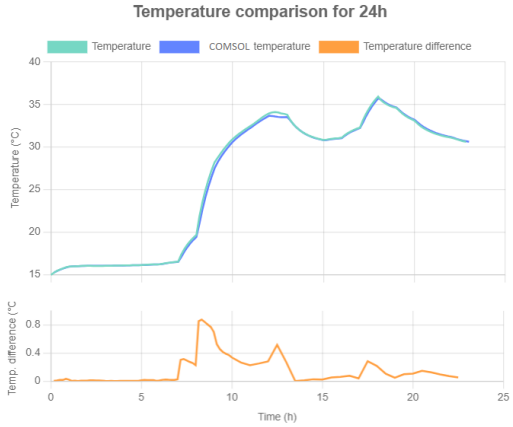

Figure 5.5: Daily load comparison between COMSOL and numerical model in *Ampwise*

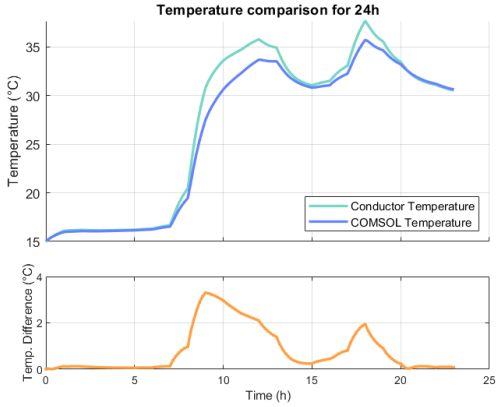

Figure 5.6: Daily load comparison between COMSOL and analytical model

3. **Short transient**: Last, here a constant current of 2000A is applied to the cable for 10 min. Figure 5.7 shows the difference between the numerical model and the COMSOL model. The largest deviation of 0.04 °C occurs in the end after 10min, on the safe side. Figure 5.8 shows the difference between the analytical model and the COMSOL model. The deviation rises relatively quickly to 6 °C.

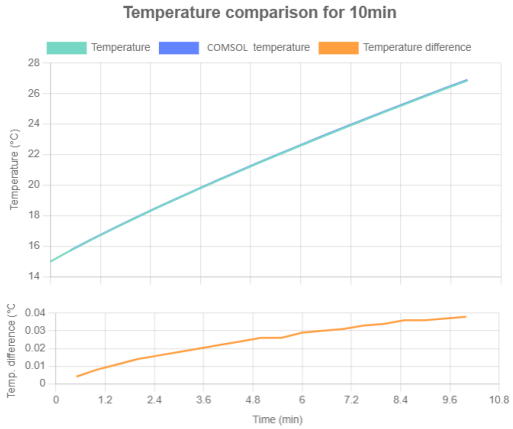

Figure 5.7: Short transient comparison between COMSOL and numerical model in *Ampwise*

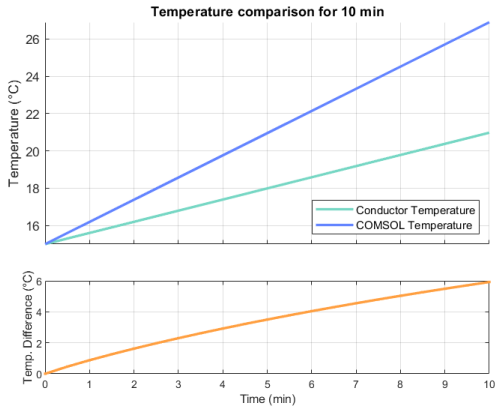

Figure 5.8: Short transient comparison between COMSOL and analytical model

Conclusion

The numerical method demonstrates a better match to the COMSOL model in all test cases, with smaller deviations in temperature predictions. This suggests that it has higher accuracy and is more reliable for both short- and long-term assessment of cable temperatures under varying electrical loads. This is expected since it inherently utilizes the same technology. The small discrepancies that are still present can be attributed to the difference in mesh quality. COMSOL has better refinement near the edges.

The analytical model, while useful, shows a larger margin of error, especially in the short term, which might limit its application in precision-critical scenarios. In the short term, this error might be due to the use of the steady-state Van Wormer coefficient p, instead of the dynamic Van Wormer coefficient.

Still, this should not solve for longer-term errors. The analytical model is 120 times faster to get the results than the numerical model; it can solve for the temperature in less than a second. For long load profiles, such as one year, this difference in computation speed could be useful. However, the accuracy lacks too much for this to be practically useful for dynamic scenarios.

The numerical model would be the recommended approach for detailed thermal analysis due to its overall higher accuracy in reflecting the complex dynamics of cable heating. From now on, only the numerical model will be used in this thesis.

5.1.4. Validation of model with CIGRE TB 880

To make the tool self-standing, the performance and characteristics of the numerical model in *Ampwise* are compared with those outlined in the CIGRE Technical Brochure 880 [41]. The comparison aims to highlight the differences in the results.

The Technical Brochure 880 covers 10 case studies for various scenarios with extended methodologies and results. It only covers steady-state ampacities calculated with IEC 60287 [5]. However, the numerical dynamic model can still be used to compare with steady-state scenarios to see if it will give a similar result after an extended amount of time when the temperature has saturated to a constant value to determine the ampacity.

The main difference in methodologies is that IEC 60287 converts the different layers (cable, soil, ...) into thermal resistances and the numerical model converts the whole domain into finite elements, so the thermal resistances are inherently an approximate value, but for simple cases with homogeneous materials, it can be considered a good model. A simple case is used to compare the accuracy of the FEM model.

Case #1 is chosen for comparison, since this scenario can be modeled in *Ampwise*. The other cases are in air, in ducts or in other formations that can not yet be modeled in the present version of the tool. This case study consists of two parts, the 132 kV cables in direct buried trefoil formation and in direct buried flat formation. The Trefoil scenario is chosen and the results can be seen below.

In *Ampwise*, steady-state ampacity is calculated iteratively using the simplified formula of Equation 3.37, excluding the Q term, until the conductor temperature is near the maximum temperature of the conductor (often $90°C$). This value of the current is then used in the time-dependent solver to obtain the dynamic temperature. A steady state with a temperature change of less than 0.001 degrees is often reached after a year, depending on the diffusivities of the materials. To ensure a steady state temperature, two years is chosen.

Finally, the main results of the tool are compared with the results of the case study, and the resulting ampacity is used in COMSOL as an additional verification of the numerical model.

Case study 1: 132kV cable directly buried

The selected cable type is a single-core extruded cable with copper round compacted conductors, XLPE insulation, copper wires screen, aluminum laminated foil and polyethylene sheath with an extruded semiconductive layer. The maximum conductor temperature is 90°C. The datasheet is shown in Figure 5.9.

Cable type	: XLPE 76/132kV 1x1200 mm2 copper	*Cable data sheet*
Standard	: IEC 60840	*25-apr-2019*

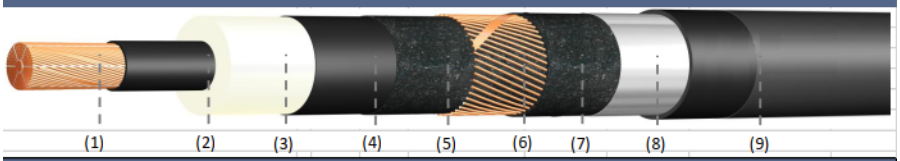

Cable construction		
Conductor	: (1)	Milliken compacted copper bare wires, bi-directional, water blocke
Conductorscreen	: (2)	semi-conducting tape + extruded semi-conducting compound
Insulation	: (3)	XLPE
Insulationscreen	: (4)	semi-conducting compound
Bedding	: (5)	semi-conducting swellable tape
Earthing screen	: (6)	copper round wires with counter helix of copper tape
Bedding	: (7)	semi-conducting swellable tape
Radial water	: (8)	aluminium laminate foil
Outer sheath	: (9)	black polyethylene jacket + extruded semi-conductive coating

Main dimensions and weight			Nominal thickness		Approx. Diameter	
Conductor	:				43,1	mm
Conductorscreen	:				46,7	mm
Insulation	:		16,1	mm	80,5	mm
Insulationscreen	:				82,9	mm
Swelling tape	:				84,3	mm
Earthing screen	:		57x1,77 mm lay-length of 500 mm		87,8	mm
Swelling tape	:				88,4	mm
Aluminum foil (excluding glue)	:				88,8	mm
Outer sheath	:		3,6	mm	97	mm
Outer semi-conductive coating	:		0,5	mm	98	mm
Cable weight	:	appr.	18,4	kg/m		

Electrical data			
Rated voltages Uo/U (Um)	:	76/132 (145)	kV
Conductor			
Maximum DC resistance at 20 °C	:	0,0151	Ω/km
Maximum temperature under normal conditions	:	90	°C
Maximum temperature under short circuit conditions	:	250	°C
Permissible short circuit current during 1 sec (adiabatic 90-250 °C)	:	>50	kA
Insulation			
Capacitance	:	0,25	µF/km
Charging current per core at Uo	:	6,0	A/km
Dielectric stress on conductor screen at Uo	:	6,2	kV/mm
Dielectric stress under insulation screen at Uo	:	3,7	kV/mm
Dielectric loss factor at Uo	:	<10	$*10^{-4}$
Earthing screen			
Maximum temperature in case of short circuit	:	180	°C
Permissible short circuit current (non-adiabatic 80-180 °C)	1s :	30,2	kA

Figure 5.9: Cable datasheet 1x1200 mm² CU/XLPE/CWS/PE 76/132 (145) kV [41]

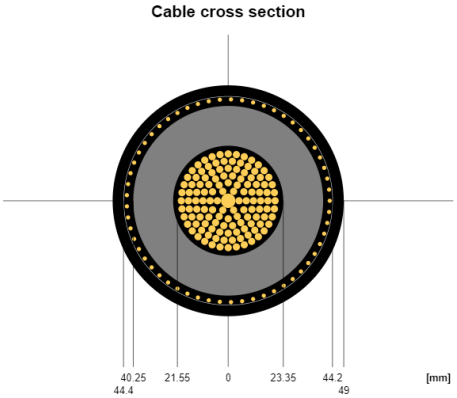

Figure 5.10: Cable model, Cross section in *Ampwise*

Trefoil formation
The three cables in the directly buried circuit are laid at a depth of 1 meter from the earth's surface to the center of the closed trefoil formation. The sheaths are solidly bonded at both ends. The soil around the cables has an ambient temperature of 20 $^{\circ}C$ and a thermal resistivity of 1 $K \cdot m/W$. The densities and heat capacities of all materials matter less now, since in a steady-state situation the speed of heat dissipation is irrelevant.

A cross section of the cable modeled in *Ampwise* can be seen in Figure 5.10 and the formation underground can be seen in Figure 5.11. The world radius is 10 meters, since then the world radius has hardly any influence on the cable. The Milliken strands are not modeled in the FEM model since that would create a large number of extra triangles while not necessarily increasing the accuracy of the model (see section 4.1). However, the cumulative area of the strands is taken into account in the calculation of the DC resistance and the sheath/armor losses.

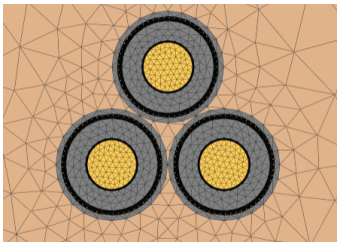

Figure 5.11: Cable model, layout formation in *Ampwise*

Calculating dielectric losses, AC resistance and sheath / armor loss factors is done as explained in the standard IEC 60287 for all methods. *Ampwise* is divided into steady-state and dynamic to verify both methods. The steady-state method calculates the final temperature using the steady-state version of Equation 3.37 ($\Theta = K \cdot H^{-1}$) to obtain the final nodal temperatures after an infinite amount of time when everything is saturated (no heat capacitances or densities are necessary for this equation since there is no matrix Q present). The dynamic method calculates the temperatures at certain time steps until a defined end time at which the heat diffuses away from the cable with a certain rate calculated using the full expression of Equation 3.37 ($\frac{\partial \Theta}{\partial t} = Q^{-1}(K - H\Theta)$). The dynamic *Ampwise* model is ran for 2 years since then, there is hardly any temperature change anymore (0.001 degrees every 3.6 days).
The results of this comparison of the CIGRE case study can be seen in Table 5.4.

Table 5.4: Results comparison CIGRE TB 880 Case 1

	Ampwise Steady state	***Ampwise Dynamic****	**CIGRE, Case #1**
DC Resistance, 90°C (Ω/km)	1.925		1.925
AC Resistance, 90°C (Ω/km)	2.215		2.215
Capacitance (F/m)	$2.55 \cdot 10^{-10}$		$2.55 \cdot 10^{-10}$
Dielectric loss (W/m)	0.465		0.465
Wire screen loss factor	0.589		0.589
Metallic sheath loss factor	0.202		0.202
Thermal resistance 1 (K.m/W)	**		0.379
Thermal resistance 2 (K.m/W)	**		0.012
Thermal resistance 3 (K.m/W)	**		0.0852
Thermal resistance 4 (K.m/W)	**		1.47
Steady-state Ampacity (A)	**982.74** (at 89.97°C)	**982.74** (at 89.88°C)	**990.54**
Conductor losses (W/m)	21.393	21.393	21.733
Wire screen losses (W/m)	12.6	12.6	12.799
Metallic sheath losses (W/m)	4.31	4.31	4.381

** Dynamic model, constant current for 2 years (17520h), to assume steady-state*
*** Calculated with FEM, no thermal resistance calculation necessary*

As expected, the DC/AC resistance, the dielectric loss, and the loss factors are all identical because they are calculated similarly. For CIGRE Case 1, the thermal resistances are calculated based on the

resistivities and their dimensions using Equation 2.1. The wire screen with 57 individual wires and a certain heat loss are also included in the calculation.

The steady-state and the long-term dynamic ampacity of Ampwise is 982.74A in both cases for a slightly different final temperature of 89.97°C and 89.88°C respectively. This ampacity has a 7.82A error (0.8%), compared to CIGRE. The difference can be attributed to a completely different way of calculating the ampacity. All individual wire strands, the metallic sheath and the core of all three touching cables have a coupling heat effect that affects each other. For the numeric model, boundary conditions are necessary, so a Dirichlet (constant temperature) is applied to all boundaries. The hottest temperature is found in the two lower cables, as the ground temperature is constant at 20 °C. Figure 5.12 shows the color map of the cables after 2 years of constant loading. The white lines are isothermal lines around the circuit.

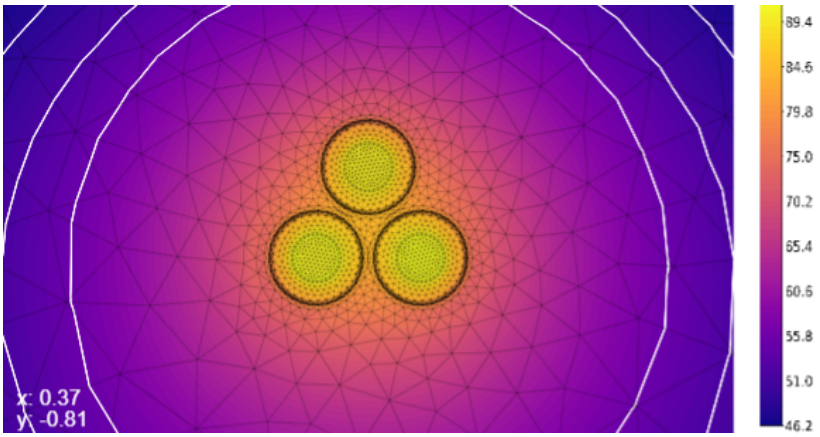

Figure 5.12: Color map of steady-state temperature after 1 year from *Ampwise*

In *Ampwise*, the steady-state calculation takes about half a second to calculate. The dynamic calculation takes around 1 minute to calculate.

Finally, COMSOL is used to give a second validation of the results using a numeric approach. The cable from *Ampwise* is imported into COMSOL in a trefoil configuration, the exact same materials and heat sources are applied and the mesh is generated. COMSOL has a better generated mesh, especially near the edges, it has refinement that *Ampwise* does not have. The study is run for 2 years and manual iteration is performed to obtain a steady state temperature of just under 90 °C. A value is found for the current at **981.8 A** for a final temperature of 89.8 °C. Figure 5.13 shows the conductor temperature for 1 year (to expand on the initial increase in temperature). The maximum temperature difference remains below 0.7 °C. The small difference present is due to the difference in mesh quality.

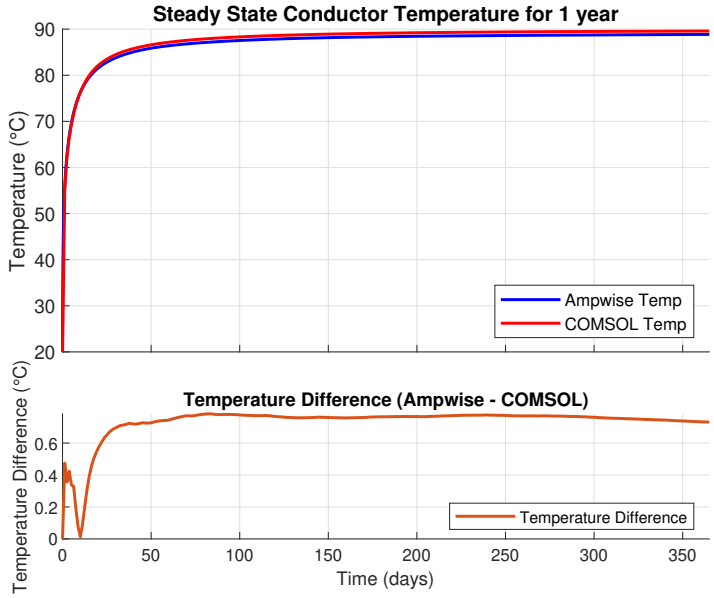

Figure 5.13: Steady state temperature comparison after 1 year

Conclusion

These results demonstrate the robustness and accuracy of the Ampwise tool in predicting cable ampacity under both steady-state and dynamic conditions. This illustrates that Ampwise is a reliable tool for such simulations. The steady-state ampacity and the dynamic long-term rating calculated by Ampwise shows only a 0.8% error compared to the CIGRE benchmark. Compared to COMSOL, both Ampwise methods have a 0.01% error, and can be considered identical. Despite the minor discrepancies observed between Ampwise, CIGRE, and COMSOL, the differences are within 1% which depending on the situation, can be considered acceptable. These variations can be primarily attributed to the different methodologies and boundary conditions applied in each simulation approach. The slight underestimation of ampacity by COMSOL compared to Ampwise and CIGRE could be due to the higher mesh refinement near the edges in COMSOL, which captures more detailed thermal gradients and may affect the overall temperature distribution and resulting ampacity. Overall, the COMSOL result can be considered more precise than the CIGRE result because of the use of the more complex numerical method that models the heat transfer equations.

In conclusion, Ampwise demonstrates a high degree of accuracy and reliability for both steady-state and dynamic cable rating calculations, aligning closely with established standards and advanced numerical tools like COMSOL.

5.2. Windpark Fryslân - a comparison with measured data

Finally, a comparative analysis of the cable temperatures predicted from *Ampwise*, against real-world monitored cable data is presented. Unlike previous comparisons with industry standards or numerical simulations using COMSOL, this analysis focuses on data collected from an actual operational environment. The temperature data was obtained from a distributed temperature system (DTS) monitoring a cable that connects the 316 MW Windplan Fryslân wind farm to the mainland.

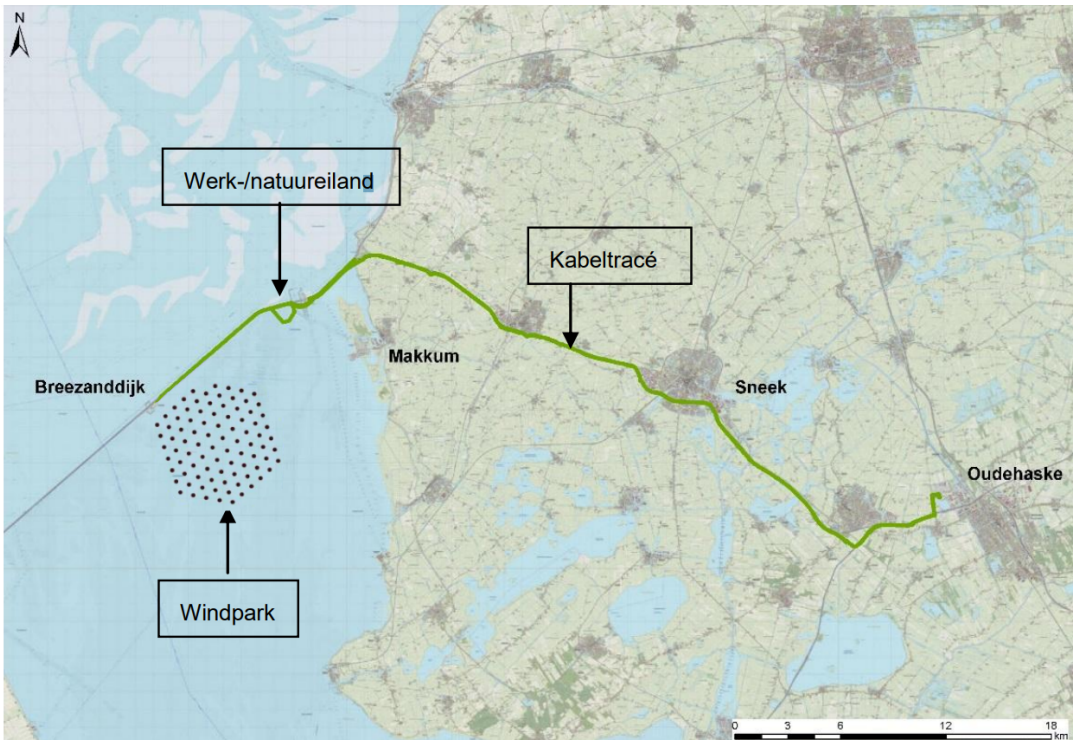

Figure 5.14: Location Windpark Fryslân and cable trace [42]

Figure 5.14 shows the location of Windpark Fryslân (WPF) and the cable trace to the mainland. WPF is a significant renewable energy project in the IJsselmeer. The wind farm comprises 89 turbines, each with a capacity of 4.3 megawatts (MW), totaling an annual production of approximately 1.5 TWh. In particular, Windpark Fryslân is the largest wind farm situated in inland waters worldwide. **Ventolines** served as project manager, overseeing the development and ensuring the successful completion of this project.

The cable trace starts at Breezanddijk on the Afsluitdijk, where two circuits of trefoil cables are buried ≈ 1 meter underground, surrounded with high quality backfill sand. Currently, the AC cables connect to a TenneT station in Bolsward, with a planned future extension to Oudehaske. The cable is a 110kV, 2500mm^2 cable from Prysmian, designed to carry at least 1010A under steady state conditions. The distance from Breezanddijk to Bolsward is approximately 24 km.

By comparing the predicted temperatures with real-world data, the precision of the dynamic rating tool *Ampwise*, can be validated. The monitored data capture variations in temperature due to both steady-state and transient load conditions, providing a robust dataset for validation. With knowledge of soil properties, laying formation, cable specifications and a load profile, *Ampwise* is able to predict time-dependent temperature variations of all the layers of the cable and the surrounding environment.

Next, the laying conditions are explained as well as the environmental parameters to compare the predicted numerical result with the real temperature measured from the DTS system.

5.2.1. Layout and environment

The layout formation consists of two circuits of trefoil-touching formation laying 1.1 meters below ground level as seen in Figure 5.15. All single-core cables are the same, except that the top cable in both circuits has a thermocouple inside to measure sheath temperatures. The cable datasheet can be found in Figure A.10 and a cross section is shown in Figure 5.16. It is a 110KV XLPE cable with an aluminium Milliken conductor. It has a rather large cross section of 2500 mm^2 and an aluminium metallic sheath that is cross-bonded. The circuits are spaced out by 1.5m and are directly buried and surrounded by high quality backfill sand with a relatively low thermal resistivity to dissipate heat quickly. The datasheet gives all the data to enter into the cable specification tab of the *Ampwise* tool.

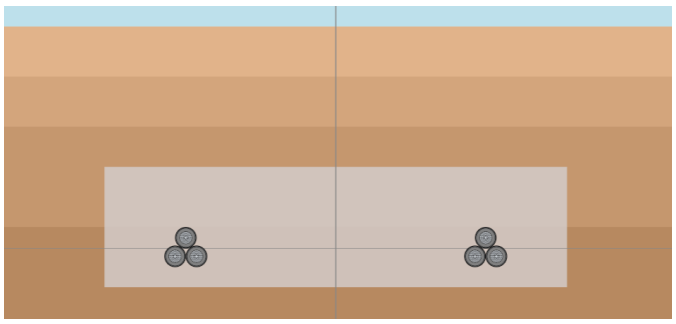

Figure 5.15: WPF circuit layout from *Ampwise*

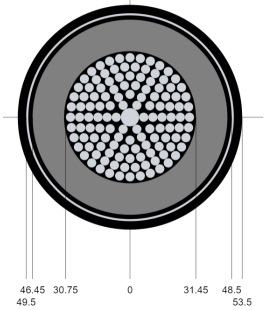

Figure 5.16: WPF cable from *Ampwise*

The material around the backfill depends on the location along the cable route. The Afsluitdijk has artificial material placed to keep the water out, so this will have a different thermal effect compared to the mainland. To determine hotspots (areas with increased temperature) and the thermal resistivity of the ground along the cable route, drillings can be performed. This creates a borehole and determines various parameters of the soil material such as porosity, degree of saturation / water level, and quartz content (sand). An empirical model like Horton's [20] can be used to calculate the thermal resistivity of the various soil layers at that location and time. Figure 5.17 shows an example drilling with labeled soil layers.

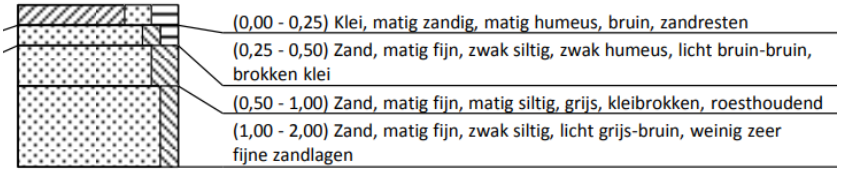

Figure 5.17: Drilling example

Figure 5.18 shows the results of such a drilling for two samples at a depth of 1.9m and 1.35m. At the end, the resulting thermal resistivity of that soil is given as well as the diffusivity of that soil. From the diffusivity, the thermal resistivity, and the moisture content, the heat capacitance can be calculated using Equation 3.13. This gives all the data to enter into the *Ampwise* tool for the Laying formation.

Sample number	Depth in relation of surface level	Depth in relation of NAP	Material	Moist unit mass	Dry unit mass	Moisture content as mass %	Porosity	Degree of saturation	Moist thermal resitivity, measured	Moist thermal resistivity, calculated	Saturated thermal resistivity, calculated	Representative thermal diffusivity	Minimum degree of saturation	Representative thermal resistivity	Representative thermal diffusivity
	m	m		γ_{wet} kg/m^3	γ_{dry} kg/m^3	w %	n %	S_r %	g m.K/W	g m.K/W	g m.K/W	δ m^2/s	S_r %	R_λ m.K/W	δ m^2/s
5	0,90	3,82	sand	1592	1473	8,1	43,3	27,5		0,68	0,41	8,1E-07	10	1,15	6,2E-07
6	1,35	3,37	sand	1726	1577	9,4	39,7	37,3	0,55	0,54	0,37	9,0E-07	10	1,06	6,5E-07

Figure 5.18: Drilling details

5.2.2. Measuring cable temperature - DTS system

Next, a load profile and some data to compare the predicted temperature are necessary. The DTS system supplies the measured temperature data.

The distributed temperature sensing (DTS) system installed on both circuits (black and white) of the WPF outputs the temperature at various parts along the cable trace. The temperature varies depending on where the thermocouple is placed, and the conductor temperature often needs to be extrapolated if it is not placed near the conductor. Often the conductor, wire screen, and thermocouple are laid conically and with a certain lay length, meaning that it spirals inside (to make the cable bend easier). This makes the temperature also differ depending on whether the thermocouple is close to other heat sources or far away, so averages are taken for segments of the cable trace.

The output of the DTS system is a list of fiber and conductor temperature readings over time for various segments along the cable trace along with the corresponding current value. The current is not the same for every location due to losses. Afsluitdijk 1 is randomly chosen as the location to make the comparison. The time step of the data is on average every 30 minutes. The fiber temperature is the measured data. The conductor temperature is the extrapolated temperature of the conductor.

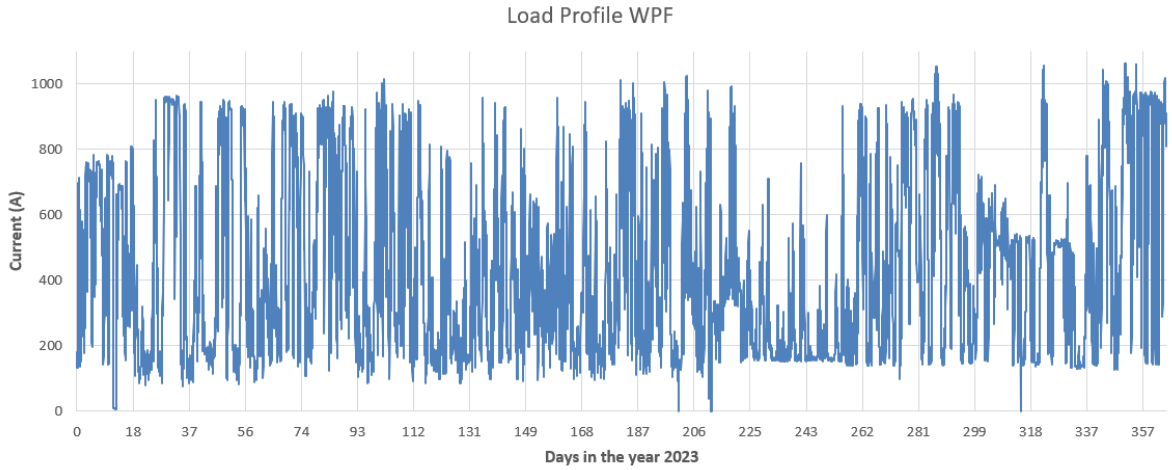

Figure 5.19: Current profile for WPF, 2023

In this report, a temperature comparison is performed for the full year of 2023 to visualize the seasonal changes with output steps every 30 minutes.

5.2.3. Weather data

To complete the operational info page of *Ampwise*, the weather profile can be included for the desired interval for which the solver needs to solve. With weather, this means the air temperature, the pressure, the solar radiation, and the precipitation for every hour or day, fetched from *Visual Weather Crossing*. Currently, the tool only works with the air temperature and solar radiation (the pressure has shown to not improve the model, see Figure 4.10). Figure 5.20 shows the air temperature for 2023 where the blue graph is the average of the days (365 points in total). This data is used in the model to calculate the heat flux and apply to the convective ground layer. In this case, the average air temperature fluctuates between 24 in summer and -1.2 °C in winter. The trendline is a fourth degree polynomial approximating the average temperature since this trendline can approximate a cosine that is not exactly one period and a temperature slope if the previous winter would be cooler or warmer than the current one for example. Only the average daily temperature is used in the model (blue line).

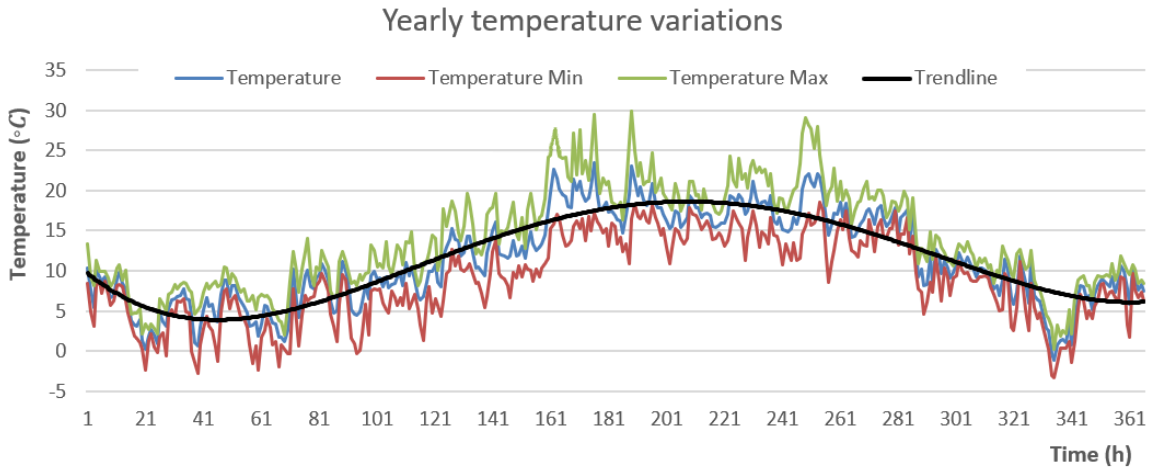

Figure 5.20: Yearly temperature trend, Data from *Visual Crossing Weather*

Next, solar radiation is incorporated into the model as a boundary heat source. As seen in Figure 5.21, during summer, the maximum solar radiation reaches 1100 W/m^2, while in winter it peaks at 120 W/m^2. Daily solar energy data are retrieved from *Visual Crossing weather* and transformed into daily bell curves. These curves are connected to form a continuous dataset for the entire year, resulting in 86400 values, representing each hour. An absorb factor of 0.3 is used

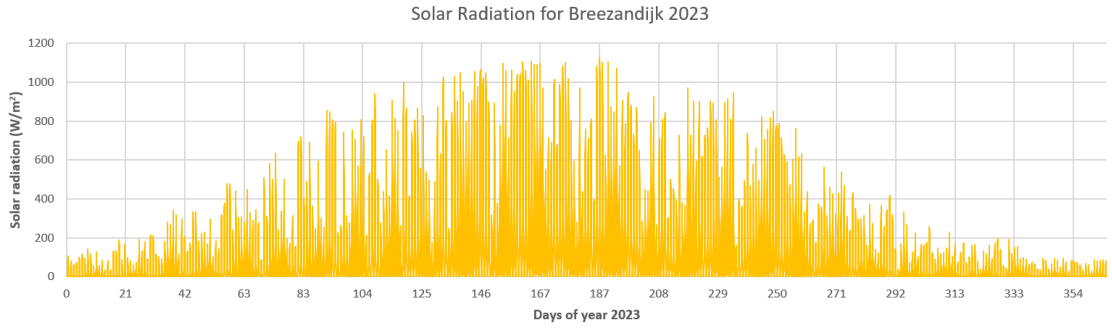

Figure 5.21: Yearly solar radiation for 2023 from *Visual Crossing Weather*

Finally, the initial temperature must be defined. The dataset begins January 1, 2023. As described in subsection 3.2.4, the ground temperature gradient changes with depth. Figure 5.22 illustrates the initial ground gradient, showing that at a depth of 1.1 meters, the cables have a starting temperature of approximately 12.1 °C. During this period, the current was very low, allowing the cable to cool to its surrounding temperature. The monitored data indicate that the fiber temperature was 12.3 °C and the conductor temperature was 12.5 °C. Therefore, this initial ground gradient serves as an accurate

approximation.

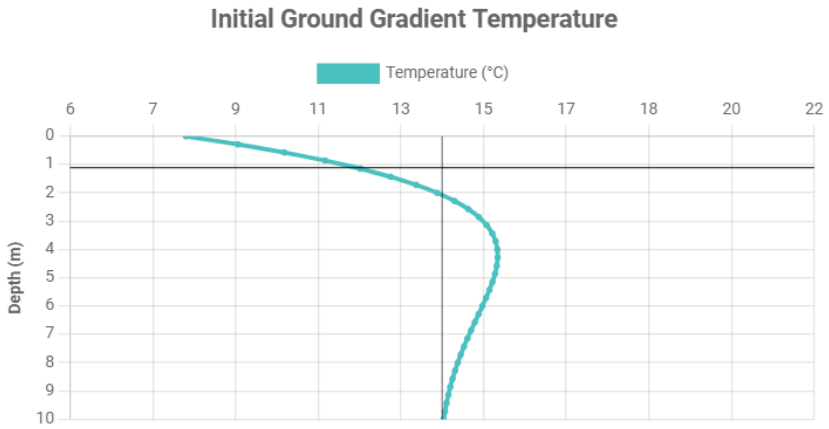

Figure 5.22: Initial ground gradient from *Ampwise*

This completes the input phase of the Ampwise tool. Next, a solver is selected and the computation can be performed. The computation time depends primarily on the complexity of the mesh and on the strength of the CPU in the computer that runs the Python server code. For an Intel Core i5-6400 CPU, the server took 6 hours to complete the entire year.

5.2.4. Comparison

The comparison between the measured DTS temperature and the predicted temperature for Windpark Fryslân (WPF) in 2023 reveals several key observations. Two comparisons are made, one with the extrapolated conductor temperature and one with the real measured fiber temperature.

Figure 5.23 shows the comparison between the predicted and measured conductor temperature. Figure 5.24 shows the comparison between the predicted and measured fiber temperature where the thermocouple is laid.
As depicted in both graphs, the predicted temperatures aligns closely with the measured data, particularly in terms of the long transient and seasonal changes. This suggests that the model is effective in capturing the broader temperature trends over extended periods.

However, the rate of temperature change in the short term is noticeably higher for the measured temperatures compared to the predicted values in both cases. This discrepancy indicates that while the model can accurately predict long-term trends, it lacks the rapid fluctuations observed under real-world conditions.

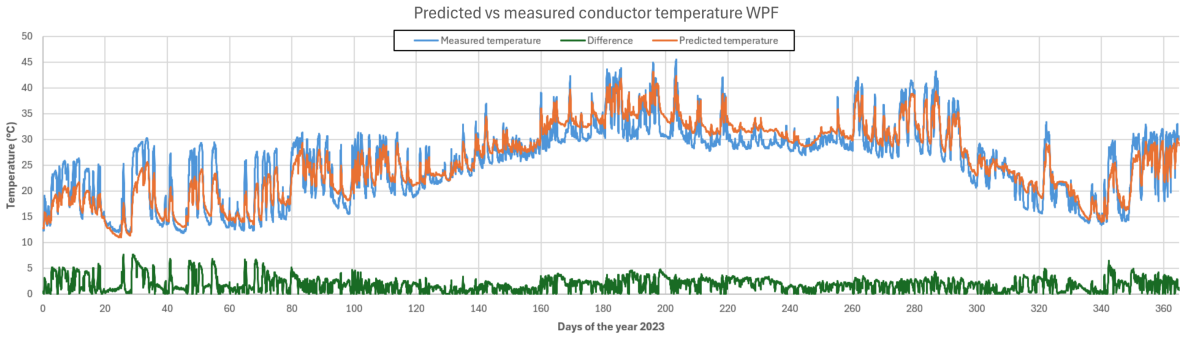

Figure 5.23: Measured vs Predicted conductor temperature for WPF 2023

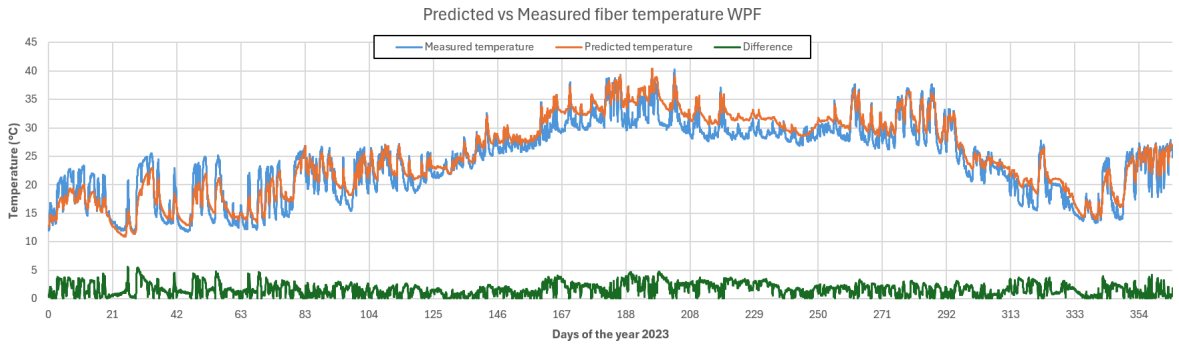

Figure 5.24: Measured DTS vs Predicted fiber temperature for WPF 2023

The green graph displays the absolute difference between the graphs. The quantitative comparison presented in Table 5.5 further supports these findings (section A.2 explains the comparison metrics in detail).
The mean absolute error (MAE) is 1.92°C/1.67°C, and the root mean square error (RMSE) is 2.34°C/1.98°C for the conductor and fiber comparison, respectively. The mean error of 0.27°C/0.86°C and a coefficient of determination (R^2) of 0.886/0.9 indicate a strong correlation between the predicted and measured temperatures. However, the maximum observed difference of 7.74°C/5.6°C at 25.9 hours highlights the limitations of the model in capturing short-term temperature spikes.

Table 5.5: Results comparison Predicted and measured conductor temperature

Comparison Metric	Conductor metrics	Fiber metrics
Mean Absolute Error (MAE)	1.92 °C	1.67 °C
Mean error	0.27 °C	0.86 °C
Root Mean Squared Error (RMSE)	2.34 °C	1.98°C
Mean Average Percentage (MAPE)	7.78 %	7.29 °C
Max difference	7.74 °C (at 25.9h)	5.6 °C (at 25.9h)
Coefficient of determination (R^2)	0.886	0.9

The higher rate of change in the real measured temperatures compared to the predicted values could be attributed to several factors:

- **Thermal Properties of Surrounding Soil**: The cable may heat up the ground near it, creating a dry zone with lower heat capacitance and density. This would result in a lower thermal mass, causing the temperature to change more rapidly.
- **Modeling Assumptions**: The model's assumptions about the conductor's thermal properties might be oversimplified. Real conductors, especially stranded ones, can exhibit more rapid heating and cooling due to their structure, which is not perfectly captured in the model.
- **Measurement Extrapolation**: The conductor temperature is extrapolated from the fiber temperature. If this extrapolation is too aggressive, it might fail to capture the rapid fluctuations seen in the real measurements.
- **Environmental Variability**: Short-term environmental variations, such as sudden changes in weather conditions or microclimatic effects, can cause rapid temperature changes that the model, which uses averaged inputs, might not fully account for.

Figure 5.25 shows the colormap from *Ampwise* at the last timestamp. The influence of the backfill can be seen in the isothermal lines.

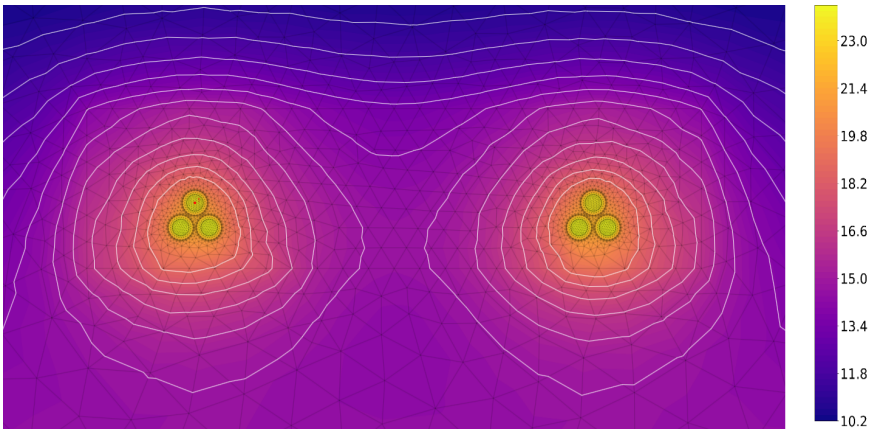

Figure 5.25: Colormap of WPF of last timestamp, from *Ampwise*

Chapter conclusion

The comparative analysis of cable temperatures predicted by the *Ampwise* tool against real-world data from the Windpark Fryslân project has provided valuable insights. The model accurately predicts long-term temperature trends and seasonal variations for both conductor and fiber temperatures, with high correlations (R^2 of 0.886 and 0.9, respectively) between predicted and measured temperatures. The mean absolute error (MAE) of 1.92°C for the conductor and 1.67°C for the fiber, and the root mean square error (RMSE) of 2.34°C for the conductor and 1.98°C for the fiber, are within acceptable ranges for long term thermal modeling.

However, the model struggles with short-term temperature fluctuations, likely due to oversimplified assumptions about thermal properties and environmental variability. This discrepancy is evident in both the conductor and fiber temperature comparisons. Despite this, *Ampwise* performs well in predicting long-term thermal behavior.

This case study validates *Ampwise* as a reliable tool for dynamic cable rating in operational environments. Future refinements could improve short-term prediction accuracy, further enhancing its utility to manage cable temperatures in large-scale renewable energy projects such as Windpark Fryslân. The inclusion of fiber temperature data further strengthens the analysis, providing a comprehensive understanding of the thermal dynamics at play.

6

Conclusion

The objective of the master thesis to improve the dynamic cyclic rating predictions for cable temperatures using the finite element method is met. The key findings of the thesis are:

- The integration of comprehensive dynamic weather data and detailed soil thermal properties provides the most accurate technique for modeling temperature in underground power cables.
- Incorporating real-time weather data, including air temperature and solar radiation, significantly enhances the accuracy of predicted cable temperatures, reducing the maximum deviation from measured data during peak summer conditions.
- The developed model compares favorably with established models such as CIGRE and COMSOL, providing comparable predictive accuracy. In steady state scenarios, Ampwise has a 0.01% error to COMSOL and can be considered identical. Compared to the CIGRE benchmark, a 0.8% error is present.
- Sensitivity analysis reveals that higher soil thermal resistivity leads to significantly higher conductor temperatures, with soil thermal resistivity of 1.5 $K \cdot m/W$ leading to conductor temperatures around 19.5°C, compared to 17.5°C for 0.7 $K \cdot m/W$.
- The initial ground temperature gradient plays a crucial role in influencing the thermal profile of the cable throughout the simulation period and outperforms models that assume constant temperature conditions.
- The numerical method demonstrates a better match to the analytical model in all test cases, with smaller deviations in temperature predictions, suggesting higher accuracy and reliability for both short- and long-term assessments. With steady-state current and dynamic method errors within acceptable ranges compared to CIGRE and COMSOL.
- The *Ampwise* tool improves the precision and usability of dynamic cable rating predictions by incorporating real-time weather data and detailed modeling capabilities. It simplifies the process of building cable configurations and layouts, and facilitates easy comparison with measured data.
- The *Ampwise* tool's prediction for long-term temperature trends and seasonal variations in the Windpark Fryslân project shows a high correlation with measured data, with an acceptable mean absolute error of 1.9 °C and root mean squared error of 2.3 °C for the conductor temperature comparison.
- The model's performance in predicting short-term temperature fluctuations is less accurate compared to the rate of change of the measured data, likely due to oversimplified assumptions about thermal properties and environmental variability.

7

Further work

The *Ampwise* tool can be improved in various ways by adding new features, fixing current features, or making the tool more user-friendly. In the scope of this thesis, not all fixes could be patched and not all non-essential features could be implemented into the tool.

First, it is handy to figure out why the rate of change is higher in real measured data and try to model it in Ampwise to get similar results.

One handy future improvement would be the reverse process of the current one. A desired ampacity or temperature profile is entered and the output is the best cable for that situation from a certain list of cables.

Adding precipitation to the model and the link between rainfall and moisture content would also be valuable. This would dynamically change the thermal resistance and heat capacitances to account for moisture in the ground rather than using an average.

Ampwise could also improve by making it possible to model cables in ducts, water, open-air or other special situations.
To make the tool practical, it would be handy if it could automatically generate a PDF report with all the findings, graphs, and conclusions.

Finally, some of the optional improvements and fixes are listed in the Appendix. section A.3 lists the improvements that could be made to the UI and the computations but were not within the scope of the thesis to finish or there was not enough time. Improvements such as a more complete importing mechanism and adding precipitation would greatly improve the user experience and accuracy of the tool. section A.4 lists the fixes that the tool needs to make the tool better in general, such as adding an axis to the graphs or refinement in the mesh.

Bibliography

[1] D. A. Douglass and A.-A. Edris, "Real-time monitoring and dynamic thermal rating of power transmission circuits," *IEEE Transactions on Power Delivery*, vol. 11, no. 3, pp. 1407–1416, Jul. 1996.

[2] E. Fernandez, I. Albizu, M. Bedialauneta, A. Mazon, and P. Leite, "Review of dynamic line rating systems for wind power integration," *Renewable and Sustainable Energy Reviews*, vol. 53, pp. 80–92, 2016, ISSN: 1364-0321.

[3] CIGRE Working Group B1.45, "Thermal monitoring of cable circuits and grid operators' use of dynamic rating systems," International Council on Large Electric Systems (CIGRE), Tech. Rep., Feb. 2019, In B1 Insulated cables, Technical Brochure 756.

[4] J. H. Neher and M. H. McGrath, "The calculation of the temperature rise and load capability of cable systems," *Transactions of the American Institute of Electrical Engineers. Part III: Power Apparatus and Systems*, vol. 76, no. 3, pp. 752–764, 1957. DOI: 10.1109/AIEEPAS.1957.4499653.

[5] *NEN-IEC 60287-1-1: Electric cables - Calculation of the current rating - Part 1-1: Current rating equations (100 % load factor) and calculation of losses - General*, English and Dutch, International Standard, Standard, International Electrotechnical Commission, Jun. 2023.

[6] *NEN-IEC 60287-2-1:2023*, English, International Standard, Standard, International Electrotechnical Commission, 2023.

[7] *NEN-IEC 60853-1: Calculation of the cyclic and emergency current rating of cables - Part 1: Cyclic rating factor for cables up to and including 18/30 (36) kV*, English, International Standard, Standard, International Electrotechnical Commission, Mar. 1985.

[8] *NEN-IEC 60853-2: Calculation of the cyclic and emergency current rating of cables - Part 2: Cyclic rating of cables greater than 18/30 (36) kV and emergency ratings for cables of all voltages*, English, French, International Standard, Standard, International Electrotechnical Commission, Oct. 1989.

[9] G. J. Anders, *Rating of Electric Power Cables in Unfavorable Thermal Environment*. IEEE Press and Wiley-Interscience, 2005, ISBN: 0-471-67909-7.

[10] D. Vree, S. Vink, J. Van Doeland, and F. de Vries, "Ampacity calculation method for deeply buried wind farm ac submarine export cables," The Netherlands, Tech. Rep., 2018.

[11] C. Bates, K. Malmedal, and D. Cain, "Cable ampacity calculations: A comparison of methods," *IEEE Transactions on Industry Applications*, vol. 52, no. 1, pp. 112–118, 2016.

[12] T. V. M. Nielsen, S. Jakobsen, and M. Savaghebi, "Dynamic rating of three-core xlpe submarine cables considering the impact of renewable power generation," 2024.

[13] M. P. Gazzana-Priaroggia, "Computer method for the calculation of the response of single-core cables to a step function thermal transient," *Electra*, vol. 87, pp. 42–53, 1987.

[14] H. Brakelmann and G. J. Anders, "Transient thermal response of power cables with temperature dependent losses," *IEEE Transactions on Power Delivery*, Sep. 2020. DOI: 10.1109/TPWRD.2020.3026779.

[15] D. Mushamalirwa, "A 2-d finite element mesh generator for thermal analysis of underground power cables," *IEEE Transactions on Power Delivery*, vol. 3, no. 1, Jan. 1988.

[16] E. Eberg, K. Espeland, S. M. Hellesø, S. Hvidsten, and K. T. Solheim, "Development of a web-based user-friendly cable ampacity calculation tool," in *25th International Conference on Electricity Distribution*, CIRED, Madrid, Spain, 2019.

[17] D. Aegerter, "Calculation of cable thermal rating using a hybrid method based on iec 60287 and finite element method," in *11th International Conference on Insulated Power Cables (Jicable'23)*, Jicable, Lyon, France, 2023.

[18] G. Anders, M. Chaaban, N. Bedard, and R. Ganton, "New approach to ampacity evaluation of cables in ducts using finite element technique," *IEEE Transactions on Power Delivery*, vol. PWRD-2, no. 4, Oct. 1987.

[19] N. Flatabø, "Transient heat conduction problems in power cables solved by the finite element method," in *IEEE Power Engineering Society Summer Meeting*, (The Norwegian Institute of Technology, Division of Electrical Power Engineering, Trondheim, Norway), IEEE, San Francisco, CA: IEEE, Jul. 1972.

[20] S. Lu, T. Ren, Y. Gong, and R. Horton, "An improved model for predicting soil thermal conductivity from water content at room temperature," *Soil Science Society of America Journal*, vol. 71, no. 1, pp. 8–14, 2007.

[21] F. Suárez, M. Hausner, J. Dozier, J. Selker, and S. Tyler, "Heat transfer in the environment: Development and use of fiber-optic distributed temperature sensing," in Sep. 2011, ISBN: 978-953-307-569-3. DOI: 10.5772/19474.

[22] P. N. B.V., "Basic design 110 kv export cable part 2b," Windpark Fryslân BV, Technical Report, Feb. 2020.

[23] "IAC - DTS Design Report," Windpark Fryslân BV, Netherlands - Fryslân, Technical Report, Oct. 28, 2020.

[24] "Design DTS-RTTR system WPF Fryslân," Windpark Fryslân BV, Netherlands - Fryslân, Technical Report, May 16, 2019.

[25] H. J. Li, K. C. Tan, and Q. Su, "Assessment of underground cable ratings based on distributed temperature sensing," *IEEE Transactions on Power Delivery*, vol. 21, no. 4, pp. 1763–1769, 2006.

[26] J. van Oosterom, "Wp groen - dynamische berekeningen," Windplan Groen, Technical Report, Nov. 2022.

[27] TKF, "Ampacity calculation for all hotspots - 240mm2 and 400mm2 cables," Windpark Fryslân, Technical Report, Nov. 2019.

[28] TKF, "Ampacity calculation - 630mm^2 cables," Windpark Fryslân, Technical Report, Apr. 2020.

[29] F. Arends, "Cable design 33 kv export cables wp groen," Windplan Groen, Technical Report, May 2021.

[30] M. Verheijen, "Cable calculation - 33kv transformer cables," Hitachi Power Grids, Technical Report, Jun. 2021, Windplan Groen project, Dronten Olsterpad site.

[31] B. Klomp, "Design calculations wp hanze," Van den Heuvel Aannemingsbedrijf BV, Technical Report, Oct. 2022, Project: Windpark Hanze.

[32] G. Anders, *Rating of Electric Power Cables: Ampacity Computations for Transmission, Distribution, and Industrial Applications* (IEEE Press power engineering series). McGraw-Hill, 1997, ISBN: 9780070017917.

[33] P.-Y. Wang, H. Ma, G. Liu, *et al.*, "Dynamic thermal analysis of high-voltage power cable insulation for cable dynamic thermal rating," *IEEE Access*, vol. 7, pp. 56 095–56 106, 2019. DOI: 10.1109/ACCESS.2019.2913704.

[34] R. J. Millar, "A Comprehensive Approach to Real Time Power Cable Temperature Prediction and Rating in Thermally Unstable Environments," Nov. 2006.

[35] O. T. Farouki, "Thermal properties of soils," pp. 81–1, Dec. 1981.

[36] T. E. ToolBox, *Specific heat capacity of materials*, https://www.engineeringtoolbox.com/specific-heat-capacity-d_391.html, 2024.

[37] H. Goldenberg, "Thermal transients in linear systems with heat generation linearly temperature-dependent: Application to buried cables," *Proceedings of the Institution of Electrical Engineers*, vol. 114, no. 3, p. 375, 1967. DOI: 10.1049/piee.1967.0081.

[38] "Electric cables - calculations for current ratings - finite element method," International Electrotechnical Commission, Geneva, Switzerland, Tech. Rep. IEC/TR 62095:2003, Oct. 2003.

[39] M. Lees, "A linear three-level difference scheme for quasilinear equations," *Maths. Comp.*, vol. 20, pp. 516–622, 1966.

[40] F. P. Incropera, D. P. DeWitt, T. L. Bergman, and A. S. Lavine, *Fundamentals of Heat and Mass Transfer*, 6th ed. John Wiley & Sons, 2007, ISBN: 978-0-471-45728-2.

[41] CIGRE Working Group, "Dynamic rating systems," International Council on Large Electric Systems (CIGRE), Paris, France, Technical Brochure TB 880, 2022.

[42] Ventolines and Zuiderzeewind, *Windpark fryslân*, `https://www.windparkfryslan.nl`, 2021.

[43] International Electrotechnical Commission, *NEN-IEC 60287-3-3: Electric cables - Calculation of the current rating - Part 3-3: Sections on operating conditions - Cables crossing external heat sources*, International Standard, Geneva, Switzerland, May 2007.

A

Appendix

A.1. User Interface - Ampwise

For this master's thesis, a web-based tool is developed to facilitate dynamic and interactive cable rating calculations. This tool, now known as *Ampwise*, enables users to easily modify input parameters and visualize results in a user-friendly format. The primary objective of *Ampwise* is to streamline the process of calculating the dynamic or steady state current carrying capacity (ampacity) of electrical power cables under various conditions.

The user interface (UI) of *Ampwise* is organized into several tabs, each dedicated to a different stage of the cable rating process. Specifically, there are three tabs to input different types of data and two tabs to view the results. This organization helps to manage the complexity of the calculations and present the information in a logical sequence.

Below the tabs, a console is present, showing important information about the server status and progress, so that the user has an idea of what the server is doing or what has gone wrong.

The interface is designed to be intuitive for the user, with dropdown buttons, sliders, and input boxes to accommodate various data types, and presets are proposed. However, the user still can input custom materials or values. This tool can be considered a black box, so no manual calculations should be necessary to use it, compared to COMSOL where all necessary calculations should be known and done in advance, and a know-how of cable heating is needed.

The tool can be started by double clicking on the *Ampwise.bat* file. This will automatically install all necessary packages and start the program in the Web browser. The process takes around 30 seconds to boot up.

The tool works on any browser and scales based on resolution, scrollbars appear when the boxes cannot be fully displayed.

The tabs are explained in detail below.

A.1.1. Cable specification

The Cable Specification tab is the starting point for defining the dimensional, thermal, and electrical properties of the cable used in the calculations.

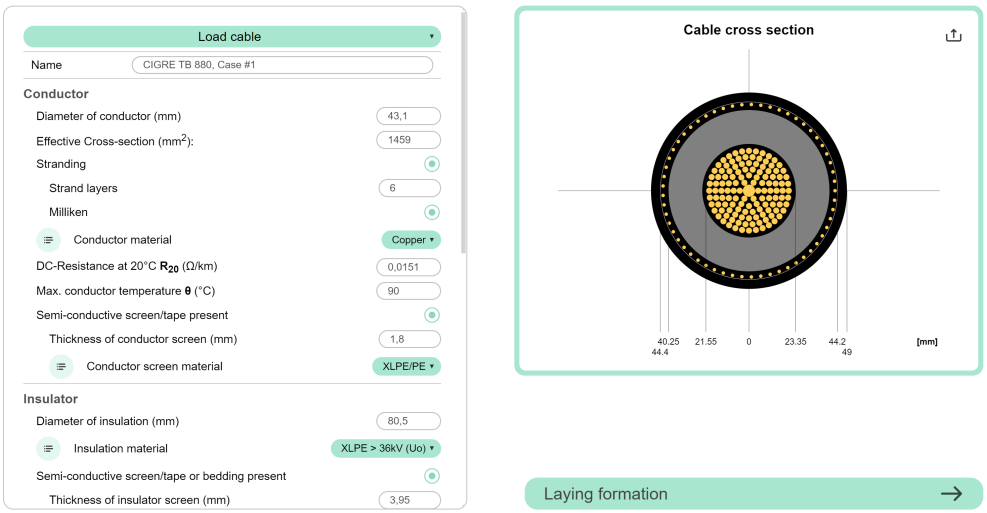

Figure A.1: Cable Specification tab of *Ampwise*

As shown in Figure A.1, the Cable Specification tab allows users to input several key parameters about the cable, including the following:

- **Conductor**: Diameter, Stranding Milliken, Effective cross section (area due to strands), Material (copper or aluminium), DC-resistance at 20°C, max temperature
  - **Conductor screen**: Thickness and material (Carbon black, Graphite, XLPE/PE, EPR)
- **Insulator**: Diameter, material (EPR <= 36kV (Uo), EPR > 36kV (Uo), PVC, XLPE <= 36kV (Uo), XLPE > 36kV (Uo), PE)
  - **Insulator screen**: Thickness and material (Carbon black, Graphite, XLPE/PE, EPR)
- **Metallic Sheath**: Thickness, bonding (Single-end, both-end/solid, cross bonded), material (Copper, Aluminium, Lead, StainlessSteel, Bronze, Steel)
- **Armor**: Outer diameter, material (Copper, Aluminium, Lead, StainlessSteel, Bronze, Steel), Wire screen option, wire count, lay length, wire diameter
- **Outer sheath**: External diameter, material (EPR <= 36kV (Uo), EPR > 36kV (Uo), PVC, XLPE <= 36kV (Uo), XLPE > 36kV (Uo), PE)

Only a conductor and insulator is needed for a completed cable, the rest are optional.

In addition, cables can be saved and loaded, so the user does not have to fill in everything all the time and can load in previously made cables. These cable presets are saved in the browser and can be given a name by the user. If the user opens the tool in another browser, the cables will not be present.

To the right of the input section, a cable preview is present where the cable can be seen based on the dimensions and materials that the user has entered with the radii on the bottom. Furthermore, the developed cable and all its layers and optional wire screen can also be exported to a DXF file using the export button in the cable view. This 2D DXF file can be imported into other CAD software or COMSOL. This makes the modeling workflow easier since all the individual wire screen cables do not have to be manually entered.

When the cable is completed, the user can go to the next tab.

A.1.2. Layout formation

The Layout Formation tab allows users to define the geometric arrangement of the cables as well as the environmental conditions to which they are exposed.

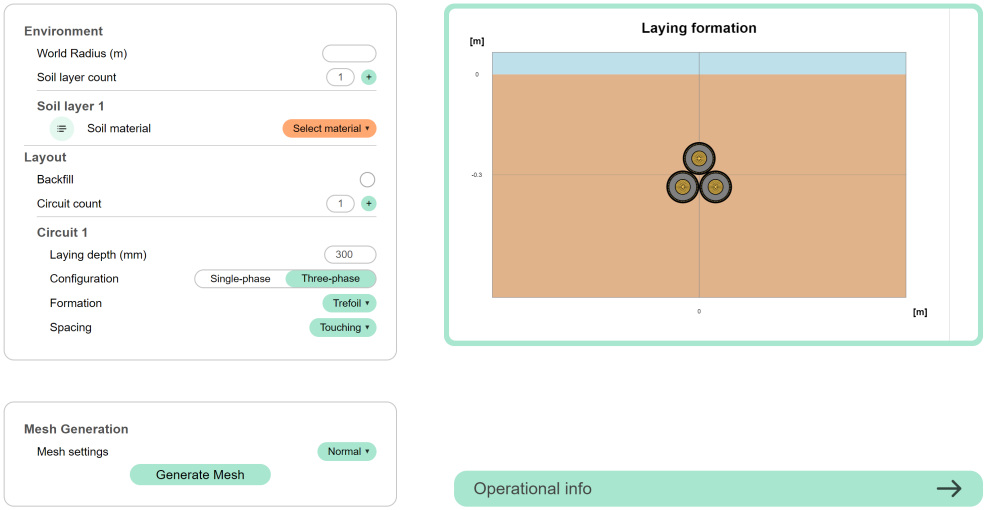

Figure A.2: Laying formation tab of *Ampwise*

As illustrated in Figure A.2, the Layout Formation tab provides a range of inputs that allow users to customize the spatial configuration of the cables and the surrounding environment. Here are the key features and inputs provided in this tab:

- **Environment**: World radius, Soil layer count, Soil layer material, soil layer depth
- **Layout**: backfill option, backfill material, backfill depth, backfill width, backfill height, circuit count, distance between circuits, circuit laying depth, circuit configuration (single-phase, three-phase), Formation (Trefoil, Flat-horizontal, Flat-vertical), spacing (touching, not-touching), spacing distance
- **Mesh generation**: mesh setting (fast, normal, precise to decide mesh size), mesh generation button

When the geometric arrangement of the circuits and the environment is done, the domain can be modeled by FEM in the mesh generation section. This will generate the finite element model of the specified domain and show it to the right of the input tab.

To the right of the input tab is the display of the model. There are two viewing options. One is the real view, and the other is the mesh view. For the real view, this is the rapidly generated world on how it should look like. The mesh view is the FEM model with a certain world radius. Zooming options are available for the mesh view to inspect the generated mesh. The mesh does not need to be generated manually; when it is not generated, the tool will do it automatically at the start of a simulation. The display can also be saved to a PNG or enlarged for greater inspection.

When the laying formation is completed, the user can go to the final input tab, the operational info.

A.1.3. Operational info

The Operational Info tab allows users to input specific electrical and operational parameters that directly impact the performance and thermal rating of the cables.

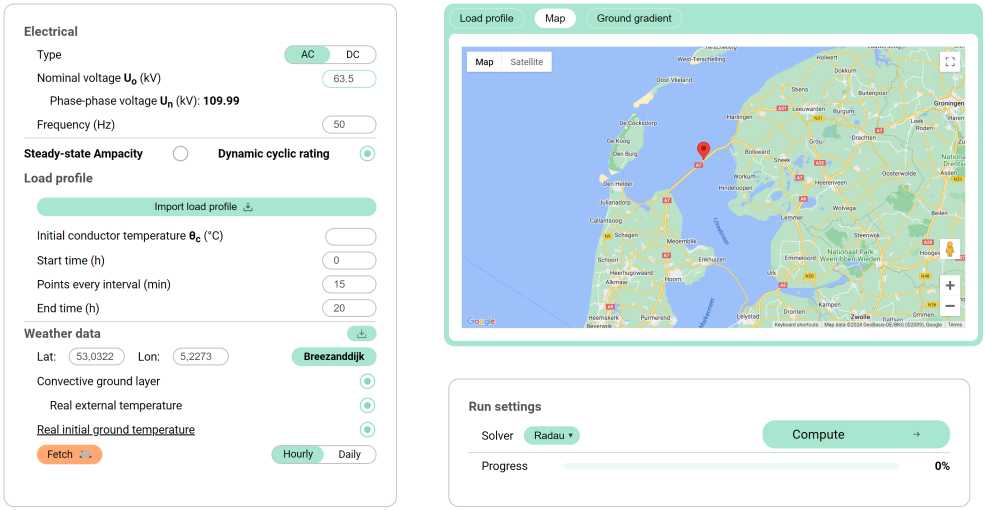

Figure A.3: Operational info tab of *Ampwise*

As depicted in Figure A.3, this tab enables the user to specify a wide range of operational settings, most importantly, a steady-state ampacity or a dynamic cyclic rating simulation. Here are the key features and inputs provided in this tab:

- **Electrical**: Type (Alternating current or Direct current), Nominal voltage (calculated phase voltage for three-phase), frequency (for AC)
- **Steady state ampacity**: Ambient temperature
- **Dynamic cylic rating**: Initial conductor temperature, output time interval (start time, points every interval, end time)
  - **Import load profile**: Import dataset window (select a csv, xlsx, xls), identify column type (Timesteps, conductor temperature, current, air temperature, measured temperature), add button to add the dataset. The measured data, load profile, and weather can be imported as can be seen in.

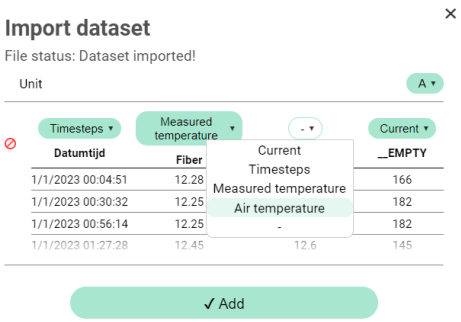

Figure A.4: Import dataset screen from *Ampwise*

  - **Weather data**: Latitude, Longitude, select location button,
    - **Convective ground layer**: Real or constant external temperature
    - **Real initial ground temperature**: Average temperature, temperature deviation, time after coldest day, temperature slope
  - Fetch location button for daily or hourly values

- **Run settings**: Solver (BDF, Radau), progress bar

To the right of the input tab, three other tabs can be selected to display graphs and a map, only relevant for a dynamic cyclic rating:

- Load profile: Here the imported load profile is visible, either power (W) or current (A), a real date is required since then the tool knows for when to fetch the weather data. The start- and end-time can be seen by the full line, the excluded graph remains a dotted line. The day can be changed by the buttons on the right and the graph can also be saved
- Map: Here a Google map is shown. The user has the ability to place a pin for where the cable is present on the world. The longitude and latitude is then saved of the dropped pin. The user can also enter the latitude and longitude manually.
- Weather: The location is used to fetch the weather data from Visual Crossing Weather API for the duration of the selected start and end time for every hour. The included weather data is the air temperature, the pressure, the precipitation and the solar radiation. The latter two are currently not incorporated into the model.

  Furthermore, if the *set initial ground temperature* checkbox is checked, the monthly temperature of the year before will also be fetched to set the realistic ground gradient temperature at the start of the simulation.

Upon completing the input in the Operational Info tab, and if everything is correctly entered, the study can be computed.

During the computation, progress is shown in the progress bar.

All the input data are sent to the Python back-end and after a couple of minutes the study is computed and the Ampacity tab is automatically shown with the results of the simulation.

A.1.4. Ampacity

The Ampacity tab is where the user can view the results of the cable rating calculations, either the steady-state ampacity or the dynamic cyclic rating results.

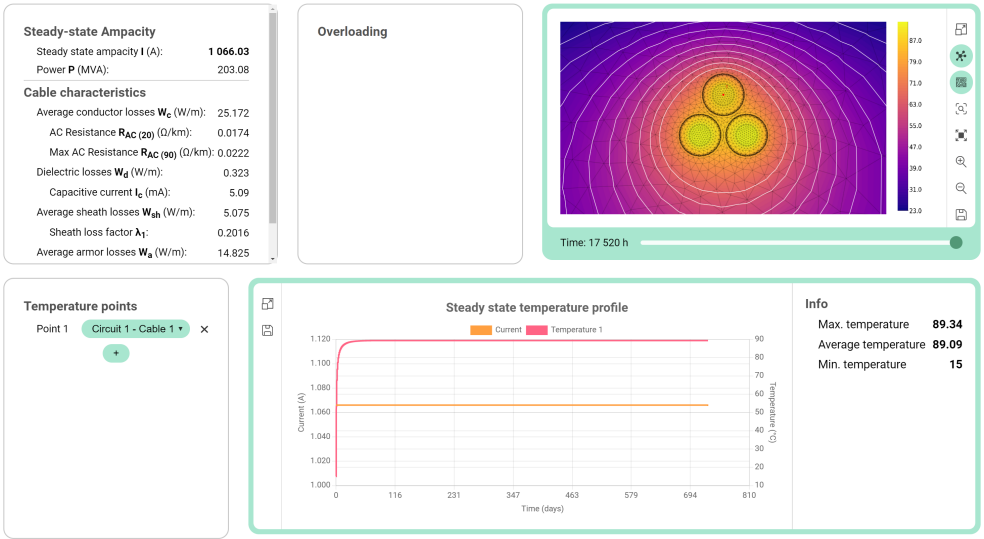

Figure A.5: Ampacity tab of *Ampwise*

The Ampacity tab shown in Figure A.5, is divided into several sections:

- **Cable characteristics and Steady-state ampacity**: Here, the analytically calculated cable characteristics are displayed like the AC resistance, loss factors, losses, etc. If a steady-state ampacity simulation is performed, then the resulting ampacity is displayed with its respective power value.
- **Overloading**: This section is currently not finished; this can display the current overloading and how long it can be overloaded with example values.
- **Colormap**: This displays the colormap for every node in the domain over time. Zooming options are available, and the user can choose between a simple display of the cables or the mesh display, where the mesh overlaps the colormap. In addition, the isotherms can be toggled between on and off. Cutpoints are shown with a red dot. The colormap is generated in the back-end by the *matplotlib* library, so there is a slight delay between a change in the front-end and the back-end image loading.
- **Cutpoint selection**: Here, cutpoints can be selected of the center of cables, or a custom cutpoint can be manually entered (x and y position).
- **Cutpoint temperature**: The temperatures of all cutpoints are displayed in the graph along with the load profile. The min, max and average temperature values are shown to the right.

Clearly, this tab is not finished but the main rating results can be viewed.
Lastly, the results can be compared with other data, like real measured data or COMSOL data in the *Real vs Computed* tab.

A.1.5. Real vs computed

The Real vs Computed tab is where the user can compare the predicted temperature with another dataset like the measured temperature.

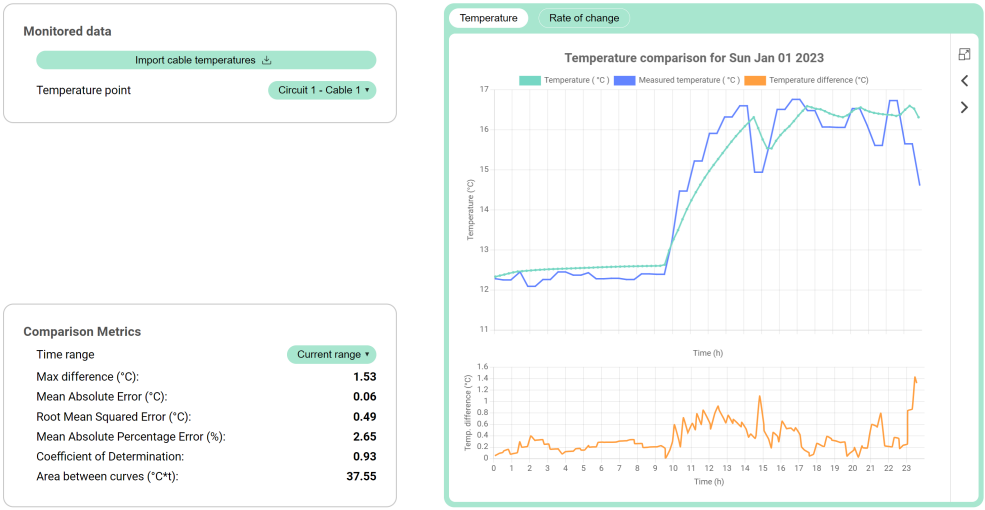

Figure A.6: Real vs Computed tab of *Ampwise*

The Real vs Computed tab shown in Figure A.6, is divided into several sections:

- **Import dataset**: The same button as in the Electrical Info tab to import a reference dataset
- **Select temperature point**: The temperature graph for a certain cutpoint to compare against
- **Comparison Metrics**: Metrics to determine fit of two graphs (current selection or total selection): Max difference, Mean absolute error, Root Mean Squared Error (RMSE), Mean absolute difference error, Coefficient of determination, Area between curves. (**See below for explanation*)

The graph on the right shows the result of the difference between the datasets in graph format. The two temperature graphs can be seen as well as its rate of change in the second tab. Both sections are divided into two graphs. The temperature comparison and the difference between the two graphs with both the same timestamps.

A.2. Explanation of Comparison Metrics

The following metrics are used to quantify the fit of the predicted temperature to the measured temperature.

- **Mean Absolute Error (MAE)**: This metric represents the average of the absolute differences between the predicted and observed temperatures. It provides an overall indication of how accurate the predictions are. The formula for MAE is:

$$\text{MAE} = \frac{1}{n}\sum_{i=1}^{n}|y_i - \hat{y}_i|$$

  where y_i is the observed value, $\hat{y}_i$ is the predicted value, and n is the number of observations.

- **Mean Error**: This metric measures the difference between the predicted and observed average temperature. It can indicate whether the predictions are generally overestimating or underestimating the actual values. The formula is as follows:

$$\text{Mean Error} = \frac{1}{n}\sum_{i=1}^{n} y_i - \frac{1}{m}\sum_{j=1}^{m}\hat{y}_j$$

- **Root Mean Squared Error (RMSE)**: This metric is the square root of the average of the squared differences between the predicted and observed temperatures. It emphasizes larger errors more than MAE and provides a measure of the overall prediction accuracy. The formula is:

$$\text{RMSE} = \sqrt{\frac{1}{n}\sum_{i=1}^{n}(y_i - \hat{y}_i)^2}$$

- **Mean Average Percentage Error (MAPE)**: This metric represents the average of the absolute percentage differences between the predicted and observed temperatures. It gives an indication of prediction accuracy as a percentage. The formula is as follows:

$$\text{MAPE} = \frac{100\%}{n}\sum_{i=1}^{n}\left|\frac{y_i - \hat{y}_i}{y_i}\right|$$

- **Max Difference**: This metric indicates the maximum observed difference between the predicted and observed temperatures. It highlights the largest single discrepancy in the dataset.

- **Coefficient of Determination (R^2)**: This metric measures the proportion of the variance in the observed temperatures that is predictable from predicted temperatures. It indicates the goodness of fit of the model. The formula is:

$$R^2 = 1 - \frac{\sum_{i=1}^{n}(y_i - \hat{y}_i)^2}{\sum_{i=1}^{n}(y_i - \bar{y})^2}$$

  where $\bar{y}$ is the mean of the observed values.

A.3. Ampwise Code Improvements

The following list of improvements are things that could make the tool better and more complete but were not in the scope of this thesis subject and not enough time was available to cover all improvements in the tool.

- Opposite workflow, where it starts with an ampacity and finally a cable is chosen that fits best in that situation.
- Iteratively find the best parameters of the environment by checking the fit of the predicted temperature graph with the real measured temperature
- More import options of the dataset:
  - RMS or P-P
  - Able to import power also next to current
  - Unit of the imported dataset, currently only Ampere (A)
  - Remove/Include more headers
  - Check the timestamps format, date or seconds: mm/dd or dd/mm
  - Correct timezone and winter/summer time
- Automatic API Key entering for the weather fetching, a place to enter the API Key and save it locally or on the server with user account?
- Use precipitation in environmental model
- Dry zone around the cable due to heating
- Axis around the cable/layout and colormap
- Show the user when to refresh or generate new mesh when inputs have changed
- Check data in front end before sending to back end
- Variable resistance for flat formation!
- Sheath/proximity factor based on tb 880
- user account and server on a real server or launch front end on a website and server local, no need to install packages, nodejs and git
- Real Milliken conductor
- Date and interval selector for the profiles to see more than just a day and color where the selection is
- Overloading field
- Being able to save the project and open it
- Try with CUDA to improve speed
- include the cable crossings code in the Ampwise tool to compute the derating factor for crossed cables

A.4. Ampwise Code Fixes

The following list of fixes needs to be performed to make the program more correct but were not in scope or not high enough on the list to fix in time and not enough time was available to fix all of them.

- Cleanup mesh, straight line for soil layers touching the backfill or cables.
- Refinement of the mesh near the edges
- No need for the empty graph, every graph should be able to handle null datasets or undefined items
- Font, point radius should reload when resizing graph
- Switching days does not work when on another temperature point
- Graph container shifts based on content
- Break out of nested loops instead of continuing
- Progress bar runs multiple times for steady state due to iterations
- Full-screen options and resetting of size (colormap)
- Temperature comparison for steady state or non-date datasets is not showing
- Slow solving after extended time, detect and restart solver

A.5. Cable crossings

As a potential academic continuation, the study of cable crossings on cable ampacity was considered. When other cables (or general heat sources) are installed in the vicinity of the cable, the permitted current-carrying capacity of the cable should be reduced to avoid overheating, see Figure A.7. However, applying formulae that are valid for parallel routes would overestimate the thermal influence of the heat source at the crossing of the cable [43].

The international standard IEC 60287-3-3 has already researched this topic for a steady state scenario and assumes all cables to be horizontal.

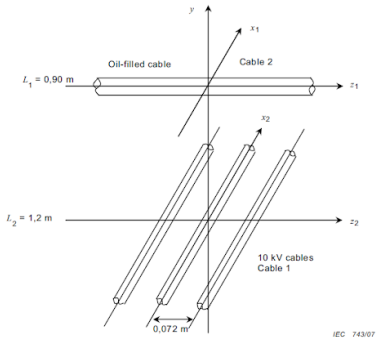

Figure A.7: Cable crossing example of IEC60287-3-3[43]

The essential goal is to calculate a Derating Factor (DF) for every heat source that is multiplied with the steady-state ampacity.

$$DF = \sqrt{1 - \frac{\Delta\theta(0)}{\Delta\theta_{max} - \Delta\theta_d}} \tag{A.1}$$

where $\Delta\theta(0)$ is the temperature increase of the conductor due to the heat source at the crossing point. The temperature rise is maximum at the crossing point and decreases with the distance from the crossing.

To calculate the maximum permissible current in each cable, an iterative procedure is necessary. The first stage of the procedure is to calculate the derating factor for one cable, assuming that the other cable is carrying its maximum permissible current, when isolated. The derating factor for the second cable is then calculated, assuming that the first cable is carrying its derated current. This is repeated for each cable until there is no change in the calculated derating factors. The iterations are repeated until there is no change in the calculated derating factors.

Python code is written to calculate the Derating factor for the scenario given in Figure A.7. The results can be seen below, and the code is given in A.8.

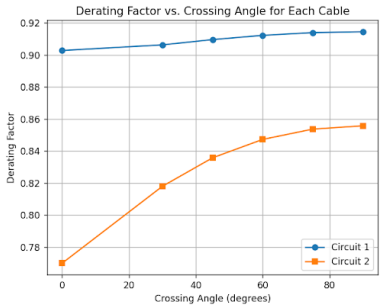

Figure A.8: Derating factor vs crossing angle

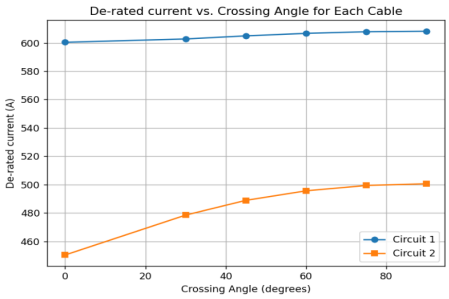

Figure A.9: Ampacity vs crossing angle

It is clearly visible that the cable ampacity of both cables gets higher the more perpendicular the crossing cable is and for parallel cables, the ampacity of both heat sources is lowest.

Cable Crossings was eventually not chosen to pursue in this master's thesis since it is already documented extensively in the international standards.

It would be interesting to model the changed (dynamic) cyclic rating due to the crossing cable. Then the iterations would have to be done every time stamp.

A.6. Daily load profile example

The load profile used for various sensitivity analysis or verification purposes:

Time	Current (A)	Time	Current (A)
0h	302	12h	892
1h	248	13h	770
2h	228	14h	772
3h	232	15h	800
4h	234	16h	854
5h	246	17h	996
6h	290	18h	854
7h	600	19h	790
8h	1000	20h	740
9h	950	21h	740
10h	940	22h	722
11h	950	23h	600

Table A.1: Hourly Current Values for One Day.

A.7. Datasheet

A.7.1. WPF cable

The datasheet for the WPF Prysmian cable used int the case study.

Prysmian Group

PRYSMIAN Draka

Cable type	:	**EYAKrvlwdgv 64/110kV 1x2500 mm² aluminium +2xOE**
Article number	:	**520.16.0307.120** *Cable data sheet*
Standard	:	HD632 S2:2011 *12-apr-2019*

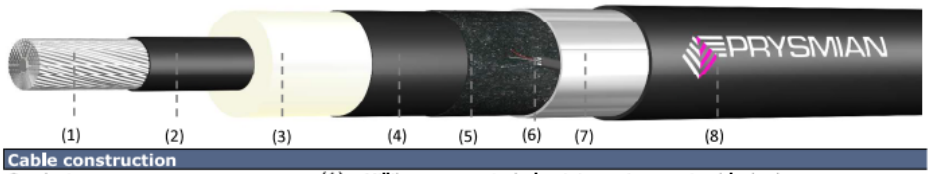

Cable construction

Conductor	: (1)	Milliken compacted aluminium wires, water blocked
Conductorscreen	: (2)	semi-conducting tape, semi-conducting compound
Insulation	: (3)	XLPE
Insulationscreen	: (4)	semi-conducting compound
Bedding	: (5)	semi-conducting swellable tape
	(6)	Two optical elements (OE) with integrated optical fibers, 2x(2xSM 2xMM), semi-conducting swellable tape
Metallic sheath	: (7)	Welded Aluminium Sheath
Outer sheath	: (8)	black polyethylene jacket
Identification	:	Prysmian - year - cable type - length identification

Main dimensions and weight		Nominal thickness	Diameter
Conductor	: (1)		61.5 mm
Conductorscreen	: (2)		62.9 mm
Insulation	: (3)	14.9 mm	92.9 mm
Insulationscreen	: (4)		94.7 mm
Metallic sheath	: (6)	1.2 mm	102 mm
Outer sheath	: (7)	5.0 mm	114 mm
Cable weight	:	appr. 14.0 kg/m	

Electrical data

Rated voltages U_0/U (U_m)		: 64/110 (123)	kV
Conductor			
Maximum DC resistance at 20° C	:	0.0119	Ω/km
Maximum temperature under normal conditions	:	90	°C
Maximum temperature under short circuit conditions	:	250	°C
Permissible short circuit current during 1 sec (adiabatic 90-250°C)	:	>50	kA
Insulation			
Capacitance	:	0.34	µF/km
Charging current per core at Uo	:	6.8	A/km
Dielectric stress on conductor screen at Uo	:	5.2	kV/mm
Dielectric stress under insulation screen at Uo	:	3.6	kV/mm
Dielectric loss angle at Uo	:	<10	$*10^{-4}$
Metallic sheath			
Maximum temperature in case of short circuit	:	250	°C
Permissible short circuit current (non-adiabatic 70-250°C)	1.0s :	43.9	kA

(* = according IEC 61443-1999)

Cable laying data

Maximum pulling force on cable with cable grip	:	12.9	kN
Maximum pulling force on conductor with pulling head	:	75.0	kN
Minimum bending radius during laying	:	2.8	m
Minimum bending radius when installed	:	2.3	m
Minimum temperature of cable during laying	:	-10	°C

Figure A.10: Prysmian cable for WPF [22]

A.8. Code

Matlab code - Analytical model

This matlab code is the analytical model based on IEC 60853. The numerical model proved to be more viable for this thesis topic and this code is not used outside of the comparison.

```
%clear all
close all

tic

%default laying formation
amount_cables = 1;
dList = []; % empty array
cable_distance = 0; % Distance between cables

%Long duration
current_profile = [2000];
time_step = 1000;
short_transient = false;
%TODO: insert reference data here
comsol_list = 0;

% Define the time parameters for simulation
N = length(current_profile);
resolution = 1/6;
time = 0:resolution:N*time_step;

% Define thermal and physical properties of the cable system
AmbTemp = 15;                   % Soil temperature at burial depth

D_cond = 0.0615;                % Conductor diameter [m]
A_cond = (pi*D_cond^2)/4;       % Conductor area [m^2]
D_ins = 0.097;                  % Insulation diameter [m]
t_ins = (D_ins-D_cond)/2;       % Insulation thickness [m]
t_sheath = 0.004;               % Sheath thickness [m]
D_cable = 0.107;                % Cable diameter [m]
L = 1;                          % Burial depth [m]

% Specification of material properties (can be found from COMSOL)
rho_ins = 3.2;                  % Thermal resistivity insulation (XLPE)
rho_sheath = 3.5;               % Thermal resistivity sheath (PE)
rho_soil = 0.82;                % Thermal resistivity soil
density_soil = 1600;
heat_cap = 1180;
diff_soil = getDiffusivity(rho_soil, density_soil, heat_cap);       % Diffusivity of soil
c_ins = 930*1900;               % Specific heat insulation (XLPE)
c_sheath = 950*1900;            % Specific heat sheath (PE)
c_cond = 2760*897;              % Specific heat conductor (aluminium)
c_metal_sheath = 2760*897;      % Specific heat screen (aluminium)

lambda1 = 0.000115;             % sheat loss factor
qs = 1 + lambda1;               % factor for ladder network

%-------------------------------------------------------------
% Calculation of thermal resistances, heat capacitances and Van Wormer
% coefficients from the thermal equivalent circuit using laplace code to solve

T1 = rho_ins/(2*pi)*log(D_ins/D_cond);                      % Thermal resistance of
    insulation layer
T3 = qs*rho_sheath/(2*pi)*log(D_cable/(D_cable - 2*t_sheath)); % Thermal resistance of sheath
     layer

% Heat capacitance of conductor
Qc = A_cond*c_cond;
% Heat capacitance of insulation layer
Qins_1 = pi/4*D_cond*(D_ins - D_cond)*c_ins;
Qins_2 = pi/4*D_ins*(D_ins - D_cond)*c_ins;
Qins = Qins_1+Qins_2;
% Heat capacitance of metali sheath layer
Qmscr = pi/4*((D_cable-2*t_sheath)^2 - D_ins^2)*c_metal_sheath;
```

```
% Heat capacitance of outer sheath layer
Qos = pi/4*(D_cable^2 - (D_cable-2*t_sheath)^2)*c_sheath;

%TODO dynamic van wormer coefficient for better results in short transient
% Van Wormer coefficient for insulation layer
p = 1/(2*log(D_ins/D_cond)) - 1 / ((D_ins/D_cond)^2-1);
% Van Wormer coefficient for sheath layer
p_ = 1/(2*log(D_cable/(D_cable-2*t_sheath))) - 1 / ((D_cable/(D_cable-2*t_sheath))^2-1);
pstar = 1/(log(D_ins/D_cond)) - 1 / ((D_ins/D_cond)-1);

%short transient
QA_t = Qc + pstar*Qins_1;
QB_t = (1-pstar)*Qins_1 + pstar*Qins_2;
QC_t = ((1-pstar)*Qins_2 + (Qmscr + p_*Qos))/qs;

%long transient
QA_t_long = Qc + p*Qins;
QB_t_long = ((1-p)*Qins + (Qmscr + p_*Qos))/qs;

%From laplace in vscode, 3-loop network short transient
time_constant = (T1+T3)*(Qc+Qins+Qos+Qmscr);
if short_transient
    poles = [-0.00832074339651749, -0.00389594298261375, -0.000352196776322375];
    T_coef_cond = [0.000143802948539010, 0.00453891745829447, 0.270717279593167];
else
    poles = [-0.00435808875040096, -0.000334806901487790];
    T_coef_cond = [0.000367801844840335, 0.275032198155160];
end

% Specifying properties to calculate initial heat loss in the conductor
rho_cond = 2.84E-8;             % Electrical resistivity of conductor (aluminium) at
    reference temperature
R_20dc = 0.00001293;            % Conductor (aluminium) resistance
alpha_cu = 0.00403;             % Copper temperature coefficient
max_temp = 90;

% ------------------------------------------------------
% Calculate SR and Wc
CondTempTot = zeros(1, length(time));
CondTempTot(1) = AmbTemp;
Ic20star = zeros(1,length(time));
SR_cond = zeros(1,length(time));
SRE = zeros(1,length(time));
Done = 0;

for t_idx = 1:length(time)
    t = time(t_idx);  % Current time from the 'time' array
    t_seconds = t * 3600;

    % ---GET CURRENT FROM SPECIFIC TIME----
    current_profile_idx = floor(t / time_step) + 1;
    current_profile_idx = min(current_profile_idx, length(current_profile));

    % ----------PRE-ALLOCATION-------------
    % Calculate Wc for the current time step, if it has not been done yet
    % and if there is a change in current
    if t_idx == 1 || (current_profile_idx ~= Done && current_profile_idx > 1 &&
    current_profile(current_profile_idx) ~= current_profile(current_profile_idx-1))
        Ic20star(round((current_profile_idx-1)*time_step/resolution + 1)) =
    getIcFromTempAndTime(current_profile, current_profile_idx);
        Done = current_profile_idx;
    end
    SR_cond(t_idx) = getStepResponse(T_coef_cond, poles, t_seconds);
    SRE(t_idx) = getEnvironmentalReponse(D_cable, L-cable_distance/2, t_seconds, diff_soil,
    rho_soil, dList, amount_cables);

    % ----------------------------------------
    % Attainment factor
    Afacs_cond = SR_cond(t_idx)/(sum(T_coef_cond));

    % ----CALCULATE Temperature Rise By Superposition (TRS)----
```

```
131     TRS_cond = 0;
132     for j = 1:t_idx
133         Wc = R_20dc*Ic20star(t_idx-j+1);
134 
135         TRS_cond = Wc*(SR_cond(j)+Afacs_cond*SRE(j)) + TRS_cond;
136 
137         % if Wc20star(t_idx-j+1) ~= 0
138         %     fprintf('For t is %d\n', t_idx);
139         %     fprintf('j is %d\n', j);
140         %     fprintf('time(j) is %f\n', time(j)*3600);
141         %     fprintf('use SR_j: %f\n', SR_j);
142         %     fprintf('use SRE_j: %f\n', SRE_j);
143         %     fprintf('* Wc at %d as %f\n', (t_idx-j+1), Wc20star(t_idx-j+1));
144         %     fprintf('TRS is %f\n', TRS_t);
145         %     fprintf('-------------\n');
146         % end
147     end
148 
149     %----CALCULATE CONDUCTOR TEMPERATURE----
150     % Heating of metallic parts
151     C_20_star = 1 - alpha_cu*20;
152     CondTempCabRise = ((C_20_star + alpha_cu*AmbTemp)*TRS_cond)/(1 - alpha_cu * TRS_cond);
153     CondTempTot(t_idx) = CondTempCabRise + AmbTemp;
154 end
155 
156 toc
157 
158 %see Step responses
159 %figure
160 %hold on
161 
162 %plot(time, SRE);
163 %plot(time, SR_cond);
164 %plot(time, SR_cond+SRE);
165 
166 difference_color = [255, 159, 64] / 255;
167 comsol_color = [99, 132, 255] / 255;
168 calculated_color = [118, 215, 196] / 255;
169 
170 % Create a new figure
171 f = figure;
172 f.WindowState = 'maximized'; % This makes the figure fill the entire screen
173 
174 % First subplot (Temperature/Current vs Time) - occupies the top position
175 subplot(3,1,1:2);
176 grid on;
177 hold on;
178 title('Temperature plot');
179 
180 yyaxis right;
181 stairs(0:time_step:N*time_step, [current_profile 0], 'LineWidth', 2);
182 
183 yyaxis left;
184 condtemp_handle = plot(time, CondTempTot, "-", 'LineWidth', 2, 'Color', calculated_color);
185 
186 ylabel('Temperature (degC)');
187 %set(gca, 'XTickLabel', []);
188 
189 % Calculate the difference
190 if (comsol_list ~= 0)
191     comsol_time = linspace(0, N*time_step, length(comsol_list));
192     interp_CondTempTot = interp1(time, CondTempTot, comsol_time, 'linear', 'extrap');
193     difference = abs(comsol_list - interp_CondTempTot);
194 
195     legend([condtemp_handle, comsol_handle], 'Conductor Temperature', 'COMSOL Temperature','
    Location', 'southeast');
196     ylim([15, max([CondTempTot interp1(comsol_time, comsol_list, time, 'linear')])]);
197 
198     comsol_handle = plot(time*60, interp1(comsol_time, comsol_list, time, 'linear'), "-", '
    LineWidth', 2, 'Color', comsol_color);
199 
```

```
200     % Second subplot (Difference per hour) - occupies the bottom position and can be thinner
201     subplot(3,1,3);
202     plot(comsol_time*60, difference, '.-', 'LineWidth', 2, 'Color', difference_color);
203     grid on;
204     xlabel('Time (min)');
205     ylabel('Temp. Difference (degC)');
206 end
207
208 % ----------------------------------------
209 % Functions
210 function SR = getStepResponse(T, P, t_seconds)
211     SR = 0;
212     for j = 1:length(T)
213         SR = SR + (T(j) * (1 - exp(t_seconds*P(j))));
214     end
215 end
216
217 function SRE = getEnvironmentalReponse(D_cable, L, t_seconds, diff_soil, rho_soil, dList,
        amount_cables)
218     if t_seconds ~= 0
219         sumPart = 0;
220         if ~isempty(dList)
221             for i = 1:amount_cables-1
222                 y1 = (dList(i)^2) / (4 * t_seconds * diff_soil);
223                 %Only for trefoil
224                 tempR = dList(i)/2;
225                 imageD = sqrt((2*L-D_cable+sqrt(3)*tempR)^2 + (tempR)^2);
226                 y2 = (imageD^2) / (4 * t_seconds * diff_soil);
227
228                 Ed1 = expint(max(y1, 0));
229                 Ed2 = expint(max(y2, 0));
230
231                 sumPart = sumPart + (Ed1 - Ed2);
232             end
233         end
234
235         x1 = D_cable^2/(16*t_seconds*diff_soil);
236         x2 = L^2/(t_seconds*diff_soil);
237
238         Ei1 = expint(max(x1, 0));
239         Ei2 = expint(max(x2, 0));
240
241         % Temperature rise due to influence of soil
242         SRE = rho_soil/(4*pi) * ((Ei1 - Ei2) + sumPart);
243     else
244         SRE = 0;
245     end
246 end
247
248 function Ic20star_i = getIcFromTempAndTime(current_profile, i)
249
250     % Handle NaN values by taking the previous non-NaN current value
251     I_temp = 0;  % Initialize with zero for the first iteration
252     if i ~= 1
253         idx = i - 1;
254         % Loop backwards to find the previous non-NaN value
255         while idx > 0 && isnan(current_profile(idx))
256             idx = idx - 1;
257         end
258         % If a non-NaN value is found, use it; otherwise, I_temp remains 0
259         if idx > 0
260             I_temp = current_profile(idx);
261         end
262     end
263
264     % Calculate Wc20star_i with the valid previous current value
265     if isnan(current_profile(i))
266         Ic20star_i = 0; % If current is NaN, no heat is generated
267     else
268         Ic20star_i = (current_profile(i))^2 - (I_temp)^2;
269     end
```

```
end

function delta = getDiffusivity(pT, density, heat_cap)
    delta = 1/(pT.*density.*heat_cap);
end
```

Python code - Solve ladder network

To solve the lalpace transform of an RC ladder network, the following code can be used to acquire the poles, zeros and coefficients.

```
import sympy as sp

def TCoefficients(P, Z, a, b, n, i, j):
    num = 1
    for k in range(1, n-i+1):
        num *= (Z[k-1] - P[j-1])

    den = P[j-1]
    print("Pj = ", den)
    for k in range(1, n+1):
        if k != j:
            print("Pk = ", P[k-1])
            print("in array Pj = ", P[j-1])
            den *= (P[k-1] - P[j-1])

    print("den = ", den)
    print("num = ", num)

    T_ij = - (a[0]/b[0]) * (num/den)

    return T_ij

def compute_transfer_function(T, Q, i):
    s = sp.symbols('s')
    n = len(T)
    H_s = 1 / (Q[n-1] * s + 1/T[n-1])

    print("Z_n = ", H_s)

    if i == n:
        H_s = H_s / (1 + Q[0]* s * (T[0] + H_s))
    else:
        for i in range(n-2, -1, -1):
            H_s = 1 / (Q[i] * s + 1/(T[i] + H_s))

    print("H_s = ", H_s)
    H_s = sp.simplify(H_s)

    poles = [p.evalf(chop=True) for p in sp.solve(1/H_s, s)]
    zeros = [z.evalf(chop=True) for z in sp.solve(H_s, s)]

    # Extracting coefficients of numerator and denominator
    numerator, denominator = H_s.as_numer_denom()
    a_coeffs = sp.Poly(numerator, s).all_coeffs()
    b_coeffs = sp.Poly(denominator, s).all_coeffs()

    #divide every coefficient from a and b by b[length(b)-1] to get 1 for s^0
    a_coeffs = [a / b_coeffs[-1] for a in a_coeffs]
    b_coeffs = [b / b_coeffs[-1] for b in b_coeffs]

    return H_s, a_coeffs, b_coeffs, poles, zeros
```

Python code - Cable Crossings (Solve derating factors)

The following code is used to solve the derating factor for cable crossings. It works but is not implemented into Ampwise.

```
print("Testing cable crossing...")

```

```
    # define two circuits
    n_circuits = 2
    A_cr = [0.0003, 0.0004]  # m^2

    I = [665, 585]  # A
    R = [0.0000781, 0.0000615]  # Ohm/m
    alpha_20 = [0.00393, 0.00393]  # 1/K

    l1 = [0.089, 0.135]
    l2 = [0, 0]
    T1 = [0.214, 0.835]  # Km/W
    T2 = [0, 0]
    T3 = [0.104, 0.09]  # Km/W
    T4 = [1.427, 0.445]  # Km/W

    n = [1, 3]

    Wd = [0, 2.01]

    L = [1.2, 0.9]  # m
    S = [[-0.072, 0, 0.072], [0]]  # m

    max_temp = [90, 85]  # Celsius
    ambient_temperature = 25  # Celsius

    p_soil = 0.8  # Km/W
    p_cr = [0.0026, 0.0026]  # Km/W
    crossing_angle = [0, 30, 45, 60, 75, 90]  # degrees, right angles

    z_max = 5
    deltaZ = 0.01
    N = int(z_max/deltaZ)
    print(">>>N:", N)

    print(">>>Calculating characteristics")

    DF_angle_cable1 = []
    DF_angle_cable2 = []

    deltaT = [0, 0]
    deltaT0 = [0, 0]
    attenuations = [0, 0]

    W_joule_sum_tot = [0, 0]

    for angle in crossing_angle:
        print(">>>Angle:", angle)

        DF = [1, 1]
        old_DF = [0, 0]
        while not np.allclose(old_DF, DF, rtol=1e-3):
            old_DF = DF.copy()

            for i in range(n_circuits):
                Tl = p_cr[i] / A_cr[i]
                Tr = T1[i] + n[i] * (T2[i] + T3[i] + T4[i])
                T = T1[i] + n[i] * ((1 + l1[i])*T2[i] +
                                    (1 + l1[i] + l2[i]) * (T3[i] + T4[i]))

                deltaTemp_max = max_temp[i] - ambient_temperature
                deltaTemp_dielectric = Wd[i] * \
                    (T1[i]/2 + n[i] * (T2[i] + T3[i] + T4[i]))

                deltaW_0 = deltaW0(R[i], alpha_20[i], DF[i]*I[i], max_temp[i])
                # print(">>>deltaW_0:", deltaW_0)

                # sum up the W_joule of the other cables
                W_joule_sum = 0
                Lh = 0
                S_new = [0]
                for j in range(n_circuits):
```

```
                    if j != i:
                        Wc = R[j] * (DF[j]*I[j])**2
                        W_joule_sum += (Wd[j] + Wc*(1 + l1[j]))*n[j]
                        Lh = L[j]
                        S_new = S[j]
                        break  # only one cable now

                W_joule_sum_tot[i] = W_joule_sum

                # print(">>>W_joule_sum:", W_joule_sum)

                attenuation_0 = 0
                delta_T = 1
                old_delta_T = 0

                iteration = 0
                while not np.allclose(old_delta_T, delta_T, rtol=1e-2):
                    old_delta_T = delta_T
                    delta_T = SingleSourceCrossing(
                        W_joule_sum, p_soil, attenuation_0, deltaZ, N, L[i], Lh, angle,
    iteration, n[i], S_new)
                    deltaT[i] = delta_T
                    if iteration == 0:
                        deltaT0[i] = delta_T
                    # print(">>>delta_T:", delta_T)

                    delta_W = deltaW(deltaW_0, delta_T, deltaTemp_max)
                    # print(">>>delta_W:", delta_W)

                    attenuation_0 = attenuation(delta_W, T, Tl, Tr)
                    attenuations[i] = attenuation_0
                    # print(">>>attenuation_0:", attenuation_0)
                    iteration += 1

                DF[i] = DeratingFactor(
                    delta_T, deltaTemp_dielectric, deltaTemp_max)

            print(">>>DF:", DF)

        DF_angle_cable1.append(DF[0])
        DF_angle_cable2.append(DF[1])

        print(">>>DF for angle {}: {}".format(angle, DF))

    print(">>>Final deltaT:", deltaT)
    print(">>>Final deltaT0:", deltaT0)
    print(">>>Final attenuations:", attenuations)

    plt.figure(figsize=(8, 5))
    plt.plot(crossing_angle, DF_angle_cable1, '-o', label='Circuit 1')
    plt.plot(crossing_angle, DF_angle_cable2, '-s', label='Circuit 2')
    plt.xlabel('Crossing Angle (degrees)')
    plt.ylabel('Derating Factor')
    plt.title('Derating Factor vs. Crossing Angle for Each Cable')
    plt.legend()
    plt.grid(True)

    plt.figure(figsize=(8, 5))
    print(DF_angle_cable1)
    # multiply every element in the list with the current*
    I_derated_1 = [DF_angle_cable1[i]*I[0] for i in range(len(crossing_angle))]
    I_derated_2 = [DF_angle_cable2[i]*I[1] for i in range(len(crossing_angle))]
    plt.plot(crossing_angle, I_derated_1, '-o', label='Circuit 1')
    plt.plot(crossing_angle, I_derated_2, '-s', label='Circuit 2')
    plt.xlabel('Crossing Angle (degrees)')
    plt.ylabel('De-rated current (A)')
    plt.title('De-rated current vs. Crossing Angle for Each Cable')
    plt.legend()
    plt.grid(True)

    plt.show()
```

Javascript code - Fetching weather data

The following javascript code is used in Ampwise to fetch the weather data from *Visual Crossing Weather*.

```
// Function to fetch weather data
const fetchWeatherData = async () => {
    // Extract latitude and longitude from coordinates
    const lat = coordinates.lat;
    const lng = coordinates.lng;

    // Check if coordinates are available
    if (!lat || !lng) {
      console.log("No coordinates found");
      return;
    }

    // Check if load profile timesteps are available
    if (!electricInfo.load_profile.timesteps || electricInfo.load_profile.timesteps.length
    === 0) {
      console.log("No load profile timesteps found");
      return;
    }

    // Get the start and end dates from the load profile timesteps
    const startDateTotal = electricInfo.load_profile.timesteps[0];
    const endDateTotal = electricInfo.load_profile.timesteps[electricInfo.load_profile.
    timesteps.length - 1];

    console.log("Start date total:", startDateTotal);
    console.log("End date total:", endDateTotal);

    // Validate the start and end dates
    if (!(startDateTotal instanceof Date) || !(endDateTotal instanceof Date) ||
    startDateTotal > endDateTotal) {
      console.log("Invalid dates");
      return;
    }

    // Get the start and end times from run settings
    const startTime = electricInfo.run_settings.start_time;
    let endTime = electricInfo.run_settings.end_time;

    // Validate the start and end times
    if ((!ifNotNullOrUndefined(startTime) && startTime !== 0) || !ifNotNullOrUndefined(
    endTime) || startTime > endTime) {
      console.log("Start/end time invalid");
      console.log(startTime, endTime);
      return;
    }

    // Define the API key for Visual Crossing API
    const apiKey = ""; // Example API key

    if (
      electricInfo.weather_profile.fetch_weather &&
      electricInfo.weather_profile.convective_ground_layer
    ) {
      const startDateWeather = new Date(startDateTotal.getTime());
      startDateWeather.setHours(startDateWeather.getHours() + startTime);

      console.log("Start date:", startDateWeather);

      const endDateWeather = new Date(startDateTotal.getTime());
      endDateWeather.setHours(endDateWeather.getHours() + endTime);

      console.log("End date:", endDateWeather);

      const startUnixTime = Math.floor(startDateWeather.getTime() / 1000);
      const endUnixTime = Math.floor(endDateWeather.getTime() / 1000);

      let dayFormat = "hours";
      if (fetchTimeSetting === "Daily") {
```

```
65          dayFormat = "days";
66        }
67
68        const url = `https://weather.visualcrossing.com/VisualCrossingWebServices/rest/services
        /timeline/${lat},${lng}/${startUnixTime}/${endUnixTime}?unitGroup=metric&key=${apiKey}&
        include=${dayFormat}&elements=tempmax,tempmin,temp,pressure,datetimeEpoch,solarradiation,
        solarenergy,precip,windspeed&options=nonulls`;
69
70        console.log("URL:", url);
71
72        try {
73          const response = await fetch(url);
74
75          if (!APICodes(response)) {
76            return;
77          }
78
79          const data = await response.json();
80          console.log("data: ", data);
81
82          if (!data.days || data.days.length === 0) {
83            console.log("No days data found");
84            return;
85          }
86
87          let temperatureTimesteps = [];
88          let temperatureMinValues = [];
89          let temperatureMaxValues = [];
90          let temperatureValues = [];
91          let pressureValues = [];
92          let solarRadiation = [];
93          let precipitationvalues = [];
94          let windSpeed = [];
95          let dailySolarEnergy = [];
96
97          //loop over the days
98          data.days.forEach((day) => {
99            if (dayFormat === "hours") {
100             if (!day.hours || day.hours.length === 0) {
101               console.log("No hours data found");
102               return;
103             }
104
105             //loop over the hours
106             day.hours.forEach((hour) => {
107               let timestep = hour.datetimeEpoch * 1000;
108               //convert to a date
109               let date = new Date(timestep);
110
111               let temp = hour.temp;
112               let tempMin = hour.tempmin;
113               let tempMax = hour.tempmax;
114               let pressure = hour.pressure;
115
116               let solarRad = hour.solarradiation;
117
118               let precipitation = hour.precip;
119
120               let windspeed = hour.windspeed;
121
122               temperatureTimesteps.push(date);
123               temperatureValues.push(temp);
124               temperatureMaxValues.push(tempMax);
125               temperatureMinValues.push(tempMin);
126               pressureValues.push(pressure);
127               solarRadiation.push(solarRad);
128               precipitationvalues.push(precipitation);
129               windSpeed.push(windspeed);
130             });
131           } else {
132             let timestep = day.datetimeEpoch * 1000;
```

```
133             //convert to a date
134             let date = new Date(timestep);
135 
136             let temp = day.temp;
137             let tempmax = day.tempmax;
138             let tempmin = day.tempmin;
139             let pressure = day.pressure;
140 
141             let solarRad = day.solarradiation;
142             let solarEnergy = day.solarenergy;
143 
144             let precipitation = day.precip;
145 
146             let windspeed = day.windspeed;
147 
148             temperatureTimesteps.push(date);
149             temperatureValues.push(temp);
150             temperatureMaxValues.push(tempmax);
151             temperatureMinValues.push(tempmin);
152             pressureValues.push(pressure);
153             solarRadiation.push(solarRad);
154             precipitationvalues.push(precipitation);
155             windSpeed.push(windspeed);
156             dailySolarEnergy.push(1000000 * solarEnergy);
157           }
158         });
159         //console.log("Temperature timesteps:", temperatureTimesteps);
160         console.log("Temperature values:", temperatureValues);
161         console.log("Temperature max values:", temperatureMaxValues);
162         console.log("Temperature min values:", temperatureMinValues);
163         console.log("Pressure values:", pressureValues);
164         console.log("Solar radiation:", solarRadiation);
165         console.log("Precipitation:", precipitationvalues);
166         console.log("Wind speed:", windSpeed);
167       } catch (error) {
168         console.error("Failed to fetch weather data", error);
169       }
170     }
171   };
```